Title	Towards improved treatment planning for head and neck microwave hyperthermia
Author(s)	Cappiello, Grazia
Publication Date	2019-10-08
Publisher	NUI Galway
Item record	http://hdl.handle.net/10379/15491

Towards Improved Treatment Planning for Head and Neck Microwave Hyperthermia

A dissertation presented by

Grazia Cappiello, M.Sc., B.Eng.

to

Electrical and Electronic Engineering
College of Engineering and Informatics
National University of Ireland Galway

in fulfilment of the requirements for the degree of
Doctor of Philosophy

Supervisor
Dr. Edward Jones

Co-Supervisors
Dr. Martin Glavin
Dr. Martin O'Halloran

December 2018

Abstract

Hyperthermia is an emerging cancer treatment modality which involves applying heat to the malignant tumor. The heating can be delivered using electromagnetic energy, mostly in the radiofrequency or microwave range. Accurate patient-specific hyperthermia treatment planning is essential for effective and safe treatment, in particular for deep and loco-regional hyperthermia. An important aspect of hyperthermia treatment planning is the ability to focus microwave energy and heating into the tumour while reducing the occurrence of hotspots in surrounding healthy tissue. Typically, a multi-element antenna phase array hyperthermia system is used to focus the electromagnetic waves at the target region. This thesis presents methods for optimising the specific absorption rate distribution and resulting temperature distribution for head and neck cancer hyperthermia treatment.

Several optimisation algorithms and objective functions have been evaluated to optimise the antenna amplitudes and phases of the hyperthermia systems. Evolutionary optimisation algorithms have been considered in this thesis and compared with a particle swarm optimisation method already in clinical use for the treatment of head and neck cancers. A differential evolution algorithm is proposed to improve target coverage. The differential evolution algorithm is shown to offer improved performance compared to the particle swarm optimisation algorithm. Most optimisation techniques reported in literature use static antenna settings throughout the treatment; however, in this thesis a dynamic approach is investigated. A time-multiplexed hyperthermia strategy is developed in order to better focus heating on the tumour while preserving predetermined areas in the healthy tissue. First, a multi-objective genetic algorithm is introduced, which generates multiple antenna settings which are applied sequentially. Thermal simulations are used to evaluate the performance of time-multiplexed steering. The results demonstrate the ability to enhance target heating while reducing hotspot temperatures. Finally, the time-multiplexing steering is evaluated against thermal tissue properties variation and is shown to be robust to temperature dependent thermal tissue properties.

Acknowledgements

Firstly, I would like to thank my principal supervisor, Dr. Edward Jones and co-supervisors Dr. Martin O'Halloran and Dr. Martin Glavin for their valuable guidance and advice throughout my research work and for giving me the opportunity to pursue the PhD in Electrical & Electronic Engineering at NUI Galway. I would also like to thank Galway University Foundation for funding this research through the structured PhD programme in Biomedical Engineering and Regenerative Medicine (BMERM), directed by Professor Peter McHugh. I would also like to thank the European Union COST Programme (Action TD1301 MiMed and Action BM1309 EMF-MED) for providing travel grants to support this research. I am also grateful to the discipline of Electrical & Electronic Engineering at NUI Galway for providing facilities to conduct this research. Some of the simulation work carried out in this thesis was completed using the SEMCAD X software kindly made available on loan by ZTM Zurich MedTech AG.

I am very grateful to Dr. Brian Mc Ginley and Dr. Adnan Elahi for their constant support and constructive discussions during the duration of this project.

My sincere thanks also go to Prof. Gerard van Rhoon and Dr. Maarten Paulides, who gave me the opportunity to spend time at their research team at the Hyperthermia Unit of the Erasmus MC Cancer Institute in Rotterdam, who provided patient data for use in this research and who contributed significantly throughout this research. I am also grateful to Dr. Tomas Drizdal for his support and highly constructive discussions and assistance. This collaboration proved to be extremely important, allowing a broader understanding of hyperthermia, its real clinical needs and the opportunities to contribute to the improvement of hyperthermia treatments.

The PhD has been a challenging experience during which I received great moral and practical support from my friends in Galway and in Italy. In particular, many thanks to Lilia, Milena, Alessandra, Lei, Maria Vittoria, Mykhaylo, Laura, Enza, Silvia, Adnan, Leonie, Ana, Dave.

Thanks to Kieran who reminded me there is Life beyond the PhD and for his love.

Last but not the least, I would like to thank my family: my parents, my brothers and my nephews for their love and unconditional trust on me.

Contents

List of Figures

List of Tables

Glossary

HTQ_{HS} Hotspot-Target SAR Quotient for a specific HotSpot. 78, 79, 84, 85, 99

2D two-dimensional. 38–41

3D three-dimensional. 14, 24, 26, 33, 34, 36, 40, 41, 70, 79, 91, 99, 107

cfSAR Cubic Filtered Specific Absorption Rate. 44, 63, 80, 83, 84, 86–91

CP Crossover Probability. 51, 53

CT Computerised Tomography. 24

CTM Constant Thermal Model. 103–112

CTV Clinical Target Volume. 43, 79, 91–94, 96, 97, 99, 105–107, 109, 110, 112, 113, 118

DE Differential Evolution. 3, 6, 48–53, 55–63, 70, 71, 73, 75, 115, 116

DNA Deoxyribonucleic acid. 10, 11

EM Electromagnetic. 1, 2, 4, 14, 15, 17, 24–26, 32, 34, 39, 55, 70, 79, 114, 116, 117

F Factor. 53

FDTD Finite Difference-Time Domain. 24, 34, 37, 38, 41

FIR Finite Impulse Response. 34, 35

GPU Graphical Processing Unit. 60

H&N Head and Neck. 1, 3, 4, 6, 8, 9, 15–18, 21, 23, 43, 45, 48, 52, 73, 75, 76, 79, 82, 97, 99, 114, 115, 117

HSF-1 Heat Shock Factor. 11

HSPs Heat Shock Proteins. 11, 13

HT Hyperthermia. 1, 6, 23, 26, 44, 48, 73

HTP Hyperthermia Treatment Planning. 2, 4, 6, 21, 23, 24, 26, 43, 44, 48, 52

HTQ Hotspot-Target SAR Quotient. 2, 6, 7, 25, 44, 47, 48, 52, 56–61, 63, 73, 76, 79, 80, 83–85, 99, 106, 116

i-mf-OCPF Independent Multi-Frequency OCPF. 40

LCA Lucite Cone Applicator. 16

mf-OCPF Multi-Frquency Optimal Constraint Power Focusing. 40

MOGA Multi-Objective Genetic Algorithm. 4, 6, 75–80, 82–84, 91, 99, 100, 104, 113, 115, 116

MRI Magnetic Resonance Imaging. 36

NSGA-II Non-dominated Sorting Genetic Algorithm. 77, 78

OCPF Optimal Constraint Power Focusing. 36, 39, 40

PDE Partial Differential Equations. 35, 36

PoptS Pareto Optimal Solution. 80, 81, 84–92, 104, 105

PSO Particle Swarm Optimisation. 3, 4, 6, 7, 48–53, 55–63, 70, 73, 75, 76, 79, 82, 99, 115, 116

RF Radiofrequency. 6, 14, 20, 21, 41, 97

SAR Specific Absorption Rate. 2–7, 21, 23–32, 37, 40, 41, 43–48, 55, 60, 63–70, 73, 75, 76, 78–80, 82–85, 91, 94, 97–99, 101, 102, 105, 106, 109, 114–118

SF Scaling Factor. 102, 103

StaticS Static Setting. 79–82, 86–91, 104, 105, 109

T-V Temperature-Volume. 70, 72, 92, 95, 105, 106, 108, 110, 111

TC Target Coverage. 6, 48, 55, 60, 61, 73, 84

TDPM Thermal Dependent Perfusion Model. 103–113

TMS Time-Multiplexed Steering. 3, 94, 109, 110, 112, 113, 116

UWB Ultrawide Band. 37, 41

VEDO Visualisation Tool for Electromagnetic Dosimetry and Optimisation. 24, 25, 50, 60

WB Water Bolus. 14, 16

1
Introduction

1.1 Motivation

One of the most common cancer categories worldwide is Head and Neck (H&N) cancer [1]. The global incidence of H&N cancers has been estimated to be between 400,000 and 600,000 new cases each year, resulting in a mortality rate of between 223,000 and 300,000 deaths per year [2], [3]. Worldwide, the number of patients dying of H&N cancer is increasing each year. In Ireland, more than 500 new cases of cancers in the H&N regions are diagnosed annually, and surviving patients suffer significant side effects from conventional therapies. A demanding challenge is to preserve the organ function in locally advanced H&N tumours [4]. Moreover, high levels of toxicity have been observed in patients treated with conventional therapies such as radiotherapy and chemotherapy [4], [5]. In order to address this problem, other procedures have been investigated. Hyperthermia (HT) has been demonstrated to be a potent tumour cell sensitizer for radio- and chemotherapy [6], [7]. Clinical trials showed to improve treatment outcomes when Hyperthermia (HT) is used as an adjunct therapy [8], [9] and significant results have been reported for many types of cancers [10]–[14]. Over the last decades, several clinical radiofrequency hyperthermia systems have been developed to heat tumours [15]. Within the hyperthermia community, systems based on radiative transfer of Electromagnetic (EM) energy to the patient are generally the most widely used [16]. Such systems typically consist of a conformal multi-element antenna array that focuses EM energy at the tumour location by constructive interference [17]–[19]. However, healthy tissue is also heated during hyperthermia, inducing the occurrence of over-heated areas, known as hotspots, which can hamper treatment quality and increase patient discomfort.

To control the EM energy deposition and the resulting temperature distribution in the tissue, a Hyperthermia Treatment Planning (HTP) stage is applied before the first treatment session. Predicted Specific Absorption Rate (SAR) calculated using appropriate amplitude and phase settings for individual antennas is used for simulation of the temperature distribution in the tissue. An important requirement in HTP and in hyperthermia systems using constructive interference to heat at depth is to heat the target regions without impairing the surrounding healthy tissue. Hence, in addition to maximising tumour heating, minimisation of hotspots in healthy tissue is also one of the major challenges in HTP. Different focusing strategies have been studied to optimise the Specific Absorption Rate (SAR) and the temperature distribution in hyperthermia systems, in terms of optimisation algorithms [20]–[25] and objective functions [26]–[28]. Most strategies employed in HTP result in fixed antenna settings that are applied throughout the treatment session. The quality of treatment depends on the balance between SAR in the target volume and SAR in the healthy tissue. Hence, during HTP the SAR distribution is optimised to maximise SAR in the tumour and minimise the energy in the hotspots.

The study in [26] found that the Hotspot-Target SAR Quotient (HTQ) was the most suitable objective function for SAR optimisation procedures and correlated best with the temperature with respect to other SAR indicators. HTQ is the ratio between the mean SAR in the 1% of healthy tissue volume with the highest SAR values, and the mean SAR in the target. However, the clinical exploitation of hyperthermia is still hampered by technical limitations. Furthermore, patients can still experience discomfort in practical application of hyperthermia. Despite HTP progress in recent years, the need for better control of EM power to minimise unwanted hotspots, as well as accurate predictions for HTP, remain demanding aspects in practical clinical application. Given this need, the main purpose of this thesis is to investigate effective objective functions and optimisation algorithms that can improve the quality of hyperthermia treatment in clinical context.

The overall objective is attained with the investigation of evolutionary optimisation algorithms. Firstly, the Differential Evolution (DE) optimisation algorithm is investigated as part of H&N hyperthermia treatment planning. Its performance is evaluated with different optimisation parameters and compared to a Particle Swarm Optimisation (PSO) algorithm, clinically employed by the Erasmus MC hyperthermia group. Although results show that both algorithms are capable of finding the optimal power deposition, the proposed DE algorithm provides consistent improvements in terms of objective function and SAR indicators.

Then, a Time-Multiplexed Steering (TMS) approach is developed for H&N hyperthermia treatment to effectively suppress hotspots in healthy tissue. The proposed method involves the use of a multi-objective genetic algorithm to find multiple antenna settings which are then combined dynamically in a sequence in thermal simulations. The antenna settings are optimised based on a novel objective function, specifically formulated to suppress a pre-defined hotspot in the healthy region. It is shown that this novel method further intensifies the heating to the tumour region while reducing the hotspot prominence.

Finally, the robustness of time-multiplexed hyperthermia is demonstrated against thermal tissue properties variation. The performance of the algorithms proposed in this thesis is evaluated using real clinical data obtained from patients treated with HYPERcollar and HYPERcollar3D systems, designed and developed at Erasmus Medical Centre (Erasmus MC) Cancer Institute, Rotterdam, the Netherlands, who were collaborators on this project.

1.2 Thesis Contributions

1.2.1 Contributions

This thesis involves the development of techniques for targeting H&N cancer with microwave hyperthermia and the use of those methodologies to improve the quality of hyperthermia treatment planning. The principal contributions in the field of hyperthermia treatment are:

1. An algorithm for HTP based on the differential evolution is proposed. The algorithm is compared to the PSO method clinically employed at the Erasmus MC for the treatment of pelvic and H&N cancers in multiple scenarios on a group of patient treated with HYPERcollar system. The efficacy of the proposed technique is evaluated across a range of SAR and thermal performance metrics.

2. A Multi-Objective Genetic Algorithm (MOGA) is proposed for hotspot suppression. A novel objective function is formulated to focus the EM energy in the target and suppress a pre-defined hotspot. The optimisation method and the novel objective function are applied on a dataset of patients treated by HYPERcollra3D and their performance is assessed using PSO as benchmark algorithm and several SAR metric.

3. A time-multiplexed steering approach is developed for H&N cancer HTP. A detailed procedure is described to implement time-multiplexed hyperthermia which mainly consists of two steps; SAR optimisation by Multi-Objective Genetic Algorithm (MOGA) and thermal simulation. A constant thermal model is used to perform thermal simulations. The proposed method is applied on a number of patients treated by HYPERcollar3D system and the improvement is demonstrated by comparing with the static thermal performance obtained by using the optimal antenna settings generated by PSO.

4. The correlation between EM energy and temperature values is investigated to measure how well the highest simulated SAR values approximate the highest simulated temperatures. The results are analysed to support hotspot identification and selection for the implementation of time-multiplexed steering.

5. The robustness of the time-multiplexed hyperthermia is evaluated against temperature dependent thermal tissue properties. The temperature dependent thermal tissue model is outlined and the performance of the novel method under thermal tissue properties variation is evaluated using thermal quantifiers.

1.2.2 Publications

The publications resulting from this research are as follows:

Journal Publications

- G. Cappiello, B. Mc Ginley, M. A. Elahi, T. Drizdal, M. M. Paulides, M. Glavin, M. O'Halloran, E. Jones, "Differential evolution optimization of the SAR distribution for head and neck Hyperthermia," *IEEE Transactions on Biomedical Engineering*, Vol. 69, Issue 8, August 2016.
- G. Cappiello, T. Drizdal, B. Mc Ginley, M. O'Halloran, M. Glavin, G. C. van Rhoon, E. Jones, M. M. Paulides, "The potential of time-mulitplexed steering in phased array microwave hyperthermia for head and neck cancer treatment," *Physics in Medicine and Biology*, Vol. 63, Issue 13, July 2018.
- G. Cappiello, M. M. Paulides, T. Drizdal, D. O'Loughlin, M. O'Halloran, M. Glavin, G. van Rhoon, E. Jones, "Robustness of time-multiplexed hyperthermia to temperature dependent thermal tissue properties," Submitted to *IEEE Journal of Electromagnetics, RF and Microwaves in Medicine and Biology*, November 2018.

Conference Publications

- G. Cappiello, B. Mc Ginley, M. M. Paulides, M. Glavin, M. O'Halloran, E. Jones, "Therapeutics Application of Electromagnetics: Hyperthermia for the Treatment of Head and Neck Cancer," *Bioengineering in Ireland (BINI)*, Galway, Ireland, January 2016.
- G. Cappiello, M. O'Halloran, M. Galvin, E. Jones, "Treatment of Breast Cancer using a Novel Microwave Hyperthermia System," *4th UL-NUIG Annual Research Day*, Limerick, Ireland, May 2014.

1.3 Thesis Outline

The reminder of this thesis is organised as follows:

Chapter 2 describes the anatomy of the different regions where H&N cancer originate. Microwave hyperthermia treatment is described and the biological and technical aspects are discussed, together with the clinical experiences. Hyperthermia treatment planning is also outlined. The chapter provides background on current objective functions and optimisation techniques used to find the best antenna settings for hyperthermia treatment. The performance metrics used throughout this research are also introduced.

Chapter 3 proposes a differential evolution algorithm to improve H&N HTP by more effectively optimising the amplitudes and phases of Radiofrequency (RF)-signals applied to the antennas. DE aims to optimise the specific SAR distribution, to avoid undesirable hotspots and better focus the heating on the target volume, while protecting healthy tissue. Data for six patients treated by the HYPERcollar applicator, developed at the Erasmus MC, have been used in order to compare the proposed DE algorithm to the PSO technique that is currently in use in clinical practice. The two techniques are evaluated with different optimisation settings, using clinically-relevant metrics including the HTQ, Target Coverage (TC) and HT temperature parameters. Results demonstrate that the proposed algorithm provides an improvement over the current clinically-used PSO at the hyperthermia unit of Erasmus MC, by more frequently and consistently locating the global optimum for all studied patients.

The purpose of Chapter 4 is to investigate the potential of time-multiplexed hyperthermia, i.e. application of multiple SAR patterns in a time-multiplexed way to improve the temperature pattern. A multi-objective genetic algorithm is used to find the time-multiplexed antenna settings, aimed at diversity between the SAR distributions. Two antenna settings derived by MOGA are applied sequentially within the time-multiplexed thermal simulations to evaluate the performance of the proposed method. The time-multiplexed patterns are compared to a single optimal static pattern found by minimising HTQ using the PSO algorithm. Firstly, the SAR assessment is carried out, followed by thermal evaluation.

Chapter 5 establishes the robustness of time-multiplexed hyperthermia to thermal tissue properties variation. Time-multiplexed performance using constant thermal model parameters and thermal-dependent perfusion model are compared for five patients. The results show that varying the blood perfusion value for fat, muscle and tumour tissue has no significant impact on focusing the tumour heating and suppressing the hotspot when time-multiplexed steering is applied; furthermore an increase in temperature is observed in the target region when the static solution is obtained with the temperature dependent perfusion model.

The final chapter summaries the main contributions presented throughout this thesis and conclusions are discussed. Some suggestions for future work are also provided.

2

Background and Literature Review

2.1 Introduction

In this chapter an overview of different aspects of H&N cancer is given. The biological aspects of microwave hyperthermia are discussed together with the technology required to apply different types of hyperthermia. A description of clinical experiences follows. The procedure of the hyperthermia treatment planning at the Erasmus MC is described and relevant optimisation strategies and objective functions present in literature are reviewed. Finally, the metrics used to evaluate the performance of the optimisation algorithms and, more generally, to quantify the quality of hyperthermia treatment are outlined.

2.2 Head and Neck Cancer

Head and neck cancers originate in different regions and by definition exclude tumours that occurs in the eyes, in the brain and in the skin. H&N cancers generally begin in the squamous cells that delineate the mucosal surfaces inside the head and neck. These squamous cell cancers are usually named squamous cell carcinomas of the head and neck. Often H&N cancer occurs in the oral cavity and the larynx, while cancers in the salivary glands are relatively uncommon. H&N cancers are categorized as illustrated in Figure 2.1:

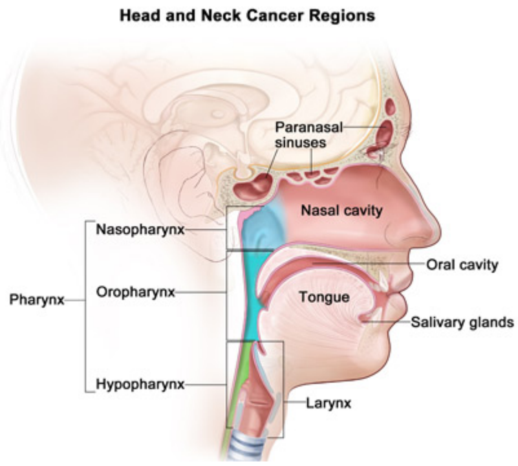

Figure 2.1: Head and neck cancer regions. Image from www.cancer.gov. (For the National Cancer Institute © 2012 Terese Winslow LLC, U.S. Govt. has certain rights)

1. Oral cavity: comprises the front two-thirds of the tongue, the lining inside the cheeks and lips, the gums, the lips, the bottom of the mouth under the tongue, the area of the gum behind the wisdom teeth and the hard palate;

2. Pharynx: the pharynx is a tube that starts behind the nose and leads to the esophagus. It includes nasopharynx, the upper part of the pharynx, behind the nose; the hypopharynx, the lower part of the pharynx, and the oropharynx, the middle part of the pharynx that includes the soft palate, the base of the tongue, and the tonsils;

3. Paranasal sinuses and nasal cavity: the paranasal sinuses are small hollow spaces in the bones of the head which surrounds the nose. The nasal cavity is the hollow space inside the nose.

4. Larynx: short hallway formed by cartilage below the pharynx in the neck. It contains the vocal cords and the epiglottis which is used to prevent food from getting into the air passages.

5. Salivary glands: located near the jawbone and the floor of the mouth.

In the H&N region, treatment of advanced tumours and the control of tumours in localised areas, i.e loco-regional control, are complex aspects [4], [29]. When treated with conventional therapies, surviving patients suffer significant side effects, such as impaired speech, hearing loss, difficulty in chewing, swallowing and breathing. Chemotherapy and radiotherapy are associated with high levels of toxicity and often fail for locally advanced or recurrent tumors. Recent research has focused on alternative or adjunct therapies, where the burden of treatment is less severe on patients. Hyperthermia has demonstrated a substantial benefit when administered in combination with radio- and chemotherapy, improving the control of the tumor locally without increasing toxicity [11].

2.3 Hyperthermia

2.3.1 Definition

Hyperthermia is a therapeutic treatment that involves increasing the temperature of the body or a specific region of it to supraphysiologic levels between 40 °C and 44 °C. It is administered as a multimodal oncological strategy; clinical studies have demonstrated hyperthermia to be a powerful therapy for the treatment of the cancer when implemented in combination with radio- and chemotherapy [11]. Hyperthermia increases the concentration of oxygen in the tumor region enhancing the effectiveness of radiotherapy, and increases the blood flow leading to an increase in perfusion which improves the drug absorption in cells for chemotherapy.

2.3.2 Thermal Biology of Hyperthermia

While much research has been conducted, and hyperthermia has successfully been used in clinical application, the biological rationale for the use of hyperthermia is not completely established. According to Kampinga *et al.* [30], the principal target of hyperthermia is proteins, but little knowledge is available about the mechanisms of cell killing. Heat-induced protein denaturation occurs randomly throughout the cell. It damages the Deoxyribonucleic acid (DNA) repair systems and leads to alterations in molecular structures and changes in enzyme complexes for DNA synthesis; nuclear proteins seem to be most sensitive and aggregation occurs in the nuclear environment, with a high heat sensitivity observed in various nuclear processes.

The amount of cell death after heat shock is dependent on cell type and heat dose. Some cells may die quickly due to apoptosis if the initiation and execution phases are not inactivated by high heat dose. If the heat damage is too significant, apoptosis defective cells will not proliferate, and they may lose their proliferative capacity via permanent cell cycle arrest, by necrosis or secondary apoptosis after S-phase or mitotic failure [30].

Elevation of temperatures transiently stimulates the production of a family of proteins, called Heat Shock Proteins (HSPs) which are produced by cells under exposure to stressful conditions, such as heating. An autoregulatory loop is responsible for the heat shock response. HSPs levels increase after heating and decrease after prolonged stress free periods. This regulation of HSPs is associated with a resistant phase of cells towards a subsequent second heat shock. The resistance phase is called thermotolerance. The higher the initial temperature, the larger the effect of thermotolerance induced in surviving cells. Thermotolerance decreases towards baseline thermosensitivity after a few days [30]. However, the inhibition of DNA repair can happen at temperatures of 40 °C which is a temperature where thermotolerance is not induced during or after heating [31]. This has been subject of discussion for combining hyperthermia with radiotherapy sessions.

Other biological effects occur over the temperature range used in clinical practice, such as changes in perfusion, re-oxygenation, induction of heat shock response and immunological simulation. During hyperthermia, the tissue metabolism increases the blood flow to counteract the temperature rise. When healthy tissue is heated, the blood vessels can enlarge to facilitate an increased blood flow which produces a temperature reduction. In contrast to healthy tissue, tumour tissues present a chaotic vascular structure with regions of low pH, hypoxia and lack of perfusion. In these circumstances, the capacity of tumour blood flow to increase upon heating is limited compared to the normal tissue blood flow; therefore, the heat dissipation is slower and the temperature of the tumour tends to rise higher than normal tissue during heating. The temperature in the healthy tissue does not increase as much and the perfusion and oxygenation enhancement in the tumour regions potentiate drug

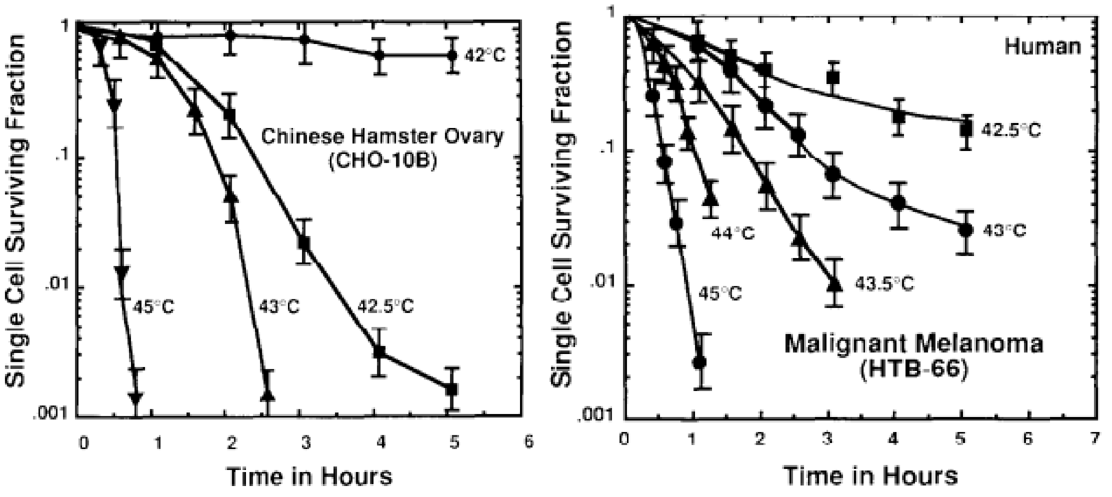

(a) (b)

Figure 2.2: (a) Survival rate of Chinese hamster ovary cells (CHO-10B cell) (b) Survival rate of human melanoma cells (HTB-66) heated over time. Measurements were made *invitro*. (Reprinted from [33], Copyright 1991, with permission from Elsevier)

and molecular uptake and radio-sensitivity [32]. As temperature increases further, the tumour cells die, or the tumour may reduce in size, facilitating surgical removal.

All these aspects can be considered to improve tumour response to radio- and chemotherapy, though the effect of hyperthermia on tumour environment related to the clinical temperature range, is still a matter of research. The rate of cell death during hyperthermia is dependent on the time and temperature of exposure. Experimental studies *in vitro* were described in [33], which used human and rodent cells propagated under the same growth conditions. The cells were contained in flask which were immersed into racks, in precision temperature-controlled water baths regulated to ± 0.05°C. Irradiation was performed with an x-ray machine operating at 300 kVp. The time-temperature relationship to the rate of cell death found in [33] is shown in Figure 2.2.

Three clear aspects of cell behavior under heating have been exploited for the thermal therapy. First of all, the rate of cell survival depends on the temperature exposure. Figure 2.2a shows a high rate of death of CHO-10B cells when heated at 42.5 °C compared to heating to 42 °C for 5 hours. Secondly, after a certain period of heating, each cell type develops a thermal resistance which is indicated

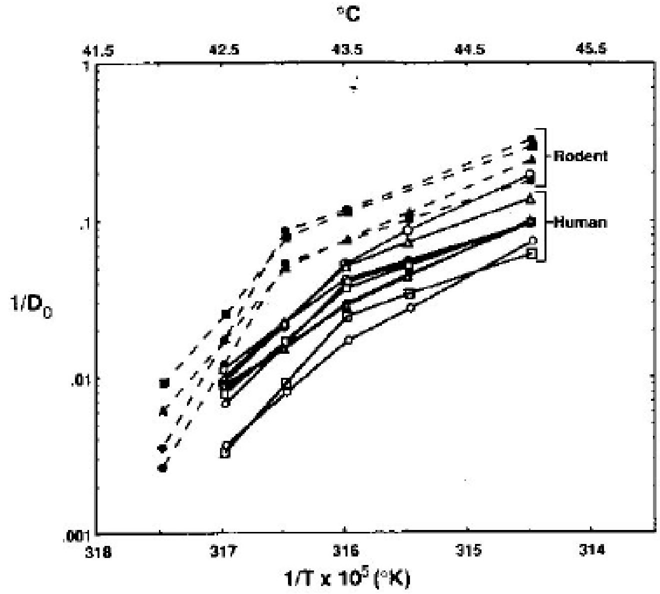

Figure 2.3: Arrhenius plots for a number of human and rodent cell lines. (Reprinted from [33], Copyright 1991, with permission from Elsevier)

by the change of slope of the curves. For example, the HTB-66 cell shows the reduction in the slope after 3 hours of heating at 42.5 °C and 43 °C, while the CHO-10B shows thermal resistance at 42.5 °C after 4 hours of heating. Ultimately, the thermo-sensitivity varies between cell type. The CHO-10B cell exhibits a lower surviving fraction (0.001) for 5 hours of heating at 42.5 °C compared to the HTB-66 cell (0.03). Hence, CHO-10B cell is more sensitive to heat than HTB-66.

A typical break temperature of 43 °C has been chosen for several cell types [34]; this is the temperature at which thermal damage, i.e cell death due to heat, starts to occur. HSPs and apoptosis may occur before the temperature of 43°C. The thermal enhancement of the treatment depends on the temperature rise in the tumour and the duration of the heating, and treatment may have a duration up to 90 minutes depending on patient tolerance. The break temperature is cell dependent and is estimated by plotting the rate of cell killing against 1/temperature (K). The rate of cell death is defined as $1/D_o$, where D_o is the period required to reduce survival by 63%. The Arrhenius plots used to calculate the break temperature related to rodent and human cells are illustrated in Figure 2.3. The break temperature occurs at the change in the slope of the Arrhenius plot.

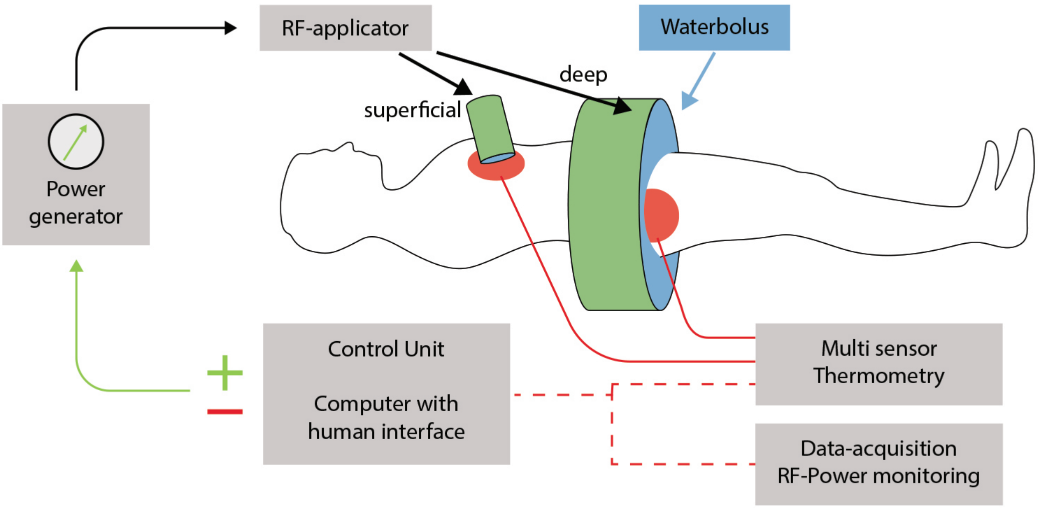

Figure 2.4: Schematic view of any hyperthermia system.

2.4 Hyperthermia Treatments and Systems

Depending on the target volume, hyperthermia can be classified as local, regional or whole-body hyperthermia [35]. Heating can be delivered using EM energy, mostly in the RF or microwave range. EM applicators can be categorized into two types: interstitial and external. Interstitial heating requires the insertion of tiny antennas into the tumour. During external heating the tumour can be heated by a conformal multi-element antenna phase array or applicators, emitting microwaves or radiowaves, to transfer the EM energy into the tissue. A Water Bolus (WB) is used to fill the space between the applicator and the patient to ensure good EM coupling and to limit hotspots at the skin. A 3D temperature distribution can be obtained by a temperature measurement system. The entire system usually has a computer-controlled feedback loop in combination with a graphical user interface for operator control. The general configuration of a microwave hyperthermia system is given in Figure 2.4.

2.4.1 Local Hyperthermia

Superficial tumours, such as lymph-node metastases of H&N tumours, chest wall recurrence, breast cancer or cutaneous metastases can be heated by waveguide

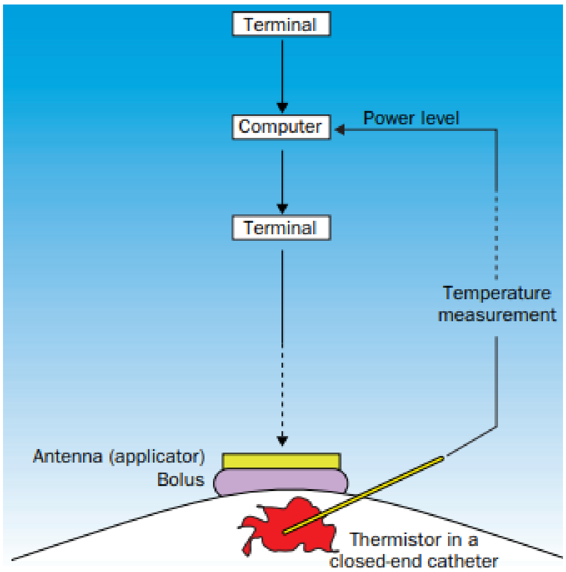

Figure 2.5: Scheme of a local hyperthermia system. (Reprinted from the Lancet, [36], Copyright 2002, with permission from Elsevier)

antennas or horn, spiral, compact applicators [36]. The applicators have a typical frequency of 150-430 MHz with therapeutic depths not more than 3 cm [36]. Figure 2.5 shows the components of such a hyperthermia system. The water bolus ensures the EM coupling of the applicator to the tissue. For the treatment of deep seated tumours, multisensory probes are placed interstitially into the tumour by inserting catheters. In the case of superficial tumours, the probes are placed on the surface of the tumour region under the water bolus. The temperature can be controlled by positioning the applicator or by controlling the output of the power generator.

The type of the applicator determines how the energy is distributed in the treated area. One of the most widely-used applicators is the waveguide applicator which is made from a section of waveguide transmission line, open at one end. A short extension of loop antenna or coaxial feed line provides the excitation. These types of applicator are usually filled with distilled water [37]. The horn applicators produce a more uniform temperature field than classical waveguides and utilise a flared opening to spread the radiated field. Another type of applicator is the microstrip antenna applicator, consisting of a resonant metallic arrangement on a continuous metallic

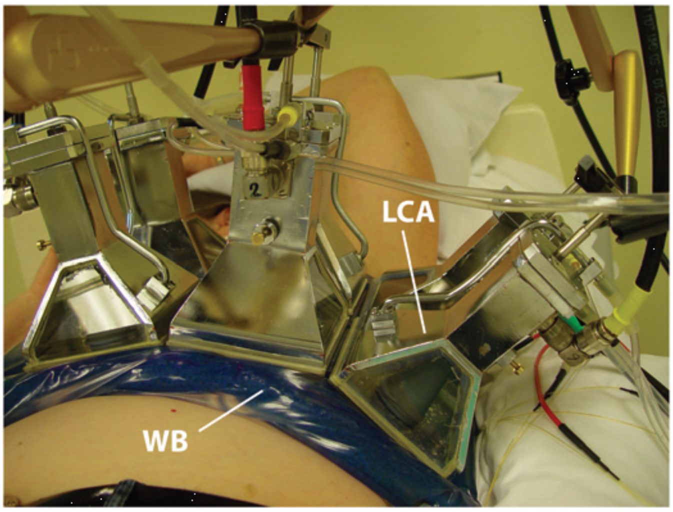

Figure 2.6: A 2x3 Lucite Cone Applicator (LCA) array and Water Bolus (WB). (Reprinted from [40], www.tandfonline.com)

plane [37]. The area of the heating patterns in local hyperthermia treatments can be shaped and enlarged by adding the antenna elements of the specific applicator.

An example of waveguide applicator is the Lucite Cone Applicator (LCA) illustrated in Figure 2.6. The LCA has been designed and clinically used at Erasmus MC to treat breast carcinoma, melanoma, mesothelioma, and lymph node metastasis of H&N squamous cell carcinoma by superficial hyperthermia, using a 433 MHz signal. The LCA antennas are fed by power amplifiers with non-coherent sources [38], [39]. The antenna array configuration is determined by the size of the hyperthermia volume (depth of up 4 cm) and the shape of the anatomy, which encompasses the re-irradiation field. Several water boli, to couple the electromagnetic waves into the patient and to cool the skin, are available according to the different LCA array configurations.

2.4.2 Interstitial and Intracavitary Hyperthermia

Rectal, prostate, vaginal, cervical or oesophageal cancers can be treated by intracavitary hyperthermia, while prostate, breast cancer, some head and neck tumours can be treated by interstitial hyperthermia. For interstitial treatments, the antennas are placed within the tumour; for intracavitary hyperthermia the antennas are inserted in natural openings such as rectum or, urethra in proximity to the tumour. These types of treatments are applicable for tumours less than 3 cm in diameter and the treatment is done in combination with brachytherapy. Interstitial techniques are also used for another cancer therapy, thermoablation, which involves invasive applicators and radiofrequency. During thermoablation, the temperature in the tumour is raised over 50 °C, causing cellular coagulation and tissue necrosis. Small focal tumour located within liver, kidney, lung or bones can be treated by thermal ablation [41].

2.4.3 Regional Hyperthermia

Regional hyperthermia can be applied to large parts of the body such as the limbs, the abdominal cavity, liver, stomach, bladder, prostate, or ovaries. Arrays of antennas can be used to treat deep-seated tumours. The goal is to focus the heating to the tumour while keeping the energy deposition in the surrounding healthy tissue under control. Multi-antenna phased array systems are normally used in such systems [17], [18], [42]–[45]. The principle of the phased array is to generate a desired electric field distribution by combining the fields of all the individual antennas. For this reason, these systems are designed in such a way that the antennas produce collinear polarizations and the total electric field can be calculated as the sum of the EM signals generated by each antenna. Focusing into the target area can be obtained by constructive interference of the EM fields that are radiated by the system. The EM wave interference can be controlled by selecting the appropriate antenna amplitude and phase settings of each RF-signal [46]. The block scheme of a regional hyperthermia system is represented in Figure 2.7.

The typical frequency used with regional hyperthermia ranges from 70 to 200 MHz for pelvic region [17], [42]–[44], and 434 MHz for H&N region [18], [45]. Examples of regional hyperthermia systems are the BSD 2000 systems (Pyrexar Medical, Salt Lake City, USA)[1] and the HYPERcollar systems shown in Figure 2.8 and 2.9. The BSD 2000 system is used at Erasmus MC for the treatment of cancer in the pelvic regions. There are two kinds of applicators: BSD Sigma 60 applicator, a cylinder-shaped applicator consisting of a ring of 8 dipole antennas that are

---

[1] http://pyrexar.com/hyperthermia/bsd-2000

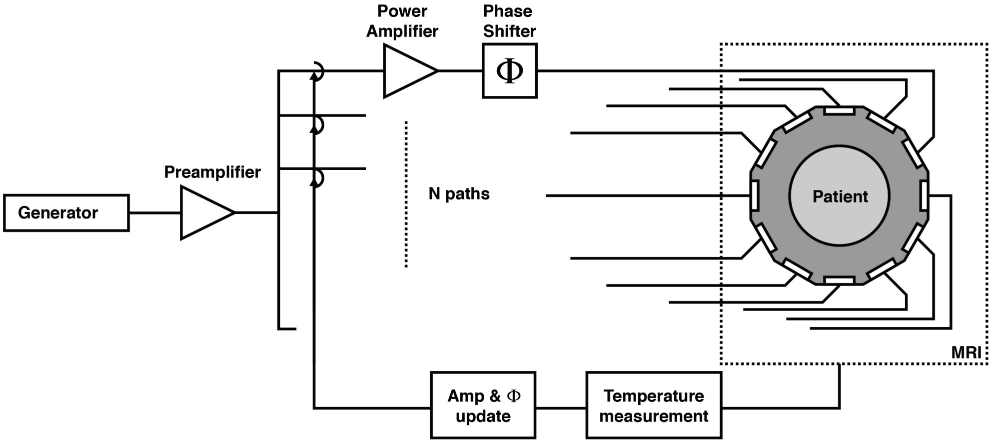

Figure 2.7: Block diagram of deep hyperthermia [37].

coupled in 4 channels of two antennas each, with an operating frequency of 77 MHz; and BSD Sigma Eye, an elliptical-shaped applicator with 24 dipole elements and 12 channels, which works at 100 MHz.

Over the last decade, two phased array applicators have been developed at the Erasmus MC for the treatment of H&N cancer. The first generation of H&N applicator is the HYPERcollar system (Figure 2.8), developed to treat regions such as thyroid, oropharynx and nasal cavity [18], [45], [47], [48]. The applicator consists of a ring-shaped phased array of twelve patch antennas, equally divided over two rings, operating at a frequency of 434 MHz. The water bolus is used to fill the space between the ring and the patient with water, whose shape is influenced by positioning and gravity. Recently a re-designed version of the HYPERcollar system, HYPERcollar3D [45], [49] (Figure 2.9), has been developed and introduced in current clinical practice, with improved antenna arrangement, twenty patch antennas over three rings, and a better configuration of the water bolus, i.e. flat margins corresponding to the antenna ring boundaries, rather than a water bolus bulging out at the antenna ring boundaries.

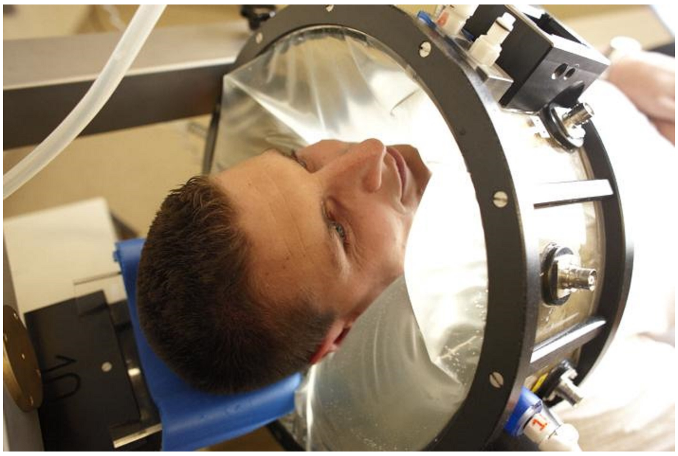

Figure 2.8: HYPERcollar system. (Taken after [50]; copyright EurAAP; used with permission)

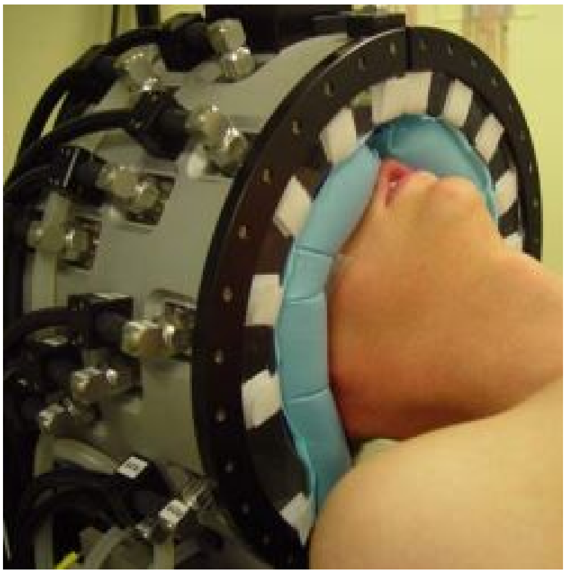

Figure 2.9: HYPERcollar3D system. (Taken after [50]; copyright EurAAP; used with permission)

2.4.4 Whole-body Hyperthermia

Carcinomas with distant metastases, i.e. cancer that has expanded from the primary tumour to distant lymph nodes or organs, can be treated by whole-body hyperthermia. Example of cancer suitable for this type of treatment are soft tissue sarcomas, melanomas or leukaemia. Various methods such as extracorporeal induction, electromagnetic induction and thermal conduction can be used to induce whole-body heating. Two systems are clinically used by employing microwave and infrared radiation with a heating time equal to 60-90 minutes [36].

2.4.5 Clinical Treatment Procedure

By way of example, this section outlines the typical procedure used in a clinical seting in Erasmus MC to treat different types of cancer. The number of hyperthermia treatment sessions depends on the patient's clinical conditions. At Erasmus MC, superficial breast hyperthermia to treat areas close to the surface is typically applied for 60 minutes, once a week, for a period of several weeks. There is an initial heat-up phase, during which the power level applied is gradually increased in order to heat the target volume up to the therapeutic temperature of 44°C, or until the patient indicates discomfort. The power steering actions are based on the interpretation of measured temperatures and patient feedback by the clinician.

The duration of H&N hyperthermia treatment is usually 90 minutes per session and the number of hyperthermia sessions varies depending on the specifics of the patients. The treatment procedure consists of different phases. The patient is positioned on a bed and the tumour is placed centrally within the applicator, adjusting the height of head and shoulders according to the positions fixed during the treatment planning phase. The water bolus is filled with demineralized water at a temperature of 20-30°C. Firstly, a power level of 200 W is applied, using the optimised phase and amplitudes settings from the HTP phase and is subsequently increased in steps of 30 W every 30 seconds [51]. The patient is asked to indicate if they feel any discomfort. If the patient feels burning sensations or pressure, the power is reduced. In this case, a SAR based re-optimisation is applied setting new phase and amplitude and aiming to reduce power limiting hotspots. After 15 minutes of treatment, defined as the start of the plateau phase, RF power increase is in steps of 15 W [51].

2.5 Clinical Trials of Hyperthermia

Clinical trials have demonstrated the benefits of using hyperthermia combined with chemotherapy and/or radiotherapy in the treatment of solid tumours, such as breast [14], carcinoma of the head and neck [12], [52], pelvic tumours [13], brain [53] and superficial tumours [54], [55]. Head and neck cancers are treated with surgery, radiotherapy, chemotherapy or a combination of these.

The three meta-analyses study conducted by Pignon *et al.* [29] showed that the combination of chemotherapy and radiotherapy results in an 8% increase of the overall 2-years survival rate and a more recent study [56], involving 87 trials, demonstrated a 4.5% benefit at 5 years. However, improvement is needed since 80% of patients experience severe toxicity associated with conventional therapies.

Four prospective randomised phase III trials prove the effectiveness of hyperthermia in H&N cancers. Table 2.1 summarises the results for these studies. In the study carried out by Valdagni *et al.* [12], [52] metastatic lymph nodes from H&N were randomised to receive radiotherapy or radiotherapy combined with hyperthermia and improvement in the complete response (i.e. complete regression or no evidence of tumour) rate of 45.5% was observed with the combined treatment versus radiotherapy alone.

The randomised study of [57] included sixty-five patients to test the efficacy of local hyperthermia together with radiotherapy and showed improvement in terms of better control after combined treatment in patients with advanced disease.

In [58] fifty six patients with cancers of the hypopharynx, oral cavity and oropharynx showed a complete response of 42.4% with radiotherapy alone compared to 78.6% in the hyperthermia group.

The study of [59] included 180 patients with nasopharyngeal cancer randomised to receive chemoradiotherapy with or without hyperthermia. The study showed significant improvement in complete response when applying chemoradiotherapy together with hyperthermia; also, five years local control and progression free survival were significant but overall survival was not significant.

The study by Zhao *et al.* [60] showed improvements in terms of survival rate and quality of life domains (swallowing, speech, dry mouth, social eating) for 83 patients with nasopharyngeal cancer when receiving chemoradiotherapy with hyperthermia. These clinical trials provide evidence that hyperthermia improves the effect of chemo- and radiotherapy in head and neck cancer treatments.

Table 2.1: Results of randomised phase III trials on Hyperthermia (HT) for H&N. RT: radiotherapy, CRT: chemo-radiotherapy, N: total number of included patient in the study, -HT: results without HT, +HT: results with HT, LC: local control, CR: complete response, PFS: progression free survival, OC: oral cavity, OP: oropharynx, HP: hypopharynx, NP: nasopharynx, QoL: quality of life. Results significant at the 5%-level are shown in bold. (After [61])

Reference	Tumour	Combi	N	Endpoint(s)	-HT	+HT
Valdagni et al. 1988 & 1994	Neck Nodes	RT	44	CR	41%	**83%**
				5 years LC	24%	**69%**
				5 years OS	0%	**50%**
Datta et al. 1990	OC, OP	RT	65	CR	31%	55%
Huilgol et al. 2010	OC, OP, HP	RT	54	CR	42%	**79%**
Hua et al. 2011	NP	CRT	180	5 years LC	79%	**91%**
				5 years PFS	63%	**73%**
				5 years OS	70%	78%
Zhao et al. 2014	NP	CRT	83	3 years OS (QoL)	54%	**73%**

2.6 Hyperthermia Treatment Planning

A hyperthermia treatment planning procedure is run for each patient before HT treatment. Appropriate amplitude and phase settings for individual antennas are used to calculate SAR and simulate the temperature distribution. The resulting temperature distribution in the tissue is monitored during HTP and modified as needed. Hence, the major benefit of HTP is to assess the SAR distribution and the temperature prior to the treatment and to guide optimisation during the treatment itself. Different focusing strategies have been studied to optimise the SAR and the temperature distribution in hyperthermia systems, and several optimisation algorithms and objective functions will be discussed in this sections. The general procedure for HTP can be divided into four steps [62]:

1. Generation of the patient model;

2. Modelling of treatment set up;

3. Calculation of the power deposition in the tissue;

4. Calculation of the temperature distribution.

The HTP procedure at Erasmus MC can be described as follows. The HTP process starts by acquiring radiotherapy-planning Computerised Tomography (CT) scan, with the patient in the same position as planned for the hyperthermia treatment. The 3D patient specific model is created using an automatic segmentation routine [63] followed by small manual correction using the iSeg software tool (Zurich Medtech, Zurich, Switzerland). The 3D patient model is afterwards combined with the applicator model in SEMCAD X (version 14.8.6 SPEAG, Zurich, Switzerland), which is an electromagnetic computation software package based on the Finite Difference-Time Domain (FDTD) method. Following this process, a 1-V sinusoidal signal with frequency 434 MHz with zero phase delay between all antennas is applied to each antenna in turn, and the resulting EM field distribution and CT scan are imported into the Visualisation Tool for Electromagnetic Dosimetry and Optimisation (VEDO) developed at Erasmus MC [51], [62] (Figure 2.10). The data stored in VEDO include EM field distributions generated from each individual antenna, density and electrical conductivity of each voxel, antenna locations, target regions and the patient's tissue profile.

VEDO is based on the particle swarm optimisation algorithm, followed by a line search method, and is used to adjust the combination of amplitudes and phases of the individual antennas to achieve the optimal SAR distribution. The SAR ($W \cdot Kg^{-1}$) is expressed as:

$$SAR = \frac{(\sigma_{eff}\,(r))\,|E\,(r)|^2}{2\rho\,(r)} \tag{2.1}$$

where σ_{eff} ($S \cdot m^{-1}$) is the effective conductivity, ρ ($Kg \cdot m^{-3}$) is the mass density, E ($V \cdot m^{-1}$) the combined electric field, calculated as the sum of the fields generated by each antenna of the system, E_j ($V \cdot m^{-1}$), where j is antenna index and r refers to the axis directions (x, y, z) of the EM propagation. The total electric field E is expressed as:

$$E\,(r,t) = \sum_{j=1}^{N} a_j e^{-i\theta_j} E_j\,(r,t) \tag{2.2}$$

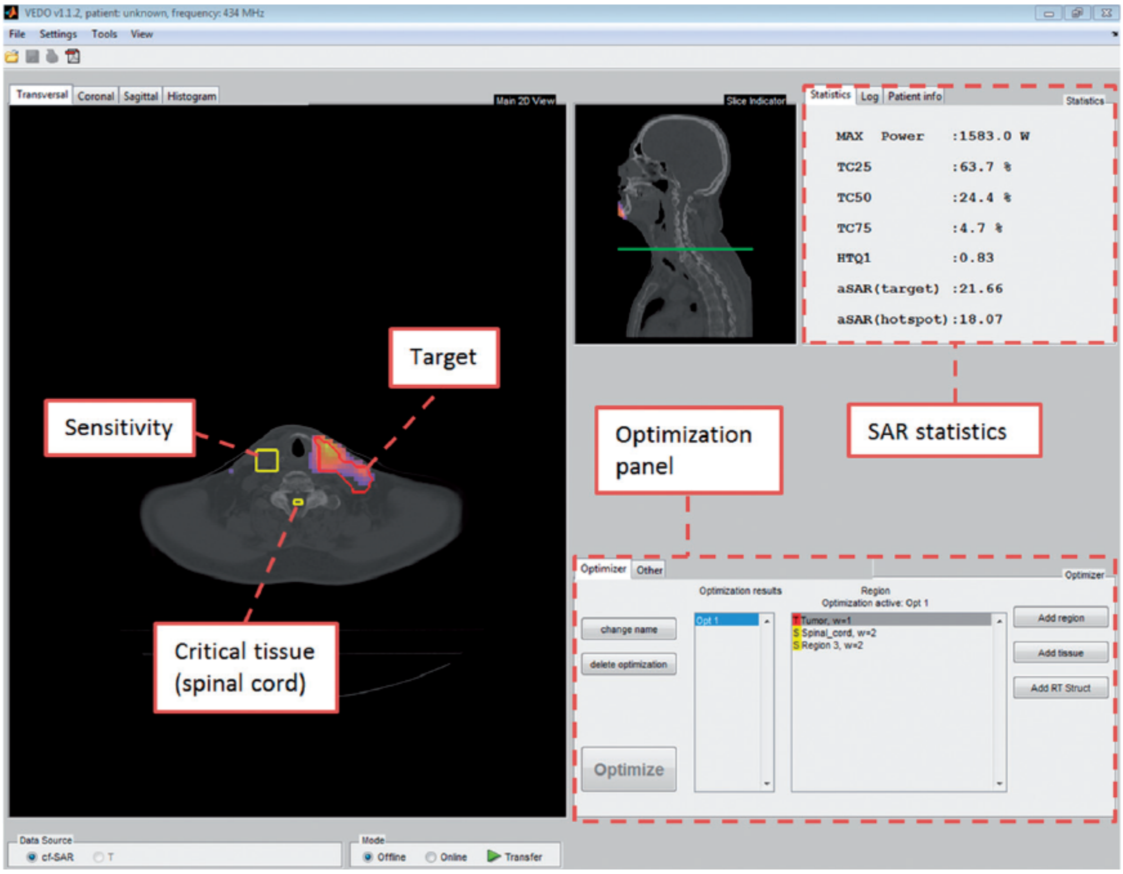

```
MAX  Power      :1583.0 W
TC25            :63.7 %
TC50            :24.4 %
TC75            :4.7 %
HTQ1            :0.83
aSAR(target)    :21.66
aSAR(hotspot):18.07
```

Figure 2.10: Graphical user interface of the Visualisation Tool for Electromagnetic Dosimetry and Optimisation (VEDO). (Reprinted from [51], www.tandfonline.com.)

where antenna j has amplitude a_j and phase delay θ_j, and N is the number of antennas. The technique aims to optimise a_j and θ_j of the EM field phasor applied to each antenna. The phasors are summed by equation 2.2 and the resultant SAR is calculated by equation 2.1. The objective (or fitness) function, the hotspot-target quotient (HTQ), is the quotient of the hotspot SAR and the average tumour SAR:

$$HTQ = \frac{SAR_a\,(V1)}{SAR_a\,(target)} \tag{2.3}$$

The hotspot SAR, referred to as $SAR_a\,(V1)$, is defined as the average SAR in the volume represented by $V1$, which is defined as the top 1 % of healthy tissue volume with the highest SAR in the total patient model. $SAR_a\,(target)$ is defined as the mean SAR in the target itself [51], [64]. Therefore, the optimisation of the fitness function aims to maximise the EM energy in the target area, while reducing the hotspots in the healthy tissue.

2.6.1 Objective Functions in Hyperthermia

Several HT studies have been carried out to synthesize the pattern of power deposition and to achieve the desired SAR and temperature distributions in the target body. Several quality indicator metrics and objective functions have been used for HTP optimisation [26], [65]. This section provides an overview of the relevant studies.

Different objective functions for both power and temperature optimisation have been considered by Wust *et al.* [66]. Their study concerns the optimisation of deep (pelvic region) electromagnetic heating based on 3D patient-specific geometry, showing the possibilities to improve the treatment by increasing the number and orientation of the hyperthermia system antennas. Related works on EM heating of the pelvis have been conducted in [67] where a single objective function has been used to minimise hotspots in healthy tissue, focusing the EM energy on the tumour position.

A further study [27] examined a variety of objective functions using a generalised mathematical formulation. Temperature-based optimisation has been applied in [28] in combination with HTP to improve treatment outcome in patients with esophageal cancer.

Canters *et al.* [26] carried out a survey of several quality indicators for SAR, followed by an evaluation based on heuristic criteria and proposed modifications of existing indicators or proposed new indicators. The correlation of the SAR indicators with the corresponding predicted temperature was evaluated and each SAR indicator was used as the target function for SAR optimisation. The quality of treatment depends on the balance between SAR in the target volume and SAR in the healthy tissue. Hence, during HTP the SAR distribution is optimised to maximise SAR in the tumour and minimise the energy in the hotspots. Many indicators have been proposed over the years and a set of criteria have been developed to allow evaluation to determine the most appropriate indicators. The criteria should enable comparison between sessions, patients, systems and institutes. The definition of the set of heuristics is described as follows:

1. Characterisation of SAR distributions: SAR_{max} independence. Inaccuracies in tissue segmentation can lead to SAR peaks that do not represent the real situation. To overcome this problem, volume-average SAR is preferred to SAR_{max} which may be affected by local details of the model.

2. Characterisation of SAR distributions: target-related criteria. Three criteria are associated with the target. The first one is the deposition of SAR in the target in absolute values (W/Kg), the second one is the quantification of SAR in the target in relation to the whole body average SAR and the third one is the homogeneity of the target, i.e. SAR or temperature homogeneity. The latter requires knowledge of perfusion in the target.

3. Characterisation of SAR distributions: hotspot-related criteria. Quantification of the absolute SAR level in hotspots, and relative to the target.

4. Optimisation criteria for SAR objective functions. Optimisation of a specific objective function which restricts hotspot SAR and maximises SAR in the target area.

To evaluate the suitability of the quality indicators, the correlation of the median temperature in the target, T_{50}, with each indicator has been investigated. The higher the correlation is, the higher the temperature is in the target. To assess the predictive value of the quality indicators, electromagnetic and temperature distributions for 36 patient models with cervical cancer were calculated using 30 different amplitude and phase settings each when heated with the BSD 2000 Sigma 60 applicator [26]. Each indicator has been used as objective function for SAR optimisation. Table 2.2 reports the quality indicators found in [26] described as follows:

1. P_{targ}: the power absorbed in the target [27].

2. P_{ratio1}: ratio between target power and total power absorbed in the patient [66], [68], [69].

Table 2.2: Quality criteria from literature. (After [26])

Indicator	Formula	Unit
1	P_{targ}	W
2	$P_{ratio1} = \frac{P_{targ}}{P_{tot}}$	-
3	$P_{ratio2} = \frac{P_{targ}}{\sum_{i=1}^{10} SAR_{max,i}}$	kg
4	$P_{ratio3} = \frac{P_{targ}}{\left[\int_{V_{targ}} SAR^2 dV\right]^{\frac{1}{2}}}$	$kg \cdot m^{-1.5}$
5	$P_{ratio4} = \frac{P_{targ}}{\left[\int_{V_{targ}} \left(\frac{SAR}{w_b}\right)^2 dV\right]^{\frac{1}{2}}}$	$kg \cdot m^{-4.5} \cdot s^{-1}$
6	$P_{ratio5} = \frac{P_{targ}}{\sum_{i=1}^{10} \left(\frac{SAR}{w_b}\right)_{max,i}}$	$m_3 \cdot s^{-1}$
7	$P_{square-ratio} = \frac{P_{targ}^2}{P_{tot}}$	W
8	$STH_{ratio} = \frac{SAR_{targ}^2}{SAR_{hotspot}}$	W/kg
9	SAR_{targ}	W/kg
10	$SAR_{ratio} = \frac{SAR_{targ}}{SAR_{tot}}$	-
11	$10gSAR_{max}$	W/kg
12	$10gSAR_{maxratio} = \frac{10gSAR_{max}}{SAR_{tot}}$	-
13	$x\%SAR_{max}coverage = \frac{V_{x\%SARmax}}{V_{targ}}$	-
14	$HC = \frac{V_{75\%SARtargmax}}{V_{25\%SARtargmax}}$	-
15	$SAR_{10max} = \sum_{i=1}^{10} SAR_{max,i}$	W/kg
16	$SAR_{hs-targetratio} = \frac{SAR1_{region}}{SAR50_{target}}$	-

3. P_{ratio2}: target power divided by the sum of the SARs at the 10 SAR peak locations [68].

4. P_{ratio3}: ratio of target power and to the volume integral over the squared SAR perfusion quotient in healthy tissue, which minimises high SAR peaks [68].

5. P_{ratio4}: target power divided by the volume integral over the squared SAR in

healthy tissue. SAR perfusion quotient is used to account for bias between SAR and temperature [68].

6. P_{ratio5}: target power divided by the sum of the 10 maximum SAR perfusion quotients [68].
7. $P_{square-ratio}$: ratio of the squared target power and the total power in healthy tissue [69].
8. STH_{ratio}: squared volume averaged SAR in the target divided by SAR in the hotspot [69].
9. SAR_{target}: target volume averaged SAR, used as objective function in [67]. In Sandrini *et al.* [70], this indicator is generally defined as the ratio of the power absorbed in a region and to the region volume.
10. SAR_{ratio}: averaged SAR in the target divided by the average SAR in the patient. Generally defined as the average SAR in a region divided by the average SAR in the patient [71].
11. $10gSAR_{max}$: maximum average SAR over 1 or 10g of tissue, defined in IEEE-1529 [72].
12. $10gSAR_{maxratio}$: ratio of maximum average SAR in 1 or 10g to average SAR in the patient, as described in Bernardi *et al.* [73].
13. $x\%SAR_{max}coverage$: part of the volume enclosed by x% SAR_{max}. Used to evaluate the quality of the treatment [18], [74], [75]
14. HC: homogeneity coefficient defined by the volume enclosed by the $75\%SAR_{targmax}$ isoSAR divided by the volume enclosed by $25\%SAR_{targmax}$ [76].
15. SAR_{10max}: sum of the 10 highest SAR spots [69].
16. $SAR_{hs-targetratio}$: ratio of the SAR exceeded in 1% of a region's volume and the median target SAR [76].

Canters *et al.* [26] evaluated the indicators based on the heuristic criteria. They found that SAR_{targ} (9) and SAR_{ratio} (10) were the most appropriate indicators for target-related characterisation of SAR distributions, while modifications of $x\%SAR_{max}coverage$ (13) and HC (14) were needed to remove dependency on the maximum SAR. For hotspot-related characterisation of SAR distributions, $SAR_{hs-targetratio}$ (16) was considered a good indicator that related SAR in the target to the hotspot SAR. The hotspot prediction from a SAR indicator is difficult because of several factors such as the perfusion, the thermodynamics of the surrounding healthy tissue and the exposed volume. However, if the energy is low, it will not cause overheating in well perfused healthy tissue. Most of the indicators were suitable for objective function optimisation; however some of them as P_{ratio2} (3), P_{ratio5} (6) and STH_{ratio} (8) depend on SAR_{max}. An indicator that related SAR in the hotspot and SAR in the target was $SAR_{hs-targetratio}$ (16), which was also found to be independent of maximum SAR in the patient. The literature survey led to the conclusion that most indicators met the criteria for target characterisation, considering the disadvantage of SAR_{max} dependency; some new indicators were also proposed for hotspot characterisation.

Table 2.3 reports the additional indicators and objective functions suggested by [26], numbered according to the criterion in Table 2.2 on which they are based.

13-m. $SAR5_{tot}coverage$: this indicator was introduced to remove the dependency on SAR_{max} of $x\%SAR_{max}coverage$. The modified indicator is defined as the part of the target where the SAR exceeds $SAR5_{tot}$, which is the SAR exceeded in 5% of the total volume.

14-m. HC_{new}: a modified homogeneity coefficient that provides the same information as HC defined above but is less sensitive to the maximum SAR in the target.

16-m. $SAR_{hs-targ-rationew}$: this indicator is similar to $SAR_{hs-targetratio}$, the ratio between hotspot SAR and target SAR, with the only difference of using averages instead of medians.

Table 2.3: Modified and new quality indicators for characterisation and SAR. (After [26])

Indicator	Formula	Unit
13-m	$SAR5_{tot}coverage = \frac{V_{targ}(SAR{>}SAR5_{tot})}{V_{targ}}$	-
14-m	$HC_{new} = \frac{SAR75_{targ}}{SAR25_{targ}}$	-
16-m	$SAR_{hs-targrationew} = \frac{SAR_{V1}}{SAR_{targ}}$	-
17a	$\rho_{hs}\left(\overrightarrow{x}\right) = \frac{1}{\frac{4}{3}\pi\cdot 0.05^3} \cdot \int_{\overrightarrow{x}\in\lvert\overrightarrow{y}-\overrightarrow{x}\rvert<0.05} dV_{hs}\left(\overrightarrow{y}\right)$	-
17b	$I_{hs}\left(\overrightarrow{x}\right) = SAR_{hs}\left(\overrightarrow{x}\right) \cdot \rho_{hs}\left(\overrightarrow{x}\right)$	W/kg
17c	$I_{hsregion} = \frac{\sum_{region} I_{hs}(n)\cdot V(n)}{V_{region}}$	W/kg
17	$I_{hsratioregion} = \frac{I_{hsregion}}{SAR_{targ}}$	-
18	$SAR_{targ-complratio} = \frac{SAR_{targ}-SAR_{complaint-region}}{SAR_{tot}}$	-

17a. ρ_{hs}: hotspot density at a specific point in the patient volume is used to estimate the hotspot volume in a sphere of 5 cm radius around that point. It was introduced to identify multiple hotspot close together.

17b. I_{hs}: hotspot intensity, which is the product of the absolute SAR level and ρ_{hs}.

17c. $I_{hs-region}$: local average hotspot intensity.

17. $I_{hs-ratio-region}$: ratio between $I_{hs-region}$ and average SAR in the patient.

18. $SAR_{targ-compl-ratio}$: objective function to optimise SAR. It is similar to SAR_{ratio} but the target is represented by the complaint region.

The evaluation metric used for both characterisation and optimisation was the median temperature in the target, $T50_{targ}$. Canters *et al.* [26] found that SAR_{targ} (9), SAR_{ratio} (10), $SAR_{hs-targ-ratio}$ (16-m), and HC_{new} (14-m) were useful indicators for target SAR analysis; while $SAR_{hs-targ-ratio}$ (16-m) was the most suitable indicator for hotspot analysis. The most suitable objective function for SAR optimisation was the hotspot-target SAR quotient (16-m) which is balanced minimising the hotspots in the healthy tissue with maximising SAR in the target.

This indicator correlated best with the temperature with respect to other SAR indicators; however, it has been noted in the literature that further investigations are needed to prove that it is the best optimisation coefficient to improve the temperature pattern. Nonetheless, it has proven to be a useful metric in clinical practice and therefore is used in this thesis as a baseline.

2.6.2 Overview of the Optimisation Techniques in Hyperthermia

Various optimisation techniques have been described in the literature to achieve optimal tumour heating by setting antenna amplitudes and phases. Among these, the eigenvector problem has been investigated by Bardati *et al.* [77] to optimise the SAR in a phased array radiofrequency system, selecting two types of targets, those to be heated and those to be protected from EM radiation. The eigenvector problem is characterised by a positive definite Hermitian matrix defined for the specific target. The solution was represented by the antenna amplitudes and phases, and the optimal solution was found as a tradeoff between the best antenna settings for individual targets. A gradient-search feedback algorithm was implemented by Fenn *et al.* [78] to control the channel amplitudes and phases of an adaptive phased array radiofrequency hyperthermia system. A homogeneous saline phantom target and a ring phased-array system of four controlled RF transmitters channels operating at a frequency of 100 MHz were used for the hyperthermia experiments. The amplitudes and phases of each transmitter channel were controlled by a gradient-search feedback algorithm which implemented the method of steepest ascent for adaptive focusing, hence for power maximisation and the method of steepest descent for adaptive nulling, for power minimisation. Invasive electric field probes were placed at one or more positions to provide necessary feedback information. The power delivered to the tumour by the transmitter was constrained to maintain constant total transmit amount, P_T, in such a way that:

$$\sum_{n=1}^{N} |\omega_n|^2 = P_T \tag{2.4}$$

where ω_n is the power transmitted for the n^{th} adaptive channel. An iterative scheme was then used to maximise the electric field at the tumour site while minimising the electric field elsewhere. The gradient-search algorithm could control the transmit weights, amplitudes and phases. Hence, the hyperthermia phased-array antenna transmitted an RF signal that generates RF power that was measured in receive field probe antennas. For any antenna configuration, the amplitudes and phases were adjusted by a small negative or positive amount and the received powers at the electric-field probes were used to calculate the total received probe array power and update the transmit weight settings. Fenn *et al.* showed a potential improvement in hyperthermia thermal dose by adaptive techniques. However, the need for invasive measurements of the electric field inside the body makes this technique difficult to employ for deep-seated tumours.

Kohler *et al.* [23] presented a fast algorithm for optimal control of multi-antenna applicators in regional hyperthermia. The study analysed functions to compute hyperthermia treatment plans to heat deep tumours. Efficient numerical methods were used to maximise the ratio of integral absorbed power inside the tumour and a weighted energy norm outside the tumour. Real patient data were used to test these fast routines and results were compared to global optimisation techniques. Kohler *et al.* developed techniques for online optimisation in a hybrid system using global optimisation methods to optimise objective functions by search algorithms as used in [66]. The study generalised the eigenvalue problem proposed by Bardati *et al.* [77] using 3D models, including temperature distribution, time dependences and weighting functions. The inverse optimisation problem was posed as follows:

$$max_{p \in \mathbb{C}^n} T_{90} \quad subject\ to \quad T\left(x\right) \leq T_c\left(x\right) \quad \forall \quad x \in G \tag{2.5}$$

where $p = (p_1, ..., p_N) \in \mathbb{C}^n$ are complex numbers describing amplitudes and phases of the emitted radiowaves, x is the tissue point of the volume of interest G, $T_c\left(x\right)$ are the critical temperatures for each point x (defined on a clinical basis), and T_{90} is the temperature exceeded by 90% of x. This functional requires the solution of a high-dimensional, nonlinear optimisation problem. Kohler *et al.* found simplifications of this functional following the optimisation criterion formulated in [79] and used a generalisation of the eigenvalue problem proposed by Bardati *et al.* [77] to maximise efficiency. Moreover, Kohler *et al.* developed efficient functionals for optimising temperature distribution, incorporating the temperature solution of the bioheat equation in a Hilbert space functional and introducing adapted weight functions. They found a computation time of less than 80 s for an updated optimisation of the Sigma-Eye applicator. This led to the flexibility in customising the antenna parameters to adapt for changes in perfusion, electrical conductivity, and individual complains of the patient.

Zastrow *et al.* [80] used a non-invasive transmit beamforming algorithm to target microwave energy at the tumour site in breasts. Four numerical breast phantoms with different breast tissue densities, including fatty scattered fibrograndular, heterogeneously dense, and extremely dense, were used to evaluate the focusing and selective heating efficacy. Transmit beamforming consisted of passing microwave signals through a set of filters, in such a way the signal emitted from each antenna adds coherently at the target location and incoherently in the healthy tissue. The beamformer signal set is designed by using a patient-specific propagation model. The model is obtained from 3D FDTD EM simulations of the numerical phantom.

Then, thermal FDTD simulations were used to calculate heating potential and steady state temperature distributions in the breast. The beamformer consisted of a Finite Impulse Response (FIR) filter in each antenna channel. By adjusting the frequency-dependent amplitude and phase of the signals, the filters focused microwave energy at the target location. Hence, the objective was to maximise the fraction of the total transmitted power delivered to the target region r_f:

$$max_{H_n(\omega)} \frac{\int \left| \sum_{n=1}^{N} H_n(\omega) T_n(\omega, r_f) \right|^2 d\omega}{\int \sum_{n=1}^{N} \left| H_n(\omega) \right|^2 d\omega} \tag{2.6}$$

where $H_n(\omega)$, $n = 1, ..., N$, is the frequency response of the FIR filter for the nth channel, and $T_n(\omega, r_f)$ represents the frequency response of the one-way propagation path from the nth source to the target location r_f. The selective heating efficacy of transmit beamforming was quantified using the following metrics:

- V_{43} (cm^3): the volume of breast tissue with temperature greater than 43°C.
- r (mm): the radial distance from r_f to the location of peak breast interior temperature.
- t_{skin} $(°C)$: peak skin temperature.
- t_{breast} $(°C)$: peak breast interior temperature.

The performance of the beamforming algorithm was evaluated as a function of operating frequency and results showed there was an optimal frequency at which the narrowband beamformer reached a predicted outcome. This frequency depended on the tissue composition and the physical structure of the breast. The beamforming proved to be a robust method to focus microwave energy at the tumour location in breasts with different volume and breast tissue density.

Schenk *et al.* [81] proposed a parallel scalable Partial Differential Equations (PDE) constrained optimisation based on a parallel iterative linear solver on distributed-memory architectures. The objective function to be minimised is formulated as in [82] and the Pennes' bio-heat equation [83] is used as a constraint as follows:

$$F = \int_{x\in\Omega_t} \left(T_{ther} - T\right)^2 d\Omega + \int_{x\notin\Omega_t, T>T_{health}} \left(T - T_{health}\right)^2 d\Omega \tag{2.7}$$

subject to

$$-\bigtriangledown \cdot \left(k \bigtriangledown T\right) + \rho_b \rho \omega \left(T - T_b\right) = \frac{\rho\sigma}{2} \left|\sum_j u_j E_j\right|^2 \quad in\ \Omega \tag{2.8}$$

$$k\theta T_n = q_{const} \tag{2.9}$$

where T is the temperature and T_b the arterial blood temperature, k the thermal conductivity, ρ the density, ρ_b the blood density, ω the perfusion rate, σ the electrical conductivity and Ω is the patient's volume of interest. The temperature is $T_{ther} = 43°C$, $T_{health} = 42°C$, $T_{lim} = 44°C$, the control of the antenna is represented by $u_j = a_j e^{-i\alpha_j}$ and E_j, where a_j and α_j are respectively the antenna amplitude and phase and E_j is the electric field generated by each antenna. The PDE-constrained interior-point algorithm makes use of a global convergent optimisation method [84] and a scalable linear solver, implemented to scale-up to thousands of computing cores.

Iero *et al.* [22] proposed a computationally effective approach to focus the heating during hyperthermia, the Optimal Constraint Power Focusing (OCPF) method. The goal was to determine the excitations of the sources in order to produce maximum focusing of the field within the target region and maintain low heating elsewhere. The method required computationally intensive global procedures based on convex programming. Two-dimensional numerical phantoms were extracted from 3D Magnetic Resonance Imaging (MRI) images of the breast obtained from researchers at University of Wisconsin-Madison and used to test the feasibility of the approach with tumours in different locations, and at different operating frequencies. A circular array of radius 20 cm was used as applicator and the synthesis procedure was performed at 2 GHz and 2.25 GHz. The proposed method was a generalisation of the "pencil beams" synthesis method through fixed geometry arrays [85]. The optimal focusing of scalar fields for the hyperthermia problem was posed as follows:

$$maximise \quad \left|E\left(r_{tumour}\right)\right|^2 \tag{2.10}$$

while

$$\left|E\left(r\right)\right|^2 \leq UB\left(r\right) \quad r \in \ \Omega \tag{2.11}$$

where r_{tumour} is the tumour location, Ω represents the healthy tissue which does not include cancer, $UB\left(r\right)$ is the upper bound mask, i.e. a non-negative function which corresponds to field amplitudes leading to sub-critical temperature increases into healthy tissue. The method assumes that the field in the direction of the tumour is purely real, hence Equation 2.10 was considered as the maximisation of the real part of the field. Therefore, the problem was formulated to determine the real and imaginary parts of the excitation coefficients $\Re\left(I_n\right)$, $\Im\left(I_n\right)$, $(n = 1, ..., N)$ such that:

$$\Psi\left(I\right) = -\Re\left[E\left(r_{tumour}\right)\right] \quad is \quad minimum \tag{2.12}$$

subject to:

$$\Im\left[E\left(r_{tumour}\right)\right]=0 \tag{2.13}$$

$$\left|E\left(r_t\right)\right|^2 \leq UB\left(r_t\right) \quad \forall\ t=1,2,...,M \tag{2.14}$$

where $I = I_1, ..., I_N$ is the vector of the excitation coefficients and $r_1, ..., r_T$ is a discretization of the domain Ω, $\left|E\left(r_t\right)\right|^2$ is a positive semidefinite quadratic form with $(t = 1, ..., M)$ where M represents the number of elements into which the space is discretized, the constraints 2.13 and 2.14 define convex sets in the space of the unknowns [86]. Since the term $\Re\left[E\left(r_{tumour}\right)\right]$ in 2.12 is a linear function of the real and imaginary parts of the excitation coefficients, the problem was formulated as the minimisation of the linear function in a convex set [87]. The study showed the capability of the method to reach a focused SAR deposition in the region of interest; however thermal analysis was needed for a complete assessment and to confirm the potential of the method in clinical use.

In 2004, Converse *et al.* [88] investigated the feasibility of using Ultrawide Band (UWB) microwave techniques to localise heating for breast cancer hyperthermia. The UWB pulses were transmitted simultaneously into the breast from a set of antennas and passed through a space-time beamformer whose filters were designed to compensate for dispersive propagation in the tissue, in such a way that the pulses added coherently at the treatment location and incoherently elsewhere. The design of the space-time beamformer was implemented using a frequency domain approach, computationally faster than the time-domain approach. Realistic numerical breast phantoms derived from magnetic resonance images of patients were used in this study.

The power density absorbed by the breast was calculated by FDTD simulations. The method was evaluated by varying the breast density and heterogeneity. The same propagation model was used for tumour localisation and for transmit-focusing beamformer design, to allow accounting for errors in estimated tumour location. The temperature distribution was also calculated by using a two-dimensional (2D) FDTD thermal model based on the bio-heat equation. The robustness of the approach was evaluated by varying the dielectric properties of breast tissue and two metrics were used to quantify the focused heating:

$$\frac{Q_{ave}\left(breast\right)}{Q_{ave}\left(tumour\right)} \tag{2.15}$$

$$\frac{Q_{ave}\left(surface\right)}{Q_{ave}\left(tumour\right)} \tag{2.16}$$

where $Q_{ave}\left(tumour\right)$, $Q_{ave}\left(breast\right)$, $Q_{ave}\left(surface\right)$, are respectively the average heating potential of the tumour, breast and surface. The value of $Q_{ave}\left(breast\right)$ was calculated from tissue in the region within a 1 cm radius of the center of the tumour, $Q_{ave}\left(surface\right)$ was determined from data in a 0.5 cm thick layer beneath the skin/breast interface. Results showed that the method was able to reach high temperatures in proximity of small tumours while maintaining temperatures under critical values in healthy tissue.

Converse *et al.* [21] also carried out a computational study of narrowband microwave hyperthermia for the breast cancer treatment as an alternative to their earlier ultra-wideband study [88]. The evaluation was performed based on EM power density and temperature profiles using three different breast phantoms with heterogeneous tissue composition and with a small tumour of 2 mm diameter. The study showed that ultra-wideband allows better focusing and greater reduction of the hotspots compared to the narrowband method.

In 2008, Cheng *et al.* [89] proposed a method for fast temperature optimisation of a multi-source hyperthermia applicator using a subset of source configurations, i.e. a subset of antennas which were called virtual sources. The sources were characterised by specific amplitudes and phases calculated based on the patient model and the tumour. The method was tested on a patient upper-leg tumour model, with and without a temperature perfusion model, and the applicator was simulated as mini-annular-phased array of ten dipole antennas. The study showed that the temperature distributions obtained from the pre-defined virtual sources were comparable to those calculated using all antennas, and hence provide a sufficiently good solution.

Bardati and Tognolatti [20] investigated three optimisation strategies under the constraint to not exceed a maximal power per channel. The first optimisation technique optimises the power-to-target; the second optimisation method maximises the ratio of power-to-tumour to the power delivered to the healthy tissue volume in order to investigate the tumour-heating selectivity; the third method maximises the ratio of power-to-tumour to the total array power to investigate the heating efficiency. The numerical analysis was done using an array of eight dipoles placed on two lines around a head/neck. They found that the EM power following the power-to-target optimisation was the largest one delivered to the tumour.

In 2005, Guo *et al.* [90] proposed a time reversal based ultra-wideband microwave method for the treatment of breast hyperthermia. Time reversal and the Capon beamformer were adopted. The technique was evaluated on two 2D breast models which included a small tumour. The first step of the method consisted of transmitting a lower-power pulsed microwave signal from one antenna and the backscattered signals were received by all the antennas and then time-gated. Capon beamforming was performed based on the time-gated signals in order to calculate the beamforming weights to focus the energy into the tumour. The time-gated signals were retransmitted into the breast from each antenna at the same time with a certain pulse repetition frequency to control the average EM power. The study was based on 2D numerical simulations and showed the ability to achieve better EM focusing compared to the space-time beamforming method.

Iero *et al.* [91] investigated the relationship between thermal and electromagnetic power focusing using the OCPF method developed in [22]. The study exploited a Green's function method to solve the Bioheat equation and carried out a quantitative assessment of the robustness of the OCPF technique against two kinds of inaccuracies; EM parameter uncertainty, i.e. incorrect values of permittivity and conductivity; and errors derived from incorrect morphology of the fibroglandular region of the breast. Two-dimensional numerical phantoms, obtained from realistic images of four breast topologies were used to carry out the evaluation. The phantoms were characterised by fatty, fibrograndular, heterogeneously dense, and very dense compositions taken from the University of Wisconsin-Madison repository. Results showed good focusing of the temperature in the target area and temperatures below critical values, i.e. 40.8 $°C$ in the healthy tissue.

In 2016, Iero *et al.* [92] extended two techniques originally developed for 2D scenarios to a 3D scenario. The study showed how to focus vector fields for hyperthermia treatments. An improved version of the Time Reversal method, the Optimised Time Reversal [93], and Optimal Constrained Power Focusing [94] were compared in two conditions, a lossless scenario surrounded by a spherical array, and a hemispherical antenna applicator. Results showed that the Optimal Constrained Power Focusing provided better focusing performance at the cost of computation time.

The work of Bellizzi *et al.* [95] concerned an optimal multi-frequency approach based on convex programming to focus the SAR distribution at a certain point in the tumour, while maintaining low SAR distribution elsewhere. The method followed the theory of the OCPF, already adopted by Iero *et al.* [91] and exploited a multi-frequency applicator, i.e. different excitations used at different frequencies. The method was called Independent Multi-Frequency OCPF (i-mf-OCPF) and based on the Multi-Frquency Optimal Constraint Power Focusing (mf-OCPF) algorithm described in [96]. The idea of the multi-frequency approach was first introduced by Zastrow *et al.* [97]. Two-dimensional breast phantoms derived from realistic 3D phantoms provided by the Wisconsin repository were used in this study.

The effectiveness of the i-mf-OCPF approach was compared to the OCPF and mf-OCPF methods confirming the optimality of SAR distribution, though still subject to undesired SAR peaks. A thermal analysis was also carried out and showed that all the methods were able to focus the temperature in the target point. However, the performance of the technique was also subject to the type of the tissue, frequencies, number of antennas and can be worse for more challenging scenarios.

In previous studies of microwave hyperthermia, the array has been constructed from simple point sources [21], [25], [90], [91] or multilayers of antenna elements around the breast model [80], while Nguyen *et al.* [24] introduced the differential beam-steering subarray approach to pre-steer each subarray separately, instead of controlling the array at the level of individual elements.

A recent study by Nguyen *et al.* [24] proposed particle swarm optimisation to optimise amplitudes and phases of the antennas to maximise power, and hence temperature at the tumour location, while preventing hotspots in healthy tissue. The proposed strategy was implemented using a 3D antenna array of 4 x 6 unidirectional antenna elements. The system was tested using a very dense 3D breast models with tumours in different locations and a frequency of 4.2 GHz which represented a compromise between the required signal penetration and focusing. Results showed the ability of the method in focusing the heating at the tumour volume.

Wiersma *et al.* [98] developed a flexible optimisation tool for hyperthermia treatments with RF phased array systems. The goal was to optimise the SAR distribution taking into considerations constraints at regions in the healthy tissue. The quantitative metric to define the optimal target volume focusing was the ratio between the SAR in the target volume and SAR in the whole tissue volume. The method was tested with a real patient case using a phased array applicator with four rectangular waveguides.

Trefna *et al.* [25] proposed a time-reversal focusing algorithm for microwave hyperthermia to treat deep-seated tumours. The method was based on the time-reversal cavity principle described by Cassereau and Fink [99] and it was applicable for both continuous and pulsed waves. An artificial EM source was placed in a model of the patient. Trefna *et al.* calculated the antenna amplitudes and phases from simulation of wave transmission and not from measured data, in contrast to other UWB approaches [88], [90], and the antenna was placed in the tumour model.

The beamforming algorithm was implemented using a FDTD algorithm. Two realistic 2D models of head and neck, and breast, were used for the study and the assessment of the technique was done based on the power absorption distributions.

To quantify the relative amount of energy that is absorbed in the tumour and to evaluate the effectiveness of the method, Trefna *et al.* calculated the ratio between the average power per voxel in the tumour volume and the average power per voxel in the healthy tissue [100]. The average power absorption ratio is defined as:

$$aPA = \frac{\frac{1}{N_{Vtum}} \sum^{Vtum} PA_{norm}\left(x, y\right)}{\frac{1}{N_{Vrt}} \sum^{Vrt} PA_{norm}\left(x, y\right)} \tag{2.17}$$

where V_{tum} and V_{rt} represent the tumour and non-tumour tissue volume, while N_{Vtum} and N_{Vrt} are the total numbers of volume elements of the tumour tissue and non-tumour tissue. The remaining tissue maximum index is defined as:

$$RTM_i = \frac{PA_1\left(remaining \quad tissue\right)}{PA_{50}\left(tumour\right)} \tag{2.18}$$

where PA_{50} is the median PA in the tumour and PA_1 indicates the highest percentile of the PA distribution in the remaining tissue. Moreover a statistical analysis was performed to calculate the maximum power absorbed in all tissues, and a quantitative evaluation of ultrawideband and narrowband beamforming was carried out on the breast model. Finally, minimisation of organ at risks was not taken into consideration in this method.

Zastrow *et al.* [97] investigated time-multiplexed beamforming for noninvasive microwave brain hyperthermia treatment by using a numerical head phantom from the Virtual Family (IT'IS Foundation) [2]. To test the effectiveness of the sequence of multiple beamformers, three target locations were chosen in different regions of the brain volume. The objective of the beamformer was to maximise the ratio of the power dissipation per unit volume at the target location and the power dissipation per unit volume at location outside the target volume with temperatures exceeding 41 °C. Thermal simulations using a time-varying heating element as source were performed to evaluate the performance of the technique. Results demonstrated the potential of the approach to minimise overheating regions of healthy tissue while maintaining the therapeutic temperature in the tumour.

In 2006, Kok *et al.* [28] carried out a treatment planning combined with high resolution temperature based optimisation to treat esophageal cancer by loco-regional hyperthermia. The study adopted a quasi-static zooming method to

---

[2] http://itis.swiss/virtual-population

calculate the power density at high resolution combined with a temperature-based optimisation technique to accomplish high resolution optimisation. The method was implemented according to the method described by Das *et al.* [101].

2.6.3 Discussion of Optimisation Techniques

In HTP, optimisation techniques based on SAR are often used to obtain the optimal antenna settings to focus the tumour heating. However, there does not seem to be clear agreement on whether SAR or temperature is most appropriate for optimisation. The work by Canters *et al.* [65] showed that the improvement from thermal optimisation may be difficult to discern in the presence of modelling uncertainties, such as tissue perfusion uncertainty and that SAR was a better predictor for the median temperature. Contrarily, a previous study [102] found that temperature-based optimisation was superior to SAR-based optimisation under the assumption of constant perfusion at hyperthermic levels. However, Lee *et al.* [103] showed that SAR based metric TC_{25} also correlates with clinical outcome. In addition, thermal uncertainties can even negate the benefit from thermal optimisations.

At Erasmus MC, SAR coverage is currently used for treatment guidance in clinical practice and thermal simulations are performed to evaluate the quality of the treatment. In the recent study of Drizdal *et al.* [104] two different temperature models were used to investigate the differences in hyperthermia treatment quality when using different hyperthermia systems for sub-superficial tumours in H&N regions. One thermal model was studied with constant values of conductivity and perfusion optimised by [105] and a second model with a temperature-dependent blood perfusion. The study found the same CTV coverage in terms of SAR (TC_{25}) and temperature (T_{50}) when comparing the performance of the Lucite Cone and the HYPERcollar applicators by using the thermal model with constant values of conductivity and perfusion values. At the same time, temperature differences up to 3 °C were found between the two thermal models, suggesting the need for further research on the most accurate thermal model. In this thesis, SAR-based optimisation techniques have been investigated to focus the heating into the tumour without impairing the healthy tissue, and thermal simulations are used as the most appropriate criterion to assess the expected benefit in the clinic.

2.7 Treatment Quality Quantifiers

The clinical metrics used to evaluate the performance of the algorithms in this thesis and to assess hyperthermia treatment quality can be divided in two groups.

2.7.1 SAR Target Coverage Indicators

Treatment quantifiers such as the Target Coverage 25% TC_{25}, Target Coverage 50% TC_{50} were used in HTP [45], where these are defined as:

$$TC_{25} = V_{target}\left(cfSAR > 0.25 * max\left(cfSAR\right)\right) \tag{2.19}$$

i. e. Target Coverage TC_{25} and TC_{50} indicate the percentage of the volume of the tumour, V_{target}, that is enclosed by the iso-contour of 25% and 50% respectively of the maximum Cubic Filtered Specific Absorption Rate (cfSAR) in the patient. Cubic filtering of SAR is a smoothing method to average the SAR over a cubic space of 1 cm^3 of tissue [51]. The larger the TC percentage, the better the treatment quality.

2.7.2 Bio-heat Equation and Temperature Indicators

Previous work has demonstrated that the hotspot-target quotient, HTQ, is correlated with the simulated temperature distributions for deep HT [26]. The Pennes' bio-heat equation is employed to describe heat transfer inside biological tissue [83], and is used in this thesis as the thermal model to predict temperature distribution in the patient model:

$$\rho c\frac{\partial T}{\partial t} = \bigtriangledown \cdot \left(k \bigtriangledown T\right) + \rho Q + \rho S - \rho_b c_b \rho \omega \left(T - T_b\right) \tag{2.20}$$

where T (^oC) is the temperature, t (s) is the time, ρ ($kg \cdot m^{-3}$) is the volume density of mass, c ($J \cdot kg^{-1} \cdot^{\circ} C^{-1}$) is the specific heat capacity, k ($W \cdot m^{-1} \cdot^{o} C^{-1}$) is the thermal conductivity, ω ($m^3 \cdot s^{-1} \cdot kg^{-1}$) is the volumetric blood perfusion rate, Q ($W \cdot kg^{-1}$) is the metabolic heat generation rate, S ($W \cdot kg^{-1}$) is the SAR and the subscript b indicates a blood property. Moreover, a mix of convective and Neumann boundary conditions are used to account for temperature losses [105].

Thermal indicators, as T_{90}, T_{50}, T_{10}, are computed to quantify the temperature in the target tumour (T_x) which is exceeded by X percent of all temperature values [106]. Larger values of T_x reflect the higher temperatures in the tumour, hence better treatment quality.

2.8 Discussion and Conclusions

This chapter has given an overview of the different areas of H&N cancer. The biological mechanisms of hyperthermia and the different types of hyperthermia treatments and systems were presented. A discussion of the hyperthermia treatment planning carried out at the Erasmus MC and the requirement to ensure a good treatment quality was provided, together with the clinic evaluation metrics. A detailed discussion of objective functions and optimization techniques was also presented.

While research has been carried out to achieve sufficient heating for the tumours while avoiding the surrounding healthy tissue, optimising the antenna settings of the hyperthermia applicator remains a difficult task. This thesis aims to improve the heating delivery for H&N hyperthermia treatments by proposing novel optimisation algorithms and assessing their effectiveness on patient models provided by the Erasmus MC.

Different numerical techniques for SAR and temperature optimisation have been described in the literature. Optimisation algorithms based on SAR are more widely applied than temperature-based methods. Important factors as perfusion, thermal conduction and bolus cooling are not taken into account in SAR-based optimisation strategies. One of the limitation of SAR optimisation is that SAR and temperature in the hotspot might not always coincide. For example, the effect of bolus cooling on superficial high SAR values might affect the temperature values, and therefore high SAR does not always imply high temperatures. Moreover, moderate SAR values in poorly perfused media can result in high temperatures. All these factors led to investigation of temperature-based optimisation methods. However, whether SAR or temperature optimisation is more appropriate is still not clear. Radiofrequency hyperthermia treatments induce a plethora of effects of which some, but not all, are temperature related. Hyperthermia is defined by the increase in temperature, but this treatment also modulates, increases and decreases perfusion. Sometimes only low temperatures are obtained in the clinic in very healthy patients due to very responsive thermoregulation. Regions with high SAR are then cooled by high perfusion. In these patients, the treatment effect can be best explained by the fact that this perfusion itself has a strong impact on treatment outcome. Hence, whether the relation between SAR and outcome is less strong than the relation between temperature and outcome is still unknown.

The reminder of this thesis presents novel SAR-based optimisation algorithms whose performance is evaluated by thermal simulations and a SAR-temperature correlation is calculated to determine the most appropriate method for hotspot selection. Thermal modeling in general is strongly affected by uncertainties; the simulations carried out in this research use tissue cooling values for fat, muscle and tumour tissue that have been specifically optimised using temperature measured during hyperthermia treatments at Erasmus MC. In this regard, the robustness of the time-multiplexed hyperthermia method is also demonstrated against thermal tissue properties variation.

Objective functions reported in the literature have been described and the correlation of the SAR indicator with the corresponding predicted temperature was evaluated; each SAR indicator was used as the objective function for SAR optimisation. HTQ was found to be the best objective function for hotspot reduction and optimisation procedures, being able to minimise the hotspots in the healthy tissue while maximising SAR in the target. The optimisation methods developed in this research aim to minimise HTQ and a novel objective function is formulated to find the optimal antenna settings to heat the tumor region and suppress pre-defined hotspots.

The next chapter discusses the optimisation method clinically employed at the Erasmus MC for the treatment of pelvic and head and neck cancer and introduces a novel optimisation algorithm to enhance heat focusing.

3

Hyperthermia Treatment Planning via Differential Evolution Optimisation

3.1 Introduction

As noted in Chapter 2, while significant advances have been made in hyperthermia treatment, challenges remain in selecting system parameters in order to optimise SAR and temperature distributions, in particular through reducing the incidence of hotspots.

In this chapter, a Differential Evolution (DE) algorithm is proposed for improving H&N HTP. Data for six patients treated by the HYPERcollar applicator developed at the Erasmus MC Cancer Institute have been used in order to compare the proposed DE algorithm to the Particle Swarm Optimisation (PSO) technique that is currently in use in clinical practice. These two techniques have been evaluated through different optimisation settings, clinical metrics including the Hotspot-Target SAR Quotient (HTQ)), Target Coverage (TC) and HT temperature parameters. The work described in this chapter has been published in Cappiello *et al.*, “Differential evolution optimisation of the SAR distribution for head and neck Hyperthermia,” *IEEE Transactions on Biomedical Engineering,* Vol. 64, Issue 8, August 2016 [107] (© [2016] IEEE. Reprinted with permission)).

The remainder of this chapter is organised as follows. In Section 3.2 the PSO and DE algorithms are introduced. The performance of the proposed technique compared to the PSO method is presented in Section 3.3. Finally, conclusions are given in Section 3.5.

3.2 Methodology

This section describes the PSO and DE algorithms and illustrates the experimental testbed, and the set of optimisation parameters chosen for the two algorithms. Details of the temperature simulations are also given.

3.2.1 PSO Optimisation of SAR Distribution

PSO is a population-based stochastic technique inspired by social behavior principles [108]. PSO adapts the trajectories of a particle population in a search problem space, according to the evaluation of a fitness function. The particles represent the candidate solutions to the problem and have their own positions and velocities, and are organised into clusters. The best particle in a cluster is called p_{best} and the global best in the population is defined as g_{best}. Generation after generation, each particle changes its velocity toward the p_{best} and g_{best} locations according to Equations 3.1 and 3.2.

$$v_i^t = w * v_i^{t-1} + c_1 * rand * \left(pbest_i^{t-1} - x_i^{t-1}\right) + c_2 * rand * \left(gbest_i^{t-1} - x_i^{t-1}\right) \quad (3.1)$$

$$x_i^t = x_i^{t-1} + v_i^t \quad (3.2)$$

where v_i^t and x_i^t are the velocity and position at iteration t with $i = 1, ..., n$, where n is the number of particles; c_1 and c_2 are the attraction weights of local optimum and global optimum of the particles, respectively, while w gives the proportion of the velocity in the previous step $t-1$ that contributes in the new step t. At each iteration, the best particle in the cluster is updated and, then the best particle in the population. Hence, the optimal solution is represented by g_{best}. An applicator

Table 3.1: Pseudocode of the PSO algorithm.

```
Pseudocode of PSO
For each particle (i)
    Initialise particle with random position and velocity
End
Do
    For each particle (i)
      Evaluate fitness function
      If the current fitness function value is better than $p_{best}$
      set current value as the new pbest
      If the current fitness value is better than the global best
      of the population, set current value as the new $g_{best}$
End
    For each particle (i)
      Calculate particle velocity according to Equation 3.1
      Update particle position according to Equation 3.2
    End
While (iterations <maximum number of generations) or
(defined minimum fitness value not achieved).
```

antenna configuration consisting of amplitude and phase values is represented by a particle in the PSO algorithm. The PSO toolbox developed by Chen [109] has been implemented in the software tool VEDO developed by the hyperthermia group at Erasmus MC and its pseudocode is given in Table 3.1.

3.2.2 DE Optimisation of SAR Distribution

The differential evolution algorithm, originally developed by Storn and Price [110], is a heuristic search and optimisation technique which belongs to the class of evolutionary optimisation algorithms. Similar to PSO, DE is initialized by a population of random solutions, called individuals. Genetically-inspired operations of crossover, mutation and selection are applied to the population in order to minimise an objective function over the course of consecutive generations (iterations). The relationship between the hyperthermia parameters to be optimised and the DE candidate solutions is proposed as follows: the chromosomes of the individual are represented by antenna amplitudes and phases, individually called genes (Table 3.2). Then, each chromosome is characterized by its corresponding complex

Table 3.2: DE Hyperthermia Parameters Relation.

DE Parameter	Antenna Array Parameter
Gene	Amplitude or Phase
Chromosome	Amplitude and phase pair
Individual	One antenna array configuration
Population	Several arrays

phasor notation P:

$$P = a \cdot e^{-i\Theta} \tag{3.3}$$

where a and Θ indicate the antenna amplitude and phase.

After randomly initializing the population, each individual is evaluated by a fitness function. At each generation, a new population is created from the current population. The individuals are named x_i, $(i = 1, \ldots, I)$, where i identifies the individuals that form the population and I is the number of individuals in the population. Firstly, for each target individual x_i, DE applies a differential mutation operator. An initial offspring y_i, is created by randomly choosing three members of the population, x_{r0}, x_{r1}, x_{r2}, and y_i is generated as:

$$y_i = x_{r0} + F \cdot (x_{r1} - x_{r2}) \tag{3.4}$$

where F is the differential weighting factor. Following mutation, the crossover operator is applied with a Crossover Probability (CP). The crossover probability determines the fraction of chromosomes that are copied from the mutant offspring to the new offspring. These newly created individuals are referred to as trial members. Each trial member is then compared to the target individual by evaluating the objective function. If the new offspring yields a superior fitness value, the trial individual will be inserted into the next generation, otherwise the old individual is retained. The procedure above is repeated until the stopping criterion (either a certain fitness value or a maximum number of iterations) is satisfied, returning the best solution from the current population. DE was implemented as described in [111].

Table 3.3: Patient and treatment characteristics: Patient identification number, location and type of the tumour, treatment number.

Patient no.	Tumour location	Type of the tumour	Treatment no.
P1	Oropharynx	Recurrent tumour	1
P2	Nasopharynx	Recurrent tumour	1
P3	Oral cavity	Primary tumour	1
P4-T1	Oral cavity	Primary tumour	1
P4-T2	Oral cavity	Primary tumour	2
P5	Retroauricular	Primary tumour	1

3.2.3 Experimental Dataset

The experimental dataset to test the performance of DE and PSO is detailed in this section. Six anonymised clinical records, related to the treatment of H&N cancer using the Erasmus MC HYPERcollar system, have been used to test the proposed DE implementation and compare it with the PSO algorithm. The patient clinical characteristics are listed in Table 3.3 and include patient identification numbers, tumour type, location and treatment number. The data related to the patients identified by P4-T1 and P4-T2 represent the first and second hyperthermia treatments on the same patient.

Figure 2.8 illustrates the HYPERcollar applicator, developed at Erasmus MC to heat deep H&N regions, such as thyroid, oropharynx and nasal cavity [18], [45], [47], [48]. As noted in Chapter 2, the applicator consists of a ring-shaped phased array of twelve patch antennas, equally divided over two rings, operating at a frequency of 434 MHz. However, Erasmus researchers have observed that in practice, four dorsal antenna often did not contribute to the heating during treatment due to issues of their practical location [45]. Therefore, only eight antennas were used for HTP.

3.2.4 Optimisation Parameters

The PSO and DE approaches have been employed to minimise the HTQ metric and obtain the optimal antenna settings (consisting of 8 amplitudes and 8 phases). The application of PSO and DE to the hyperthermia problem requires the selection

Table 3.4: Optimisation technique parameters (common to PSO and DE).

Parameter	PSO and DE
amplitude boundaries	[0,1]
phase boundaries	[-180,180]
number of individuals	$I_a = 60$, $\mathrm{I}_b = 60$, $I_c = 100$, $I_d = 200$
number of iterations	$G_a = 200$, $G_b = 400$, $G_c = 200$, $G_d = 200$

Table 3.5: Specific optimisation technique parameters of PSO and DE.

PSO Parameter	value	DE Parameter	value
c_1	0.5	F	0.85
c_2	1.25	CP	1
w	0.9		

of adjustable parameters such as: the boundary range of the antenna and phase parameters, the number of individuals per population, and the number of iterations per method; these parameters common to both optimisation algorithms are reported in Table 3.4. Four different settings of the two latter parameters have been considered to compare the PSO and DE performances; these are identified by subscripts a, b, c, and d in Table 3.4. Additional parameters specific to each technique are given in Table 3.5, and were selected from initial experimentation on the data.

Furthermore, the parameters in Tables 3.4 and 3.5 have been chosen empirically to provide a balance between the breadth of the search and the computation time. For PSO, the weight of local and global optimum of the particles, c_1 and c_2, and the weight ω in Equation 3.1 are given, while for the DE, the differential Factor (F), and the crossover probability CP, are given.

3.2.5 Temperature Simulations

To evaluate the performance of DE and PSO algorithms, temperature simulations were carried out in SEMCAD X (version 14.8.6 Speag, Zurich, Switzerland) using the Pennes' bio-heat equation expressed by Equation 2.20 in Section 2.7. Transient thermal simulations were calculated by SEMCAD X using the tissue-specific thermal properties (conduction and perfusion) used in [105], with an applicator efficiency factor of 40% for the HYPERcollar system. The applicator efficiency of the system is the percentage of the power from the antenna connectors delivered into the patient. Dielectric and thermal properties indicated in Table 3.6 were used in this study. The waterbolus temperature was fixed at 20 °C and the input total power, was tuned to reach the maximum target temperature of 44 °C in healthy tissue and 40 °C in critical organs (i.e. brain, eye and spinal cord) for all configurations. Heat dissipation represents a major factor in the clinical application of hyperthermia.

The study conducted by Verhaart *et al.* [105] shows that iterative tuning of the tissue-specific conduction and perfusion terms for matching the Pennes' bio-heat equation simulations to temperature measurements data of sixteen patients treated with the HYPERcollar leads to a substantial improvement in simulation accuracy.

This approach has been shown to provide accurate predictions for the overall temperature distribution, e.g. the median temperature in the target region. Hence, in this thesis, the optimised values for muscle, fat and tumour tissue found in [105] have been used to estimate the temperature distribution improvement for various optimisation settings. A mix of convective and Neumann boundary conditions was applied such that [105]:

$$k\frac{\partial T}{\partial n} = h\left(T - T_{outside}\right) \tag{3.5}$$

where $T_{outside}$ (^oC) is the temperature outside the boundary, n (m) is the direction normal to the surface, h $(W \cdot m^{-2} \cdot ^o C^{-1})$ is the heat transfer coefficient due to convective and radiative losses. The waterbolus temperature was set to 30 °C and the initial tissue temperature to 37 °C. The temperature of external air and headrest were set to 20 °C and $h = 8W \cdot m^{-2} \cdot ^o C^{-1}$ [105] was used for the boundary conditions. The interfaces at tissue-internal air, tissue-lung and tissue-metal implants were modelled using $h = 50W \cdot m^{-2} \cdot ^o C^{-1}$ [105], while $h = 292W \cdot m^{-2} \cdot ^o C^{-1}$ was applied for the tissue-waterbolus interface.

Table 3.6: EM tissue properties at 434 MHz and thermal tissue properties for temperature simulations at 37 °C [112] and *thermal properties in [105].

Tissue	ε_r (-)	σ_{eff} $(S \cdot kg^{-1})$	ρ $(kg \cdot m^{-3})$	c $(J \cdot kg^{-1} \cdot^{o} C^{-1})$	Q $(W \cdot kg^{-1})$	k $(W \cdot m^{-1} \cdot^{o} C^{-1})$	ω $(m^3 \cdot s^{-1} \cdot kg^{-1})$
Internal air	1.0	0.0	1.2	-	-	-	-
Lung	23.6	0.38	394	-	-	-	-
Muscle	56.9	0.81	1090	3421	0.96	0.4*	442.8*
Fat	11.6	0.08	911	2348	0.51	0.5*	255*
Bone	13.1	0.09	1908	1313	0.15	0.32	10.0
Cerebrum	56.8	0.75	1045	3696	15.5	0.55	763.3
Cerebellum	55.1	1.05	1045	3653	15.7	0.51	770.0
Brainsteam	41.7	0.45	1046	3630	11.4	0.51	558.6
Spinal cord (myelum)	35	0.46	1075	3630	2.48	0.51	160.3
Sclera	57.4	1.01	1032	4200	5.89	0.58	380.3
Lens	37.3	0.38	1076	3133	-	0.43	-
Vitreous humour	69.0	1.53	1005	4047	-	0.59	-
Optical nerve	35.0	0.46	1075	3613	2.48	0.49	160.3
Cartilage	45.1	0.60	1100	3568	0.54	0.49	35.0
Thyroid	61.3	0.89	1050	3609	87.1	0.52	5624.3
GTV	59.0	0.89	1050	3950	-	1.5*	848*

3.3 Results

Experimental results obtained by PSO and DE are given in this section. More specifically, Section 3.3.1 presents an analysis of the two algorithms. Section 3.3.2 discusses the performance of PSO and DE with clinical settings, evaluating TC parameters, and SAR distributions. Section 3.3.3 analyses the temperature measurements.

3.3.1 Performance of PSO versus DE as a Function of the Objective Function

3.3.1.1 Mean and Standard Deviation of HTQ

To obtain the fitness values, DE and PSO have been run 50 times using four different optimisation algorithm settings (through varying the number of individuals and iterations), reported in Table 3.4. The results of these experiments are illustrated in Table 3.7 and in Figure 3.1. The best performance, achieved by PSO and DE across all parameter configurations is reported in the second row of Table 3.7. The best performance corresponds to the lowest HTQ value. Both algorithms achieve the best fitness score at least once out of the 50 runs for all configurations.

Table 3.7 also includes the highest (worst) HTQ value, together with HTQ average and standard deviation for each algorithm configuration and for each patient. The percentage variation in standard deviation between the PSO and DE algorithms is also highlighted in bold for each algorithm configuration.

Substantial performance differences can be observed between DE and PSO for all settings investigated. DE exhibits HTQ standard deviation lower than PSO by between 40.1% and 96.8%, which means that DE locates the global optimum more frequently and consistently than PSO. It is also interesting to note that no particular parameter configuration for either of the optimisation algorithms consistently outperforms the others.

This finding suggests that the optimisation algorithms are not particularly parameter sensitive. The improvement of DE over PSO is graphically illustrated in Figure 3.1 where mean HTQ and standard deviation are represented. In all graphs (corresponding to the six different patient records), DE reaches a lower mean HTQ over 50 runs compared to PSO, and lower standard deviation value in each algorithm configuration considered. Hence, DE is consistently superior compared to PSO, both for accuracy and robustness results. These results mean that using DE reduces the risk of non-optimal solutions being selected during the hyperthermia optimisation process.

Table 3.7: Best and maximum HTQ, mean and standard deviation values over 50 runs. Relative percent standard deviation improvements of DE over PSO are presented.

Patient no.		P1	P2	P3	P4-T1	P4-T2	P5
PSO and DE Best HTQ		1.3269	3.399	1.0343	2.1207	1.0343	1.1056
60 individuals, 200 iterations (PSO_{60-200}, DE_{60-200})							
PSO	Max	1.4447	3.8776	1.2366	2.5844	1.2269	1.1523
	Avg.	1.336	3.4226	1.0426	2.1376	1.0437	1.1175
	Std.	**0.0237**	**0.0772**	**0.0303**	**0.0669**	**0.0292**	**0.0128**
DE	Max	1.3584	3.4505	1.0695	2.2264	1.0836	1.1282
	Avg.	1.3292	3.4029	1.036	2.1257	1.0378	1.1077
	Std.	**0.0063**	**0.0101**	**0.0055**	**0.0161**	**0.0099**	**0.0042**
DE Percent improvement over PSO		**73.4**	**87**	**81.9**	**75.9**	**65.9**	**67**
60 individuals, 400 iterations (PSO_{60-400}, DE_{60-400})							
PSO	Max	1.3788	3.6918	1.1554	2.3157	1.3049	1.1491
	Avg.	1.3327	3.4128	1.0391	2.1387	1.0466	1.1123
	Std.	**0.0119**	**0.0522**	**0.0188**	**0.0426**	**0.042**	**0.0102**
DE	Max	1.3343	3.4505	1.0377	2.2243	1.0696	1.1135
	Avg.	1.3279	3.4032	1.0344	2.125	1.0368	1.1062
	Std.	**0.0018**	**0.0108**	**0.0006**	**0.0154**	**0.0085**	**0.0016**
DE Percent improvement over PSO		**84.9**	**79.3**	**96.8**	**63.9**	**79.8**	**83.9**
100 individuals, 200 iterations ($PSO_{100-200}$, $DE_{100-200}$)							
PSO	Max	1.3757	3.8452	1.0892	2.2872	1.084	1.2467
	Avg.	1.3308	3.4286	1.038	2.1329	1.0391	1.114
	Std.	**0.0108**	**0.0907**	**0.0117**	**0.0371**	**0.0118**	**0.0207**
DE	Max	1.3546	3.6253	1.0466	2.152	1.0466	1.1133
	Avg.	1.3282	3.4069	1.0346	2.1221	1.0353	1.1063
	Std.	**0.0047**	**0.0332**	**0.0018**	**0.0048**	**0.003**	**0.0015**
DE Percent improvement over PSO		**55.8**	**63.3**	**84.8**	**87**	**74.4**	**92.5**
200 individuals, 200 iterations ($PSO_{200-200}$, $DE_{200-200}$)							
PSO	Max	1.4016	3.5392	1.096	2.2687	1.0809	1.1375
	Avg.	1.3297	3.4069	1.0374	2.126	1.036	1.1123
	Std.	**0.0118**	**0.0285**	**0.0122**	**0.0212**	**0.0081**	**0.0091**
DE	Max	1.3641	3.4247	1.0466	2.152	1.0374	1.1212
	Avg.	1.3294	3.4009	1.0347	2.1218	1.0343	1.1064
	Std.	**0.0071**	**0.0052**	**0.0018**	**0.0047**	**0.0004**	**0.0029**
DE Percent improvement over PSO		**40.1**	**81.8**	**85**	**77.9**	**94.6**	**68.3**

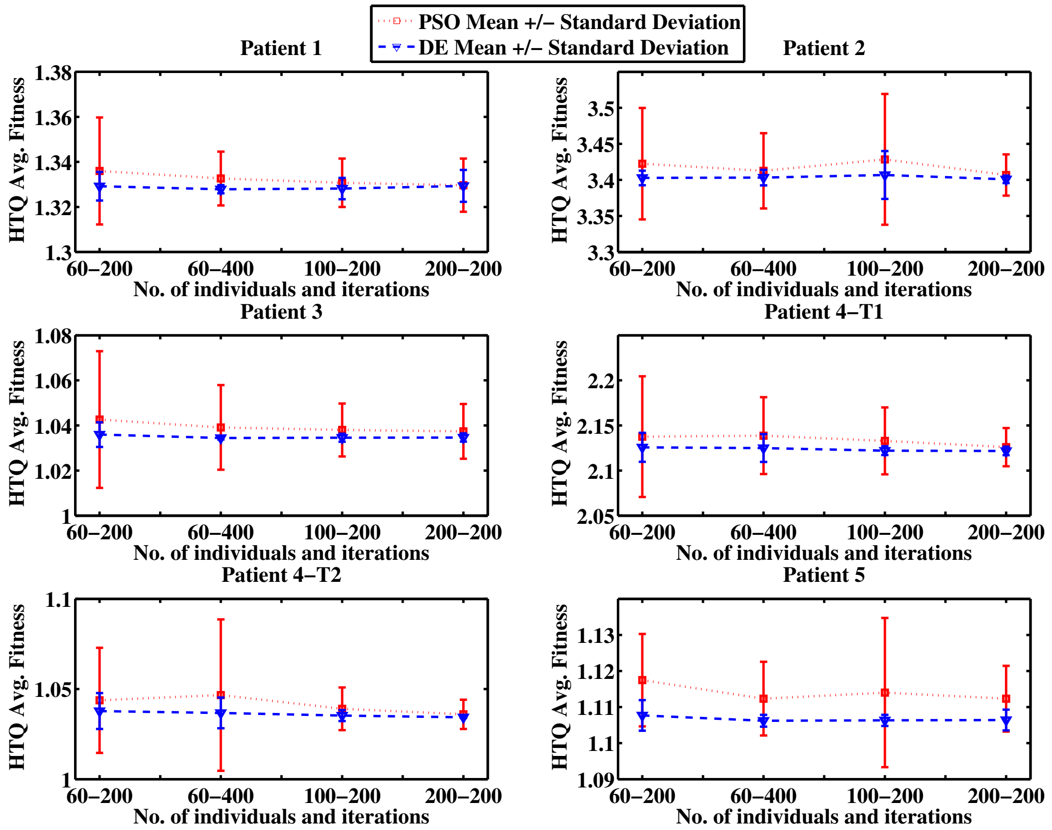

Figure 3.1: Mean and standard deviation values of the fitness solutions obtained by four PSO and DE configurations using 50 run samples for six patient records. PSO is in red, and DE in blue.

3.3.1.2 HTQ Metric in Clinical Settings

In this section, PSO and DE HTQ results are compared using a single parameter configuration from the previous results (selected among the four algorithm configurations). Since, as discussed in the previous section, the selection of optimisation parameters does not significantly affect algorithm performance, the setting of 60 individuals and 400 iterations was selected to compare with the VEDO software configuration in clinical use [51]. The PSO algorithm implemented in VEDO is referred to as PSO_{CS} while the chosen DE configuration is referred to as DE_{CS}.

The maximum percent errors between best and worst optimisation obtained by PSO_{CS} and DE_{CS} are shown in Table 3.8 and calculated as follows:

$$Max \quad Percentage \quad Error = \left| \frac{HTQ_{worst} - HTQ_{best}}{HTQ_{best}} \right| \times 100 \tag{3.6}$$

Table 3.8 reveals that the maximum percentage error between the best and worst fitness solutions of PSO_{CS} varies from 3.9% to 26.2%, whereas the maximum error of DE_{CS} ranges from 0.3 to 4.9%. Moreover, as illustrated in bold font in Table 3.8, the mean HTQ maximum error across all records is 10.6% and 1.9% for PSO_{CS} and DE_{CS} respectively. In agreement with the results presented in Table 3.7, these findings demonstrate that a more targeted and consistent heat focusing is achieved by DE_{CS} compared to the clinically-deployed algorithm.

Table 3.8: HTQ Maximum percentage errors for the PSO_{CS} and DE_{CS} optimisation strategies.

Patient no.	P1	P2	P3	P4-T1	P4-T2	P5	Error average (%)
PSO_{CS} max. percent error	3.9	8.6	11.7	9.2	26.2	3.9	**10.6**
DE_{CS} max percent error	0.5	1.5	0.3	4.9	3.4	0.7	**1.9**

3.3.1.3 HTQ Convergence Time

Convergence time to achieve the best HTQ has been calculated for PSO and DE. In general, DE exhibits faster convergence than PSO, over the 50 runs. Table 3.9 lists the number of iterations required for both DE and PSO to reach the best value achieved by PSO; this value is chosen as a common optimisation goal for the number of iterations for ease of comparison. DE converges faster than PSO for all configurations analysed, except for the $PSO_{200-200}$ setting, where PSO converges faster than DE in three out of the six patients (highlighted in bold in Table 3.9).

However, although PSO converges faster in these cases, DE still outperforms PSO when results at the stopping criterion are considered. Along with HTQ results, the computation time for a standard CPU (Intex X86) implementation of DE and PSO was investigated. Since PSO_{CS} and DE_{CS} evaluate an identical number of candidate solutions, the execution time of both optimisation approaches is similar.

The required optimisation time for one patient for PSO_{CS} is 79 s on average across all records, while DE_{CS} computation time is 94 s. Computation time on a

Table 3.9: Convergence rate for four PSO and DE individual and iteration configurations. Each result repressents the number of iterations required for DE and PSO to reach PSO's best solution.

	Patient no.	P1	P2	P3	P4-T1	P4-T2	P5
Iteration no.	PSO_{60-200}	165	129	150	147	132	180
	DE_{60-200}	76	72	70	84	67	49
	PSO_{60-400}	130	153	144	218	186	273
	DE_{60-400}	89	94	75	79	60	60
	$PSO_{100-200}$	132	120	116	164	90	158
	$DE_{100-200}$	89	67	73	79	75	48
	$PSO_{200-200}$	100	165	65	127	77	178
	$DE_{200-200}$	**138**	94	**82**	98	**90**	48

CPU points to the possibility of using a Graphical Processing Unit (GPU) accelerator as a useful computational platform. Initial GPU experiments, conducted as part of this research, suggest a speed-up factor of between 4 and 5 is achievable.

3.3.2 Performance of PSO versus DE as a Function of the SAR-Treatment Quantifiers

3.3.2.1 Mean and Standard Deviation of HTQ

The amplitudes and phases of the best solution achieved by the two optimisation methods using VEDO clinical settings, PSO_{CS} and DE_{CS}, are reported in Table 3.10.

3.3.2.2 SAR Treatment Quantifiers

The treatment quantifiers previously discussed in Section 2.7 have been used to evaluate the treatment quality and the performance of each HTQ optimisation algorithm. Tables 3.11 and 3.12 present TC_{25} and TC_{50} results. All antenna amplitudes are normalised between 0 and 1 in order to calculate the SAR for 1W total input power.

The variation between the best and worst case of the hyperthermia TC indicators, ΔTC, is reported in Tables 3.11 and 3.12. While PSO_{CS} reaches a range of ΔTC_{25} equal to 0-11%, across all the six records, the DE_{CS} ΔTC_{25} is smaller and equal

Table 3.10: Antenna amplitudes and phases of the best solution achieved by PSO and DE optimisations.

Best antenna amplitude and phase values											
P1		P2		P3		P4-T1		P4-T2		P5	
PSO	DE	PSO	DE	PSO	DE	PSO	DE	PSO	DE	PSO	DE
0.1	0.1	0.15	0.2	0.6	0.65	0.45	0.4	0.8	0.92	0.0001	0.00007
-40°	82.2°	-4.6°	-180°	-146.2°	-49.6°	-146°	56°	-171°	154.4°	10.3°	164°
0.06	0.06	0.74	0.97	0.6	0.64	0.73	0.66	0.8	0.9	0.008	0.006
-125°	-2.3°	132.6°	-43°	-66.4°	30.2°	69°	133°	-91.4°	-126°	54°	-145.4°
0.08	0.08	0.04	0.05	0.47	0.51	0.35	0.32	0.63	0.72	0.04	0.03
-28.2°	94.2°	32°	-143.3°	116.6°	-147°	138.4°	-20°	91.6°	57.3°	-134.5°	26.6°
0.43	0.43	0.63	0.83	0.63	0.69	1	0.9	0.85	0.97	0.98	0.77
51.3°	174°	143.1°	41°	40°	137°	39.6°	-118.5°	15°	-19°	16°	175.6°
0.05	0.05	0.07	0.09	0.2	0.21	0.16	0.15	0.26	0.3	0.01	0.01
-30.1°	92.4°	12°	-164°	-148.2°	-51.4°	-117.4°	84.4°	-173°	152.3°	-180°	-20.1°
0.16	0.16	0.54	0.71	0.12	0.13	0.04	0.04	0.16	0.2	0.02	0.01
-61°	62°	-179.5°	5°	3.4°	100.3°	-120°	82°	-21.3°	-56.5°	144°	-56°
0.12	0.12	0.25	0.33	0.25	0.27	0.01	0.01	0.33	0.4	0.01	0.01
103°	-134.6°	-85°	99°	98.6°	-164.5°	36°	-122.4°	74°	39.4°	159.3°	-40.1°
0.94	0.94	0.63	0.83	0.17	0.19	0.13	0.11	0.23	0.26	0.06	0.05
-106.4°	16°	117.2°	-58.6°	-68°	29°	-36°	166°	-92.5°	-127°	-7.2°	152.6°

to 0-4% for five patients. This means that DE can provide greater tumour SAR coverage and more uniform heating during the patient treatment. Moreover, TC_{50} varies from 0% to 11% in five patients for PSO_{CS} and from 0% to 3% in four out of the six patient records for DE_{CS}. Furthermore, in some cases (highlighted in bold) the worst solutions show a larger target coverage than the ones corresponding to the best fitness values. One reason for this is that HTQ accounts for energy deposited both in the tumour and in healthy tissue, while the TC metrics only consider the tumour region (without any regard to the healthy tissue). For this reason, HTQ performance can be improved with a small loss in TC in a small number of cases.

Table 3.11: TC_{25} Performance metric tested on six clinical records for the PSO and DE optimisation strategies. Percentage variation between best and worst cases are also given.

Patient no.	TC_{25} PSO_{CS} and DE_{CS} Best case (%)	TC_{25} PSO_{CS} Worst case (%)	TC_{25} DE_{CS} Worst case (%)	ΔTC_{25} PSO_{CS} (Best-worst case variation) (%)	ΔTC_{25} DE_{CS} (Best-worst case variation) (%)
P1	88	77	84	11	4
P2	17	10	**19**	7	**-2**
P3	89	85	88	4	1
P4-T1	96	85	89	11	7
P4-T2	89	**89**	85	**0**	4
P5	38	37	38	1	0
	ΔTC_{25} average (%)			5.6	2.3

Table 3.12: TC_{50} Performance metric tested on six clinical records for the PSO and DE optimisation strategies. Percentage variation between best and worst cases are also given.

Patient no.	TC_{50} PSO_{CS} and DE_{CS} Best case (%)	TC_{50} PSO_{CS} Worst case (%)	TC_{50} DE_{CS} Worst case (%)	ΔTC_{50} PSO_{CS} (Best-worst case variation) (%)	ΔTC_{50} DE_{CS} (Best-worst case variation) (%)
P1	25	16	22	9	3
P2	0	0	0	0	0
P3	32	**35**	**33**	**-3**	**-1**
P4-T1	29	18	27	11	2
P4-T2	32	28	29	4	3
P5	8	8	**9**	0	**-1**
	ΔTC_{50} average (%)			3.5	0.5

3.3.2.3 SAR Distributions

For each patient, the cubic filtered SAR distribution was plotted. While the HTQ results for all patients are presented in Section3.3.1, the cfSAR distributions of only three patients are presented here in the interest of brevity. The SAR maps related to the two methods are presented in Figures 3.2-3.7. The cfSAR distribution is visualised by varying the z coordinate on the transversal plane, where the direction of z is from the neck to the top of the head. For each patient, the coordinates specified in Figures 3.2-3.7 have been chosen according to the location of the tumour in the 3D patient model. The tumour is delineated in black in each map.

The cfSAR distributions in Figures 3.2-3.7 demonstrate that the PSO and DE hyperthermia optimisations are comparable in the best case optimisation, since both algorithms successfully locate the minimum of HTQ solution. However, in the worst case, DE better focuses the energy in the target area, compared to PSO.

Figures 3.2, 3.3 illustrate how for Patient 2, DE better focuses the heat more consistently in the target area over PSO, achieving respectively a HTQ maximum percentage error of 1.5% and 8.6% (as described in Table 3.8). Further, DE results in a greater TC_{25} in the worst case compared to the best one. This is because although there is a lower TC_{25} coverage in the tumour in the best case, the performance is compensated by the reduction in energy being transmitted to healthy tissue.

Also for Patient 4-T1 (first treatment) in Figures 3.4, 3.5 the DE optimisation results in a smaller HTQ value than PSO in the worst case. Maximum errors of 4.9% and 9.2% between the HTQ best and worst cases are observed with DE and PSO respectively. The DE ΔTC_{25} and ΔTC_{50} are also smaller than those of PSO. Patient 4-T2 (Figures 3.6, 3.7), refers to the second treatment of Patient 4. A substantial error of 26.2% is observed between the PSO best and worst scenarios, against a 3.4% error provided by DE. In the worst case optimisation, PSO presents a TC_{25} equivalent to that of the best case, with hotspots in the healthy tissue. This is not the case for DE, which shows better focusing in the worst case compared to PSO, despite of greater ΔTC_{25}.

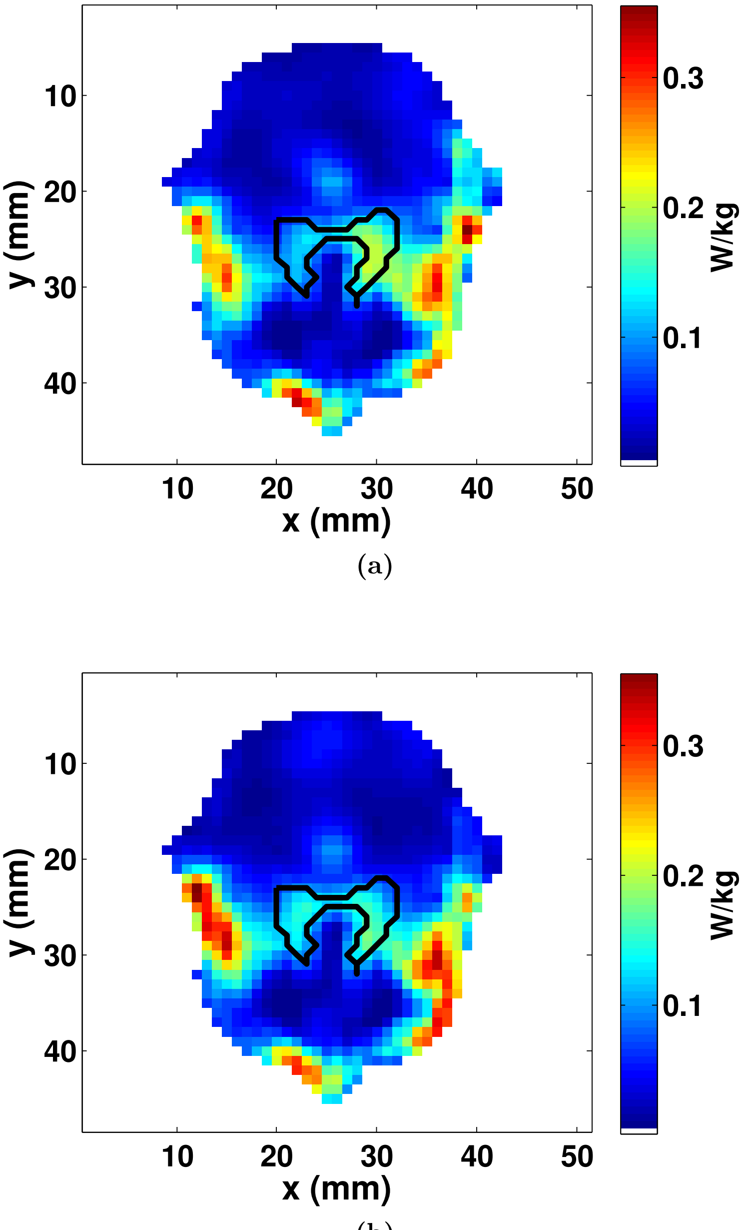

(a)

(b)

Figure 3.2: Cubic filtered SAR distributions in a transversal cut through the target location (z = 58 mm), using the optimised antenna and phase settings resulting from PSO_{CS} best (a) and worst optimisation (b) in patient P2.

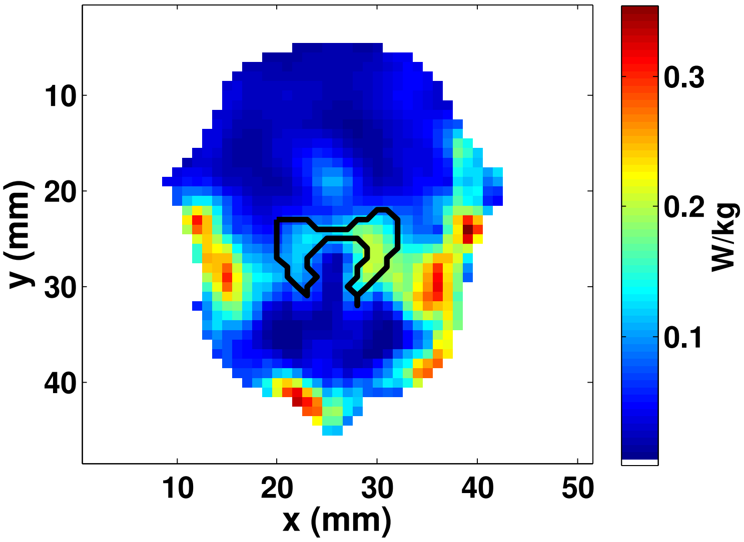

(a)

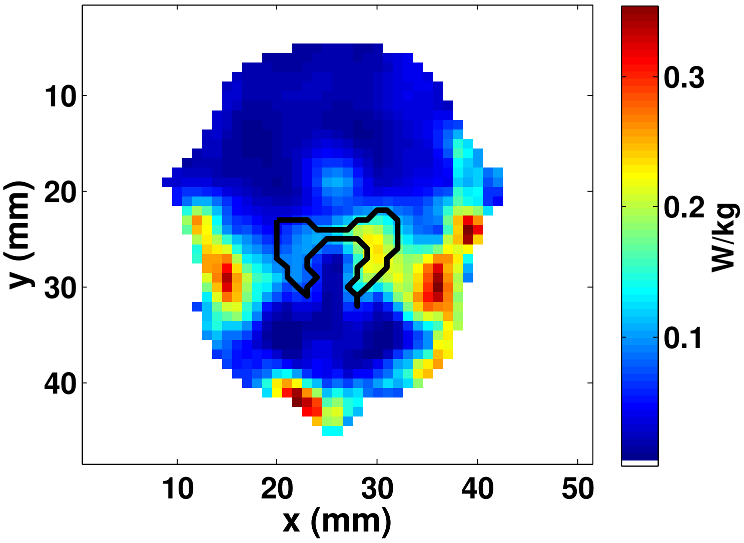

(b)

Figure 3.3: Cubic filtered SAR distributions in a transversal cut through the target location (z = 58 mm), using the optimised antenna and phase settings resulting from DE_{CS} best (a) and worst optimisation (b) in patient P2.

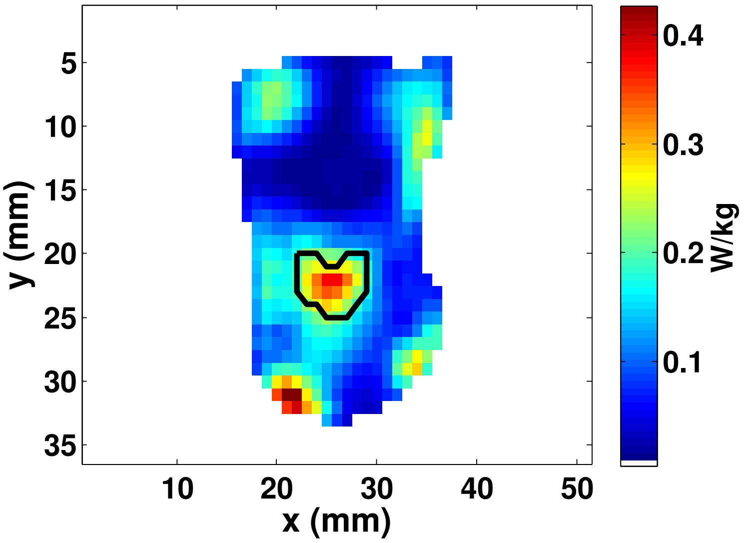

(a)

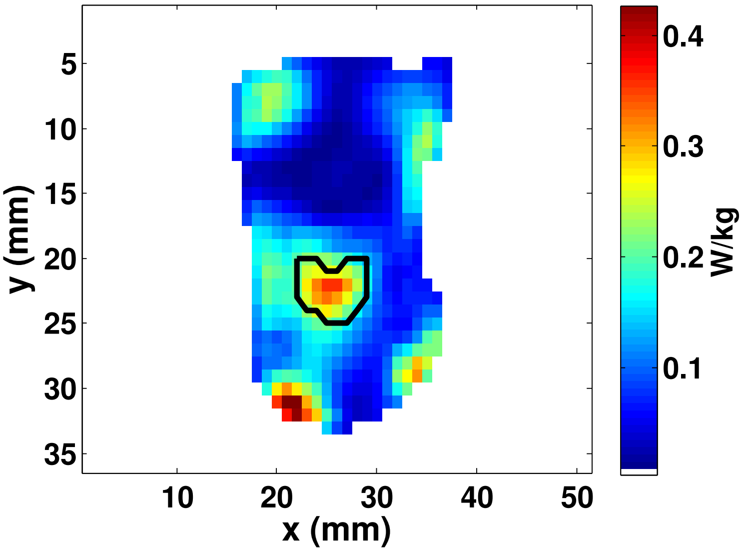

(b)

Figure 3.4: Cubic filtered SAR distributions in a transversal cut through the target location (z = 20 mm), using the optimised antenna and phase settings resulting from PSO_{CS} best (a) and worst optimisation (b) in patient P4-T1.

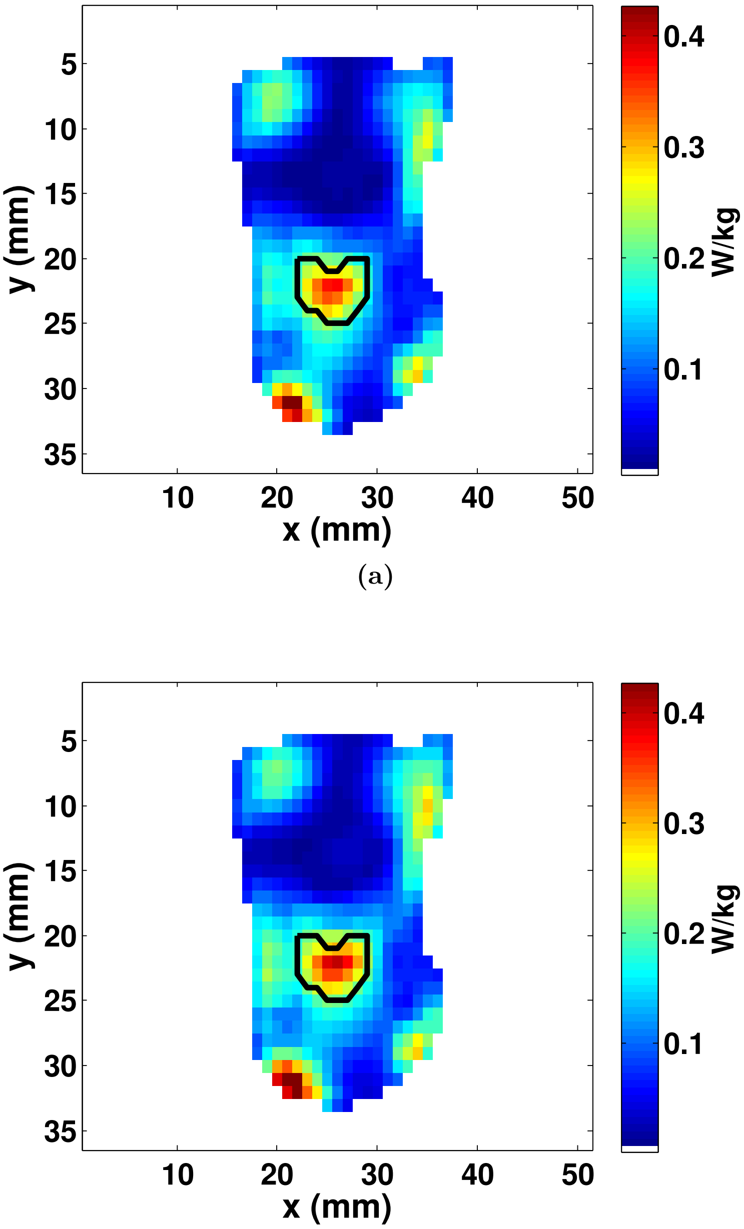

(a)

(b)

Figure 3.5: Cubic filtered SAR distributions in a transversal cut through the target location (z = 20 mm), using the optimised antenna and phase settings resulting from DE_{CS} best (a) and worst optimisation (b) in patient P4-T1.

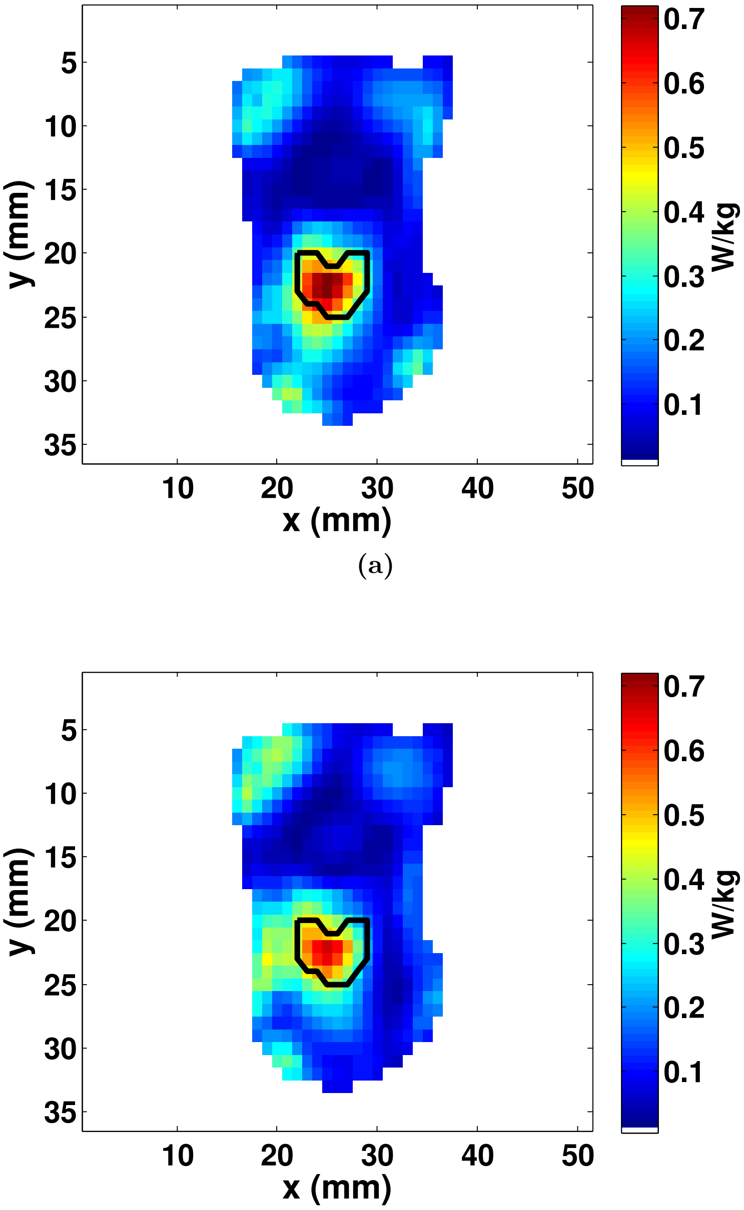

(a)

(b)

Figure 3.6: Cubic filtered SAR distributions in a transversal cut through the target location (z = 20 mm), using the optimised antenna and phase settings resulting from PSO_{CS} best (a) and worst optimisation (b) in patient P4-T2.

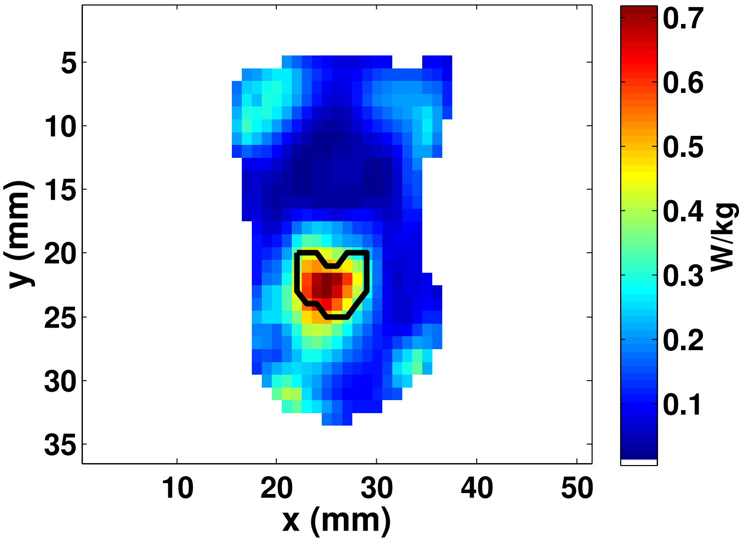

(a)

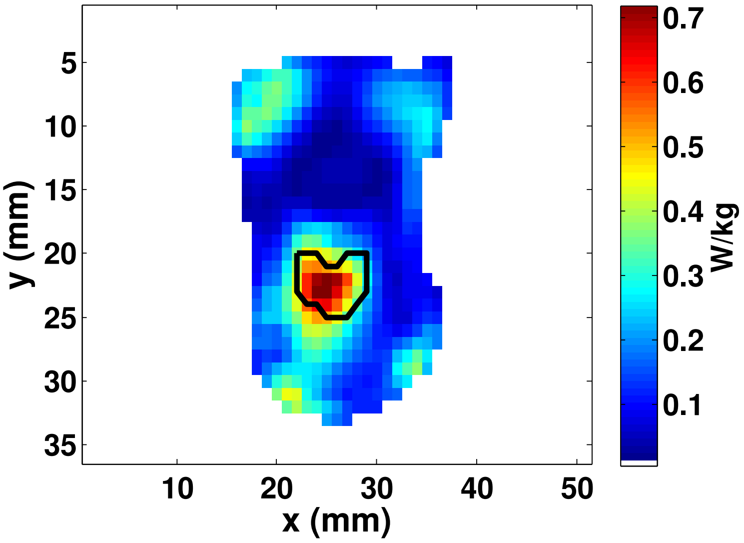

(b)

Figure 3.7: Cubic filtered SAR distributions in a transversal cut through the target location (z = 20 mm), using the optimised antenna and phase settings resulting from DE_{CS} best (a) and worst optimisation (b) in patient P4-T2.

3.3.3 Thermal Performance

Thermal modeling, which converts 3D SAR distribution to a 3D temperature field, has been performed to evaluate whether a therapeutic temperature of 40 °C is reached inside the tumour, while maintaining the temperature of the healthy tissue in a specific range. Cumulative Temperature-Volume (T-V) histograms and temperature indices were computed for PSO_{CS} and DE_{CS} in the best and worst cases for the six patients. The absorbed energy from the EM field simulation was used for the thermal calculations.

The cumulative T-V histograms related to the best and worst PSO_{CS} and DE_{CS} optimisations of three patients are illustrated in Figure 3.8. Temperature results for all records are reported in Table 3.13. The histograms show a tumour temperature difference between PSO_{CS} best (solid red) and worst (dash-dot red) case is observable in at least three out of the six records.

The corresponding temperature parameters, T_{90}, T_{50}, T_{10}, together with the maximum temperature, T_{max}, achieved in the tumour area, are listed in Table 3.13. The variations (ΔT) arising from best and worst PSO_{CS} and DE_{CS} optimisations are also reported in bold. In the worst case, PSO_{CS} shows an average ΔT_{max} of 0.9 °C (range 0.1 - 2.3 °C) over the best case and across all patients; in contrast, an average ΔT_{max} of 0.2 °C (range 0 - 1.1 °C) is measured between DE_{CS} best and worst optimisations. Also, the average variation of the temperature indices (ΔT_x) between best to worst was found to be higher for PSO compared to DE. An average ΔT_{10} equal to 0.7 °C and 0.2 °C is observed for PSO_{CS} and DE_{CS}, whose values range respectively from 0 °C to 2 °C and from 0 °C to 0.2 °C. Furthermore, PSO and DE report an average ΔTC_{50} equal to 0.5 °C (range 0 - 1.1 °C) and 0.1 °C (range -0.1 - 0.6 °C) across all the six data; whereas an average ΔT_{90} of 0.5 °C (range 0.2 – 1 °C) and 0.2 °C (range 0.1 - 0.6 °C) are measured for PSO_{CS} and DE_{CS}. The histograms also indicate that the temperature pattern in the healthy tissue remains the same for the best and worst optimisations both for PSO and DE. The median temperatures, T_{50}, in the healthy tissue range between 37 °C and 37.3 °C across all patients.

Table 3.13: T_{max} and temperature indices T_x that are exceeded by x percent of all temperature readings in the tumour target. T_{max} and T_x best and worst optimisation results arising from PSO_{CS} and DE_{CS} are given with their variation.

		T_{max} (°C)		T_{10} (°C)		T_{50} (°C)		T_{90} (°C)	
Patient no.		PSO	DE	PSO	DE	PSO	DE	PSO	DE
P1	Best	43.8	43.8	41.7	41.7	40.1	40.1	38.8	38.8
	Worst	43.7	43.8	41.7	41.7	39.9	40.1	38.6	38.7
	ΔT (°C)	**0.1**	**0**	**0**	**0**	**0.2**	**0**	**0.2**	**0.1**
P2	Best	40.6	40.6	38.7	38.7	38.7	38.7	36.8	36.8
	Worst	39.5	40.6	38.4	38.6	38	37.8	36.6	36.7
	ΔT (°C)	**1.1**	**0**	**0.3**	**0.1**	**0**	**0.2**	**0.2**	**0.1**
P3	Best	40.3	40.3	39.7	39.7	39.2	39.2	38.5	38.5
	Worst	39.6	40.3	39	39.7	38.6	39.3	37.6	38.4
	ΔT (°C)	**0.7**	**0**	**0.7**	**0**	**0.6**	**-0.1**	**0.9**	**0.1**
P4-T1	Best	43	43	41.2	41.2	39.9	39.9	39.3	39.3
	Worst	40.7	41.9	39.2	40.2	38.8	39.3	38.3	38.7
	ΔT (°C)	**2.3**	**1.1**	**2**	**1**	**1.1**	**0.6**	**1**	**0.6**
P4-T2	Best	43.4	43.4	41.9	41.9	40.1	40.1	39	40
	Worst	43.3	43.3	41.5	41.7	39.9	39.9	38.6	39.7
	ΔT (°C)	**0.1**	**0.1**	**0.4**	**0.2**	**0.2**	**0.2**	**0.4**	**0.3**
P5	Best	43.5	43.5	39.9	39.7	38.2	38.2	34.9	34.9
	Worst	42.4	43.4	39.2	39.7	37.4	38.2	34.4	34.8
	ΔT (°C)	**1.1**	**0.1**	**0.7**	**0**	**0.8**	**0**	**0.5**	**0.1**
$\Delta T_{average}$ (°C)		**0.9**	**0.2**	**0.7**	**0.2**	**0.5**	**0.1**	**0.5**	**0.2**

Overall, the temperature measurements data support the better performance of the DE algorithm, where smaller differences were found between the best and the worst optimisations.

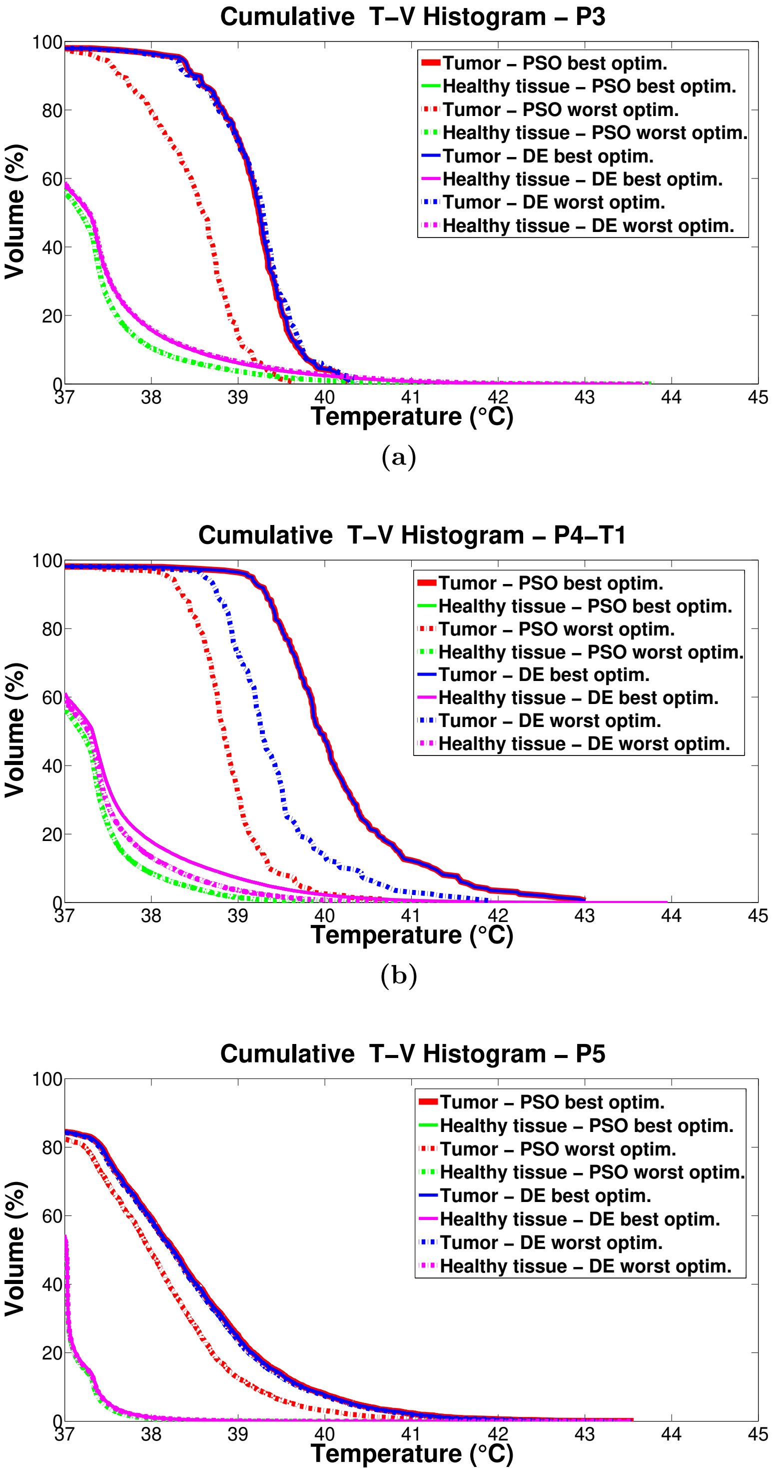

(a)

(b)

(c)

Figure 3.8: Cumulative Temperature-Volume (T-V) histograms representing the 3-D temperature distribution within the tumour and healthy tissue for patient 3 (a), 4-T1 (b), and 5 (c). Best (solid line) and worst cases (dash-dot line) for PSO_{CS} and DE_{CS} are illustrated.

3.4 Discussion

The success of microwave hyperthermia in H&N cancer treatment is strongly dependent on the power levels of the RF signals used for each antenna of the applicator. The DE optimisation algorithm proposed in this chapter provides improvements over the clinically used PSO in terms of SAR coverage and thermal performance. Although both algorithms achieve the same optimal SAR distribution, i.e. the minimum value of the objective function HTQ over 50 runs, DE outperforms PSO in the worst optimisation. This translates into a better focus of the energy in the target and minimisation of energy in the hotspots. This is confirmed by temperature results, which indicate smaller temperature differences between best and worst optimisation. More specifically, average temperature variation of 0.5 °C and 0.1 °C were observed in T_{50} for PSO and DE respectively. According to [113], [114], differences on the order of 0.3 °C in CTV temperature are relevant in clinical practice. DE optimisation leads to higher CTV temperatures in the worst case compared to PSO and hence a better treatment outcome. Therefore, thermal results show a significant clinical benefit of the DE optimisation.

There has been substantial research on the most appropriate measure to use for optimisation in HTP. As mentioned above, the optimisation algorithms presented in this work minimise HTQ and the treatment is evaluated through a set of treatment quality indicators. In fact, the study by Canter *et al.* [26] found that HTQ was a good SAR optimisation function and correlated best with the temperature compared to other SAR indicators. The parameters TC_{25} and TC_{50} were also used to assess the quality of the treatment in terms of SAR results and the temperature-based quality parameters. For H&N hyperthermia, Verhaart *et al.* [105] demonstrated that T_{50} can be predicted with a median accuracy of 0.8 °C, even when neglecting the temperature dependence of tissue cooling. Thermal modeling is highly affected by uncertainties; however, the thermal properties of tissues used in this work were validated using temperatures measured by thermometer probes which were placed interstitially [45].

3.5 Conclusions

In this chapter, a DE optimisation method for SAR distribution for H&N hyperthermia treatment was presented. DE generates a set of parameters which allows for the application of an optimal HT SAR distribution in the target treatment area of the patient. The SAR distribution was investigated in a set of data from patients treated by the HYPERcollar system in the clinic of Erasmus MC. The optimum amplitude and phase of each applicator's antenna are found by minimising an objective function, in order to focus the energy in the tumour while reducing hotspots in the surrounding healthy area.

DE is compared to the PSO optimisation technique across four algorithm parameter settings. While results illustrate that both algorithms are capable of finding an optimal power distribution, the proposed DE algorithm provides an improvement over the PSO algorithm used at the hyperthermia unit of Erasmus MC, by more frequently and consistently locating the global optimum for all studied patients. DE performs better in terms of HTQ average and standard deviation, gaining HTQ average and standard deviation improvements of 0.02-0.94% and 40.1-96.8% respectively across all patients. The clinically-employed version of PSO, PSO_{CS}, was compared to DE and the best and worst optimisations produced by the two algorithms were analysed in terms of HTQ, TC and temperature performance metrics. The best and worst DE_{CS} optimisations exhibit an average HTQ error of 1.9% compared to the 10.6% average error obtained by PSO_{CS}. Similar trends are found for TC and thermal variations.

The computation time for a standard desktop computer implementation of DE and PSO was also determined. The convergence rate for PSO and DE configurations was found to be similar, with average values of 79 s and 94 s respectively across all patients. The DE algorithm was not entirely optimised for speed purposes and was slightly slower than PSO, though there is scope for further optimization for efficiency.

Despite the improvements obtained with DE, there is scope for improvement. In the following chapter, the development and application of time-multiplexed hyperthermia will be described, in order to further improve the tradeoff between tumour heating and the generation of hotspots. A multi-objective genetic algorithm is introduced together with the formulation of a novel objective function to obtain multiple optimal heating patterns applied sequentially.

4

Time-Multiplexed Steering in Phased Array Microwave Hyperthermia for Head and Neck Cancer Treatment

4.1 Introduction

In the previous chapter, a Differential Evolution (DE) optimisation algorithm was proposed in order to improve the SAR and heating of the target region while reducing hotspots. The efficacy of the proposed algorithm was demonstrated by testing with a H&N cancer patient dataset from Erasmus MC. DE resulted in enhanced focus of microwave energy absorption to the target region during hyperthermia treatment. In particular, DE offered improved performance over the current clinically-used Particle Swarm Optimisation (PSO), by more frequently and consistently locating the global optimum for all patients in the data set. These results were confirmed by thermal simulations.

In this chapter, sequential, i.e. “time-multiplexed”, application of multiple optimal heating patterns is presented to further improve the tradeoff between increased tumour heating and reduced hotspots. A Multi-Objective Genetic Algorithm (MOGA) is introduced to balance two objectives that both focus SAR delivered to the target region but differ in the suppressing of pre-defined hotspots.

This step leads to two optimal solutions for antenna settings. These antenna settings are then applied sequentially and thermal simulations are used to evaluate the effectiveness of the time-multiplexed steering.

The proposed technique is tested using treatment planning data of a representative dataset of five H&N cancer patients for the HYPERcollar3D system, provided by the Erasmus MC hyperthermia group. Steering dynamics are analysed and the time-multiplexed steering is compared to the current static solution used in the clinic, i.e. HTQ optimisation using PSO. The results demonstrate the ability to enhance target heating while reducing hotspots and provides a better time-averaged treatment quality. The work described in this chapter is published in Cappiello *et al.*, "The potential of time-mulitplexed steering in phased array microwave hyperthermia for head and neck cancer treatment," *Physics in Medicine and Biology*, Vol. 63, Issue 13, July 2018 [115] (© Institution of Physics and Engineering in Medicine. Reproduced with permission. All rights reserved. DOI: 10.1088/1361-6560/aaca10).

The reminder of this chapter is organised as follows: Section 4.2 describes the methodology used to implement time-multiplexed steering in the phased array hyperthermia applicator, and the method used for performance analysis and the dataset used in this work. The MOGA implementation, the formulation of the novel objective function and the thermal model are also described in this section. Section 4.3 reports SAR and thermal results from the performance evaluation. Finally, the conclusions are presented in Section 4.5.

4.2 Methodology

This section introduces the time-multiplexed steering for H&N hyperthermia. Firstly, the basic principle of the multi-objective genetic algorithm is described; then, a novel objective function to suppress a pre-defined hotspot is formulated, after which the thermal model employed to carry out the thermal evaluation is discussed. Lastly, the time-multiplexed steering procedure for H&N hyperthermia is presented.

4.2.1 Multi-Objective GA Optimisation

Multi-Objective Genetic Algorithms (MOGAs) [116] apply a heuristic search and optimisation technique that can solve multi-objective problems while promoting diversity within the solutions. In most instances, there will not be a solution which is best (globally maximum or minimum) over all objectives. A MOGA generates a set of Pareto optimal solutions which may favor one objective at the expense of the others. The Pareto optimal solutions are defined as those solutions that dominate other solutions in the search space when all objectives are considered. Hence, an optimal solution can be selected based on tradeoffs between all objectives. Mathematically, the Pareto-optimality problem [117] can be posed as follows:

$$minimise \quad f\left(x\right) = f_1\left(x\right), f_2\left(x\right), ..., f_n\left(x\right) \tag{4.1}$$

where n is the number of the objective functions, and x is a vector of m decision variables: $x = x_1, x_2, ..., x_m$ in the solution space X. In a minimisation problem, given two vectors x and y, a solution x dominates another solution y if:

$$f_i\left(x\right) \leq f_i\left(y\right) \quad for\ i = \{1, ..., n\} \tag{4.2}$$

$$f_j\left(x\right) < f_j\left(y\right) \quad for\ at\ least\ j = \{1, ..., n\} \tag{4.3}$$

i.e. solution x dominates solution y if x is no worse than y in all objectives and x is strictly better than y in at least one objective. A solution is called non-dominated if none of the objective functions can be improved in value without worsening one or more objective functions. The set of all non-dominated solutions in X represents the Pareto optimal set and the plot of the objective functions is referred to as the Pareto Front [118], [119].

The MOGA used in this study is a variant of the fast Non-dominated Sorting Genetic Algorithm (NSGA-II) [116], [118]. NSGA-II starts by initializing a population of random candidate solutions, called individuals. The population is sorted in two groups (known as fronts), a first non-dominant front and a second front dominated by the individuals in the first front. The individuals in both fronts are ranked based on a quality measure called the “fitness value”, which indicates how close a given solution is to the optimum solution for the specific problem. Next, the distance between each individual and the other individuals in the front is calculated. This distance is known as the crowding distance and it is used to promote diversity whereby a larger crowding distance will encourage greater diversity in the population. The distance between individuals is calculated as the Euclidian distance between their respective solution vectors ($x1$ and $x2$). A new population is created by selecting “parents” based on the crowding distance and the fitness value. Crossover and mutation operators are applied to form the new “offspring”. Then, the offspring population is compared with the current population to ensure that only individuals that are superior to their parents (either by fitness value or crowding distance) progress to the next generation. This process is known as elitism.

The algorithm proposed in this work follows the same implementation as NSGA-II except that the elitism mechanism is slightly different. NSGA-II favors individuals with strictly better fitness value, while the proposed MOGA uses a version of elitism which improves both the fitness and the diversity of the population by examining both in the selection process.

The relation between MOGA solutions and the hyperthermia parameters to be optimised is similar to that described in Section 3.2.2 where each candidate solution is represented by the antenna array amplitude and phase configurations. Although the HYPERcollar3D consists of 20 antennas, only 12 amplitudes and phases are optimised in HTP since the number of operational channels is currently constrained by the number of available power amplifiers in the system [120]. The 12 antennas selected for the treatment are those that individually achieve the highest mean SAR in the target region [45]. This set of 12 antennas is fixed throughout all simulation experiments.

4.2.2 Hotspot Specific Objective Function

In this section, a novel objective function, the total Hotspot-Target SAR Quotient for a specific HotSpot (HTQ_{HS}), is formulated to suppress a specific hotspot that occurs in the healthy tissue. The HTQ_{HS} is defined as:

$$HTQ_{HS} = \frac{SAR_a\left(V_{HS}\right)}{SAR_a\left(target\right)} \tag{4.4}$$

where $SAR_a\left(V_{HS}\right)$ $(W \cdot kg^{-1})$ is the mean SAR in the hotspot volume V_{HS}. V_{HS} represents the region of the healthy tissue volume outside the CTV with the highest SAR in the H&N patient model. Therefore, MOGA minimises the two objective functions, HTQ and HTQ_{HS} and gives rise to a set of Pareto optimal antenna parameters that individually provide different SAR levels in the CTV and in the hotspots.

4.2.3 Temperature Simulations

To evaluate the performance of time-multiplexed hyperthermia, temperature simulations were carried out in SEMCAD X using the Pennes' bio-heat equation described in Section 2.7. As in previous research reported in Chapter 3, transient thermal simulations were carried out using the dielectric and thermal properties indicated in Table 3.6. Constant values of thermal conductivity and blood perfusion for muscle, fat and tumour tissue used in [105] have been used in this study. The total input power was tuned to reach the maximum temperature of 44 °C in the healthy tissue outside the CTV and/or 40 °C in critical organs (eyes, brains and spinal cord). A mix of convective and Neumann boundary conditions was applied as in Section 3.2.5.

4.2.4 Time-Multiplexed Steering Procedure

In this section, the methodology adopted to implement time-multiplexed steering for H&N hyperthermia is described. The methodology can be divided into three parts.

4.2.4.1 SAR-Temperature Correlation

For each patient, PSO optimisation was performed to get the best amplitude and phase settings that minimise HTQ; as noted before, these settings are referred to as StaticS. Then, the EM distributions of individual antenna were combined and the cubic filtered SAR (cfSAR) was calculated. The resulting absorbed energy was used to obtain the 3D temperature distribution. Finally, the coefficient of determination, R^2, was calculated to measure how well the highest simulated cfSAR values approximate the simulated temperatures above 40 °C in the healthy tissue, and to determine the most appropriate method for hotspot selection. R^2 was calculated based on the difference between the temperature values for HTQ optimised antenna settings and the predicted temperature values and is defined as:

$$R^2 = 1 - \frac{\sum_1^n (y_i - f_i)^2}{\sum_1^n (y_i - y_{av})^2} \tag{4.5}$$

where n is number of voxels in the hotspot volume, y_i are the observed temperature values, f_i are the predicted temperature values from the fit, y_{av} is the mean of the observed temperature data. R^2 is a measure of how well the regression line agrees with the observed temperature values. The smaller the second term is, the closer to the fit the observed data are, hence the closer the value of R^2 is to 1 [121].

4.2.4.2 SAR Optimisation

A multi-objective optimisation was performed to find the best time-multiplexed antenna settings. In a single application of the method, MOGA is able to find Pareto optimal antenna settings that yield multiple SAR distributions. The SAR fields differ in the amount of energy absorbed in the target and in the hotspot. For each patient, one Pareto Optimal Solution (PoptS) was identified to supply a balance between establishing sufficient SAR in the target and SAR reduction in the hotspot. Then, two antenna settings, StaticS and PoptS were sequentially combined to form the time-multiplexed configuration.

4.2.4.3 Thermal Evaluation

In order to assess the effectiveness of time-multiplexed hyperthermia the static and the time-multiplexed thermal performance were compared. A resolution of 2 mm was used for the thermal solver. First, the thermal simulations with StaticS and PoptS were run individually to obtain the total input power required for each static configuration. Then, the thermal simulation for time-multiplexed steering was run applying two antenna settings in the sequence StaticS followed by PoptS and the total input power of the combined steering settings was tuned. As noted

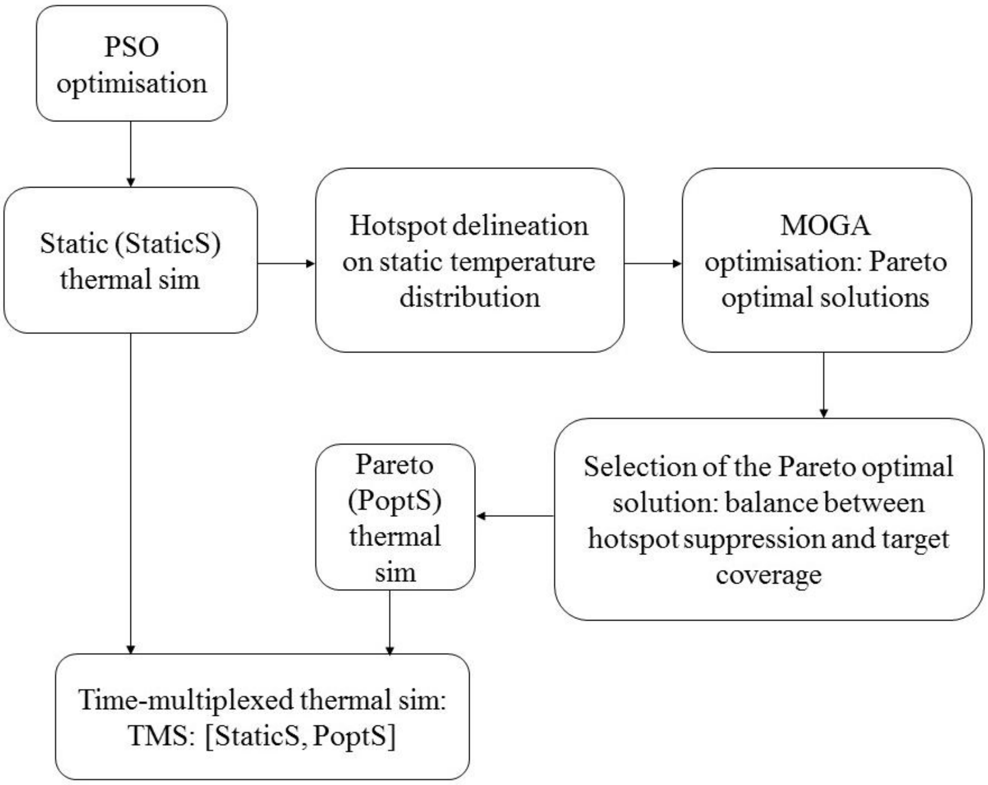

Figure 4.1: Schematic workflow of the time-multiplexed steering procedure. Two antenna settings, StaticS and PoptS, are applied sequentially in the time-multiplexed thermal simulation

above, total power was tuned to achieve the maximum temperature of 44 °C in the healthy tissue and/or 40 °C in critical organs. The sequence was repeated throughout the simulation period which was set to 1200 s. This value was found empirically to be sufficient to reach steady-state conditions.

The overall methodology is given in Figure 4.1. The steering rate was also investigated and defined as the time duration for which each antenna setting has to be applied to guarantee stable hotspot suppression and enhance heat delivery to the tumour.

4.2.5 Experimental Dataset and Evaluation Parameters

4.2.5.1 Patient models

Patient models treated using the HYPERcollar3D system in Erasmus MC have also been used in this study. The HYPERcollar3D system [49], [122] has been developed at Erasmus MC for hyperthermia treatment of deep-seated tumours in the head and neck region. The applicator is a re-designed version of the HYPERcollar system [18], [47] and consists of 20 patch antennas operating at a frequency of 434 MHz and arranged in three antenna rings (Figure 2.9).

From the group of the patients subject to treatment using the HYPERcollar3D at Erasmus MC, five patient models were selected, fully anonymised and used in this study (henceforth referred to as Patient 1 to Patient 5). The patient group selection was based on the prevalence of hotspots in the optimal SAR distribution, i.e. worst case scenarios were chosen for the StaticS cases. The hotspot occurrence was also verified in the thermal pattern. The patient group included two oropharynx tumours, one neck node metastasis, one parotid gland and one oral cavity tumour in four males and one female with mean age of 62.6 years.

4.2.5.2 Evaluation Parameters

As noted before, quantifying the quality of hyperthermia treatment is challenging. Applicators are usually compared in terms of their ability to focus the SAR. In the clinic, the temperature rise or cumulative equivalent minutes at 43 °C are used [123]–[125] but thermal simulations are affected significantly by uncertainties in thermal tissue parameters. For H&N cancer, these tissue properties were recently examined and it was shown that T_{50} can be predicted with good accuracy [105]. Hence, since time-multiplexed hyperthermia exploits the relatively large time constant of tissue cooling for averaging different SAR patterns that are applied in a sufficiently fast sequence, its performance was analysed both in terms of SAR and temperature simulation based quantifiers described in Section 2.7.

4.3 Results

In this section the results obtained by applying time-multiplexed hyperthermia are discussed. Firstly, the SAR-temperature correlation is analysed to select the hotspots. Then, PSO and MOGA are compared in terms of SAR indicators and

SAR distributions. Finally, thermal performance of static and time-multiplexed configuration is discussed.

4.3.1 SAR-Temperature Correlation

The hotspots were accurately defined before performing MOGA. An analysis was conducted to decide if the hotspots should be defined based on SAR or temperature. Figure 4.2 plots cfSAR values against temperature using the static settings for Patient 1 and shows the fitted regression line. The prediction model (red linear fit) does not fit the observed data well, and very low correlation was found ($R^2 = 0.13$). The observed temperature values lie in the 95% confidence interval of [40.8 °C, 43.7 °C]. R^2 values for all other patient models were in the range of 0.2 and 0.6. Hence, hotspot selection was based on the temperature distribution and the region with the highest temperature (i.e. 44°C) was delineated.

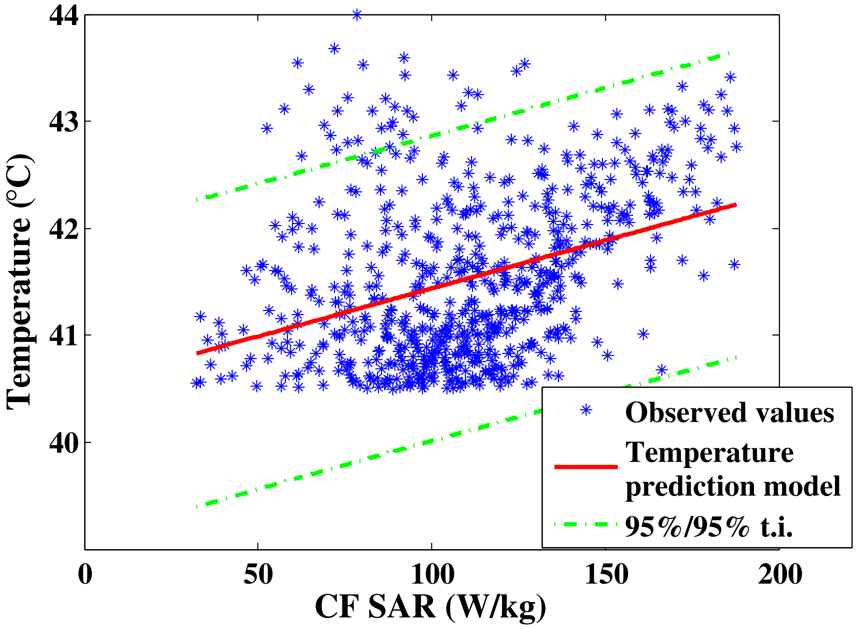

Figure 4.2: Simulated cubic filtered SAR and corresponding temperature values (after 20 minutes of simulation) for HTQ optimised antenna settings. Linear fits and R^2 values are shown for Patient 1.

4.3.2 SAR Performance of MOGA against PSO

In order to find the best solution from the set produced by MOGA, MOGA solutions were compared with the static solution, in terms of energy reduction in the hotspot, HTQ and TC metrics. The cfSAR distributions were also obtained for each patient. Thus, SAR results are presented in three parts.

4.3.2.1 Pareto Optimal Solutions

For each patient model, the MOGA optimisation was run to select the Pareto solution (PoptS) that maintained adequate focusing in the target region, i.e. $TC_{25} \geq 75\%$ [51] and provided substantial hotspot energy reduction, i.e. 30-60% SAR reduction compared to the HTQ optimised distribution for all patients. Figure 4.3 shows the set of solutions returned by MOGA when HTQ and HTQ_{HS} are minimised for Patient 1, together with the chosen PoptS solution for that patient.

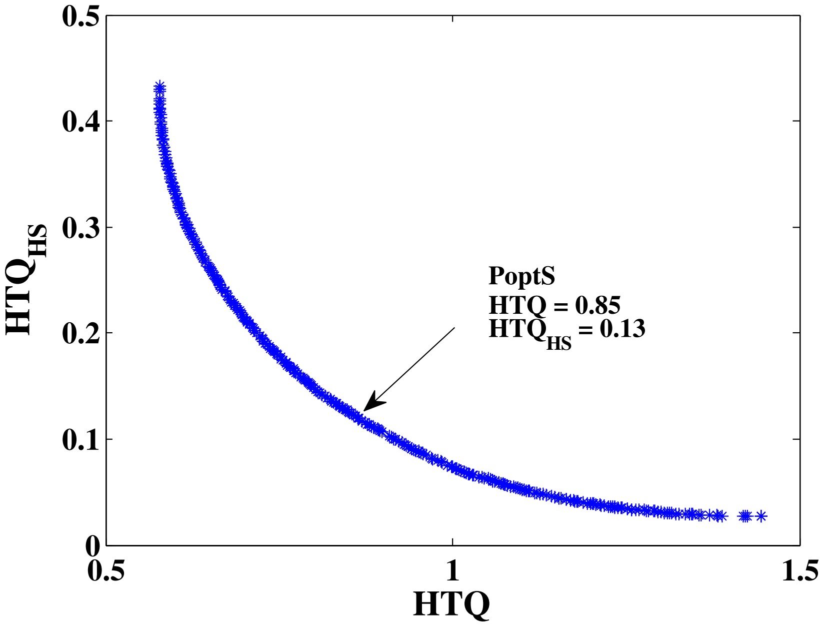

Figure 4.3: Simulated cfSAR and corresponding temperature values (after 20 minutes of simulation) for HTQ optimised antenna settings. Linear fits and R^2 values are shown for Patient 1.

4.3.2.2 SAR Quantifiers

Tables 4.1 and 4.2 report SAR performance quantifiers calculated using static and Pareto settings applied individually. Results show higher HTQ values for the Pareto solutions compared to the static solution, meaning a non-optimal ratio between the energy in the healthy tissue and in the target. However, this is counteracted by much lower HTQ_{HS} values, i.e. reduction of 59-71%, and hence more effective suppression of the energy in a specific area by the PoptS. The Pareto solutions reach a range of improvement over the static solution equal to 8-17% for TC_{25} (3/5 patients) and 3-25% for TC_{50} (4/5 patients). For two patient models, no TC_{25} improvement or reduction was found compared to the static results and TC_{50} was reduced by 15% for one patient.

Table 4.1: HTQ performance metric for static and Pareto solutions and percentage variation tested on 5 patient models.

Patient no.	HTQ		ΔHTQ	HTQ_{HS}		ΔHTQ_{HS}
	StaticS	PoptS	PoptS - StaticS (%)	StaticS	PoptS	PoptS - StaticS (%)
P1	0.57	0.85	+49.1	0.45	0.13	-71%
P2	0.45	0.54	+20	0.22	0.09	-59%
P3	0.29	0.39	+34.5	0.42	0.14	-67%
P4	0.46	0.80	+74	0.78	0.27	-65.4%
P5	0.39	0.52	+33.3	0.78	0.26	-66.7%

Table 4.2: TC_{25} and TC_{50} performance metrics for static and Pareto solutions and percentage variation tested on 5 patient models

Patient no.	TC_{25} (%)		ΔTC_{25}	TC_{50} (%)		ΔTC_{50}
	StaticS	PoptS	PoptS - StaticS (%)	StaticS	PoptS	PoptS - StaticS (%)
P1	82	82	0	65	50	-15
P2	99	99	0	81	84	+3
P3	73	90	+17	32	57	+25
P4	89	97	+8	25	42	+17
P5	73	90	+17	30	35	+5

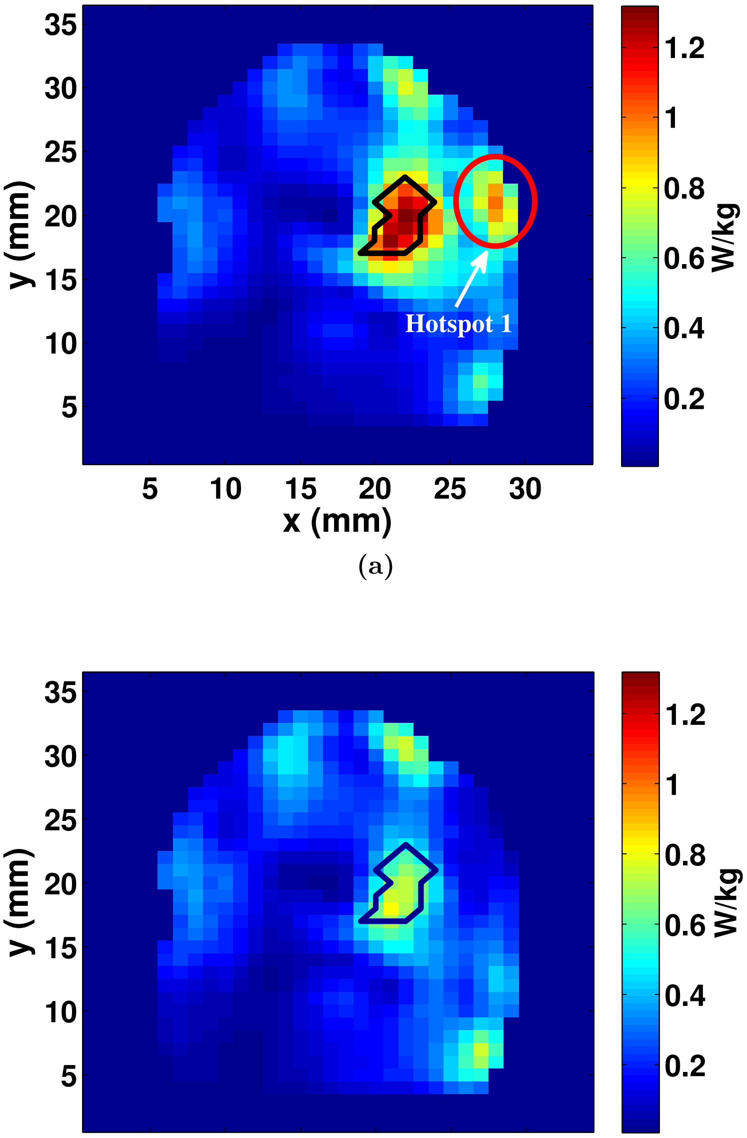

(a)

(b)

Figure 4.4: Normalised cfSAR distributions for 1W input power in the transversal cut at $z = 35$ mm through the target location obtained by the StaticS (a) and PoptS antenna settings (b) for Patient 1.

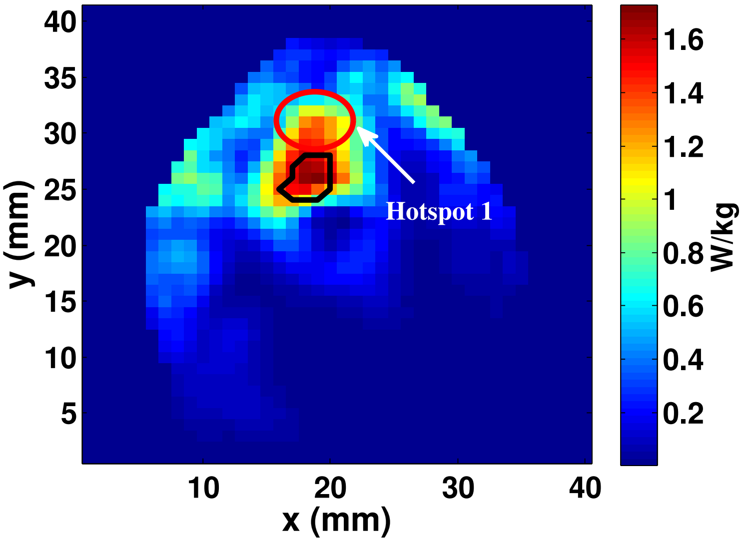

(a)

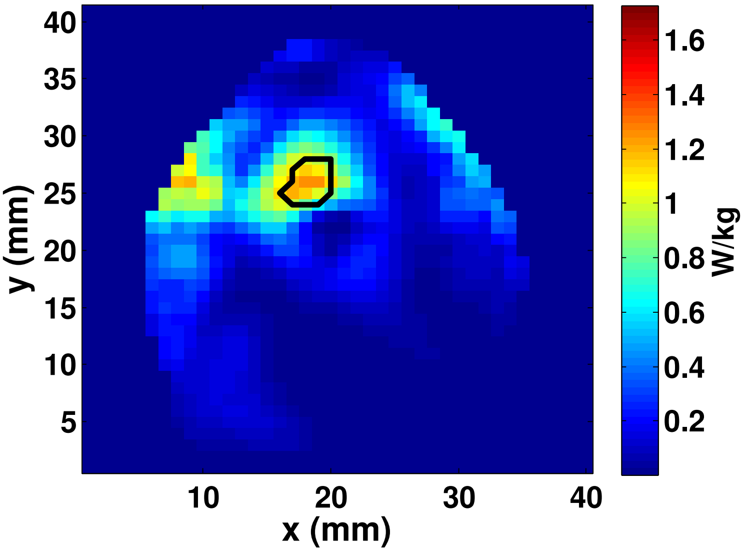

(b)

Figure 4.5: Normalised cfSAR distributions for 1W input power in the transversal cut at $z = 31$ mm through the target location obtained by the StaticS (a) and PoptS antenna settings (b) for Patient 2.

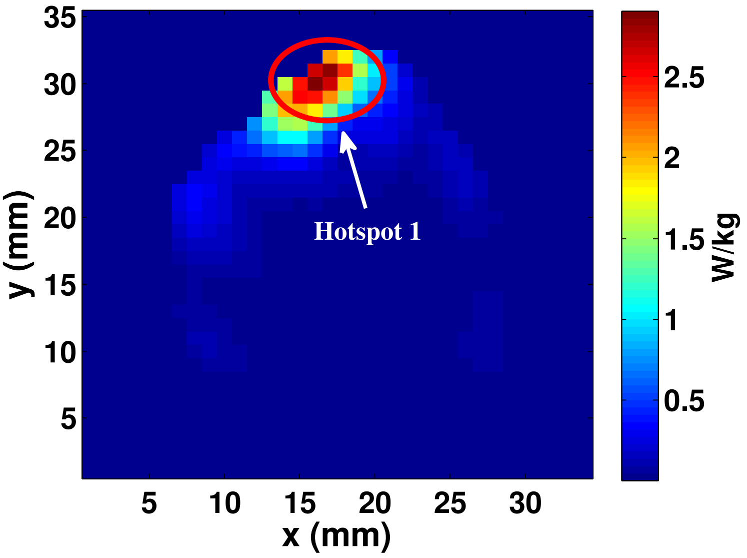

(a)

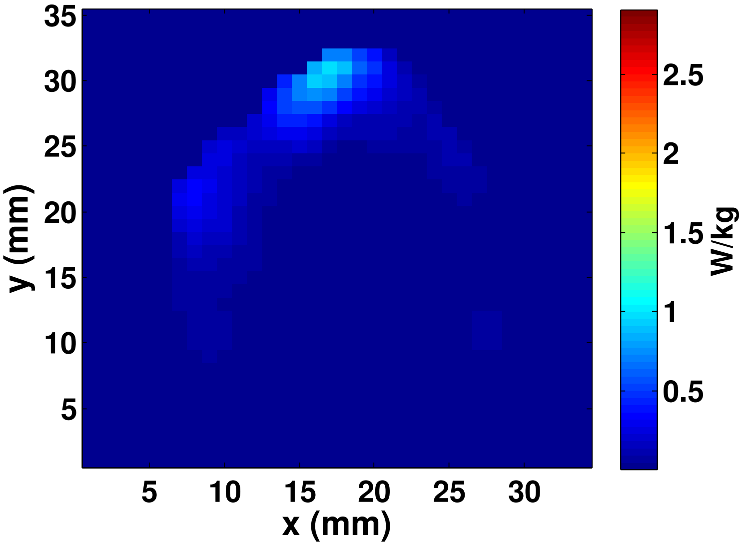

(b)

Figure 4.6: Normalised cfSAR distributions for 1W input power in the transversal cut at $z = 32$ mm obtained by the StaticS (a) and PoptS antenna settings (b) for Patient 3.

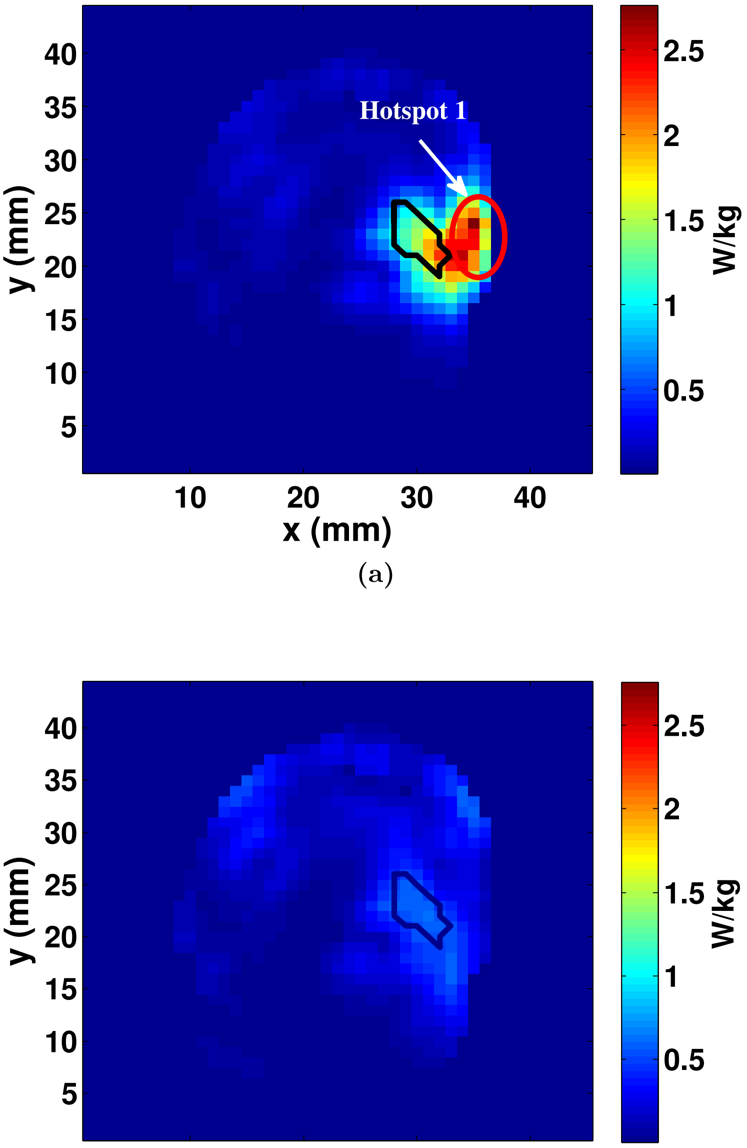

(a)

(b)

Figure 4.7: Normalised cfSAR distributions for 1W input power in the transversal cut at $z = 40$ mm through the target location obtained by the StaticS (a) and PoptS antenna settings (b) for Patient 4.

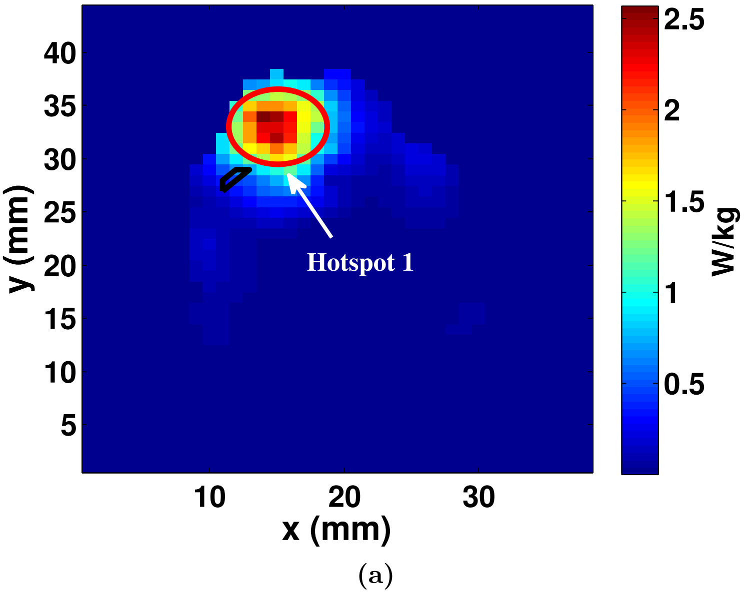

(a)

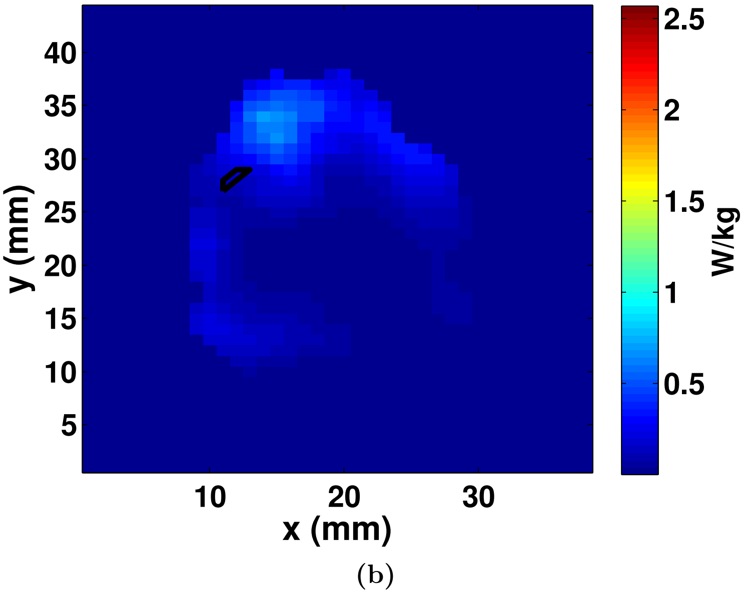

(b)

Figure 4.8: Normalised cfSAR distributions for 1W input power in the transversal cut at $z = 43$ mm through the target location obtained by the StaticS (a) and PoptS antenna settings (b) for Patient 5.

4.3.2.3 SAR Distribution

Figures 4.4a, 4.4b show two cross sections of normalised energy profile in the 3D model of Patient 1, obtained by the StaticS and PoptS settings. The CTV region is delineated in black and the most prominent hotspot (Hotspot 1) in red. While the hotspot is evident in the cfSAR map in Figure 4.4a for the StaticS case, the cfSAR map for PoptS in Figure 4.4b clearly shows the suppression of energy in the primary hotspot, still maintaining a good SAR coverage in the target when using MOGA. However, other hotspots arise in the healthy tissue in Figure 4.4b; the significance of these new hotspots is assessed by the thermal simulation and discussed later in this chapter. In general, the same behavior was observed with Patients 2, 3, 4 and 5. For example, the suppression of Hotspot 1 is also observed as shown in Figures 4.5-4.6-4.7-4.8.

4.3.3 Thermal Performance of Static and Time-multiplexed Configurations

4.3.3.1 Time-Multiplexed Steering Speed

Thermal simulations were carried out using SEMCAD X, wherein a point sensor was placed in the hotspot and in the CTV to track the temperature over time during the thermal simulation. Figure 4.9a illustrates the temperature of the tumour as a function of time, while Figure 4.9b shows the temperature of the hotspot recorded in Patient 1. The figures show the temperature evolution for the static settings (StaticS and PoptS), as well as temperatures applying the time-multiplexed settings at a total cycle time of 10, 40 and 120 s (i.e. where each individual solution is applied for 5, 20 or 60 s). Time-multiplexing periods of 10 s (red curve) or 40 s (green curve) ensured a stable temperature in the CTV, within 0.04 °C and 0.2 °C respectively, and prevented high peak temperatures. Total cycle time of 120 s resulted in a temperature ripple of 0.4 °C. Further, the simulation period of 1200 s was found to be sufficient to attain steady-state temperature in the five patient models. Figure 4.9 also shows the benefit of the time-multiplexed steering approach in the target region for Patient 1, with the temperature increased by 0.3 °C in the CTV and reduced by 1.4 °C in the hotspot.

The overall power for time-multiplexed steering was tuned to reach maximum temperature of 44 °C in the healthy tissue and allow fair comparison with the static solutions. This power tuning also compensates for the decrease in temperature observed in the CTV for the PoptS solution as shown in Figure 4.9a. This results in suppression of a specific hotspot, an increase in the temperature to 44 °C at a different location of the healthy tissue volume, and further, a temperature increment in the CTV. The results for time-multiplexed steering using a 10 second period will be discussed in more detail in the next section.

4.3.3.2 Cumulative Temperature-Volume histograms and thermal quantifiers

Static and time-multiplexed hyperthermia performance were compared for all five patients using cumulative T-V histograms. The temperature in the CTV and in the most prominent hotspot, Hotspot 1, was calculated based on the static temperature distribution. Temperatures of additional hotspots arising during time-multiplexed steering were also estimated. Thermal indicators for all clinical records are reported in Table 4.3, together with the variation (ΔT) arising from static and time-multiplexed methods. Examples of cumulative T-V histograms are shown in Figure 4.10. Consideration of the behaviour for each patient now follows.

Patient 1. The time-multiplexed steering technique provides a temperature increase equal to 0.3 °C in the CTV compared to the static method, while decreasing the temperature in Hotspot 1 from 44 °C to 42.9 °C, as indicated in Table 4.3. However, total input power was tuned to achieve a maximum temperature of 44 °C in the healthy tissue in the thermal simulation. Therefore, additional hotspots can occur in the healthy tissue during time-multiplexed steering and reach equal or higher maximum temperature compared to the maximum temperature in Hotspot 1 achieved by the static method. In fact, T_{max} of Hotspots 2 and 3 shows increases of 0.8 °C and 1.5 °C, although their median values are maintained below the CTV temperatures.

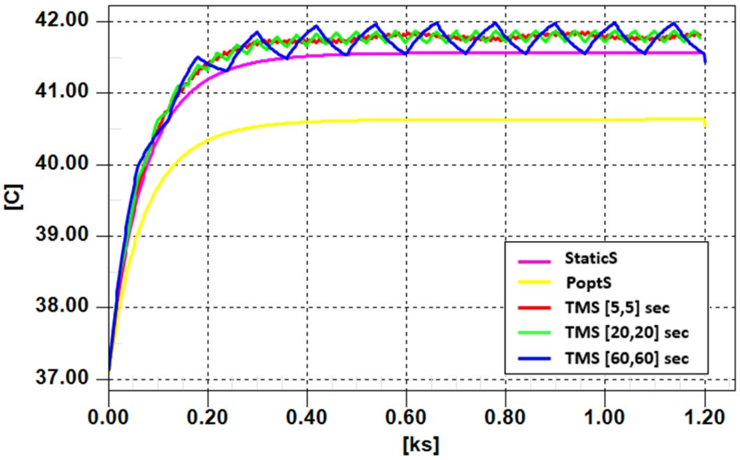

(a)

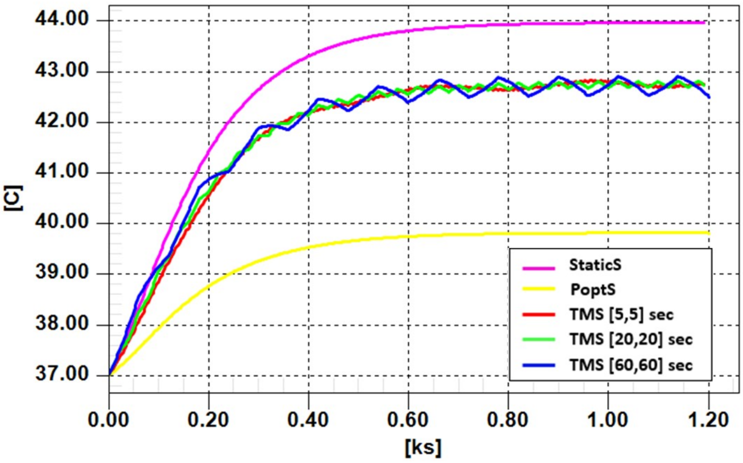

(b)

Figure 4.9: Point temperature (degrees Celsius) in the CTV (a) and in Hotspot 1 (b) over the simulation period of 1200 s (axis is labelled in kiloseconds as produced by SEMCAD X). Static (magenta), Pareto optimal (yellow) and time-multiplexed thermal performance are compared varying the steering rate of five (red), twenty (green) and sixty (blue) seconds.

Patient 2. A target temperature gain equal to 1 °C was observed when time-multiplexed steering is applied. The temperature of Hotspot 1 drops by 1.5 °C. Hence, a second hotspot is heated without exceeding the target median values. The temperature difference between static (solid) and time-multiplexed (dash-dot) configurations for Patient 2 is shown in Figure 4.10a.

Patient 3. Similarly, Patient 3 reports a CTV temperature improvement of

0.5 °C, a reduction of 1.5 °C in Hotspot 1 and a maximum temperature rise of 0.9 °C in a different healthy region.

Patient 4 and 5. The time-multiplexed approach increases the target temperature of 1.2 °C and 0.8 °C while suppressing Hotspot 1 by 0.6 °C and 1 °C and raising Hotspot 2 temperatures by 0.1 °C and 1.9 °C, respectively for Patients 4 and 5.

Across all patients studied, time-multiplexed hyperthermia provides a reduction in the hotspot average maximum temperature of 1.2 °C, at the expense of raising the maximum temperatures in other hotspots, although maintaining their median values below the CTV temperatures. The proposed method also provides a benefit through an average improvement of T_{50} in CTV about 0.8 °C.

Table 4.3: Thermal quantifiers T_x that are exceeded by x percent of all temperature readings in the CTV for a selection of worst cases treated with the HYPERcollar3D and T_{max} in the hotspots. Temperature changes from *StaticS* (single SAR steering) to TMS (time-multiplexed steering) are given in bold.

Patient no.	Antenna settings	CTV $T_{50}(°C)$	Hotspot 1 $T_{max}(°C)$	Hotspot 2 $T_{max}(°C)$	Hotspot 3 $T_{max}(°C)$
P1	StaticS	40.4	44	43.1	42
	TMS	40.7	42.9	43.9	43.5
	$\Delta_{TMS-StaticS}(°C)$	**+0.3**	**-1.4**	**+0.8**	**+1.5**
P2	StaticS	41.7	43.7	41.3	
	TMS	42.7	42.2	43.7	
	$\Delta_{TMS-StaticS}(°C)$	**+1**	**-1.5**	**+2.4**	
P3	StaticS	40.2	42.9	42.7	
	TMS	40.7	41.4	43.6	
	$\Delta_{TMS-StaticS}(°C)$	**+0.5**	**-1.5**	**+0.9**	
P4	StaticS	40.3	43.7	43.6	
	TMS	41.5	43.1	43.7	
	$\Delta_{TMS-StaticS}(°C)$	**+1.2**	**-0.6**	**+0.1**	
P5	StaticS	39.9	43.7	42	
	TMS	40.7	42.7	43.9	
	$\Delta_{TMS-StaticS}(°C)$	**+0.8**	**-1**	**+1.9**	

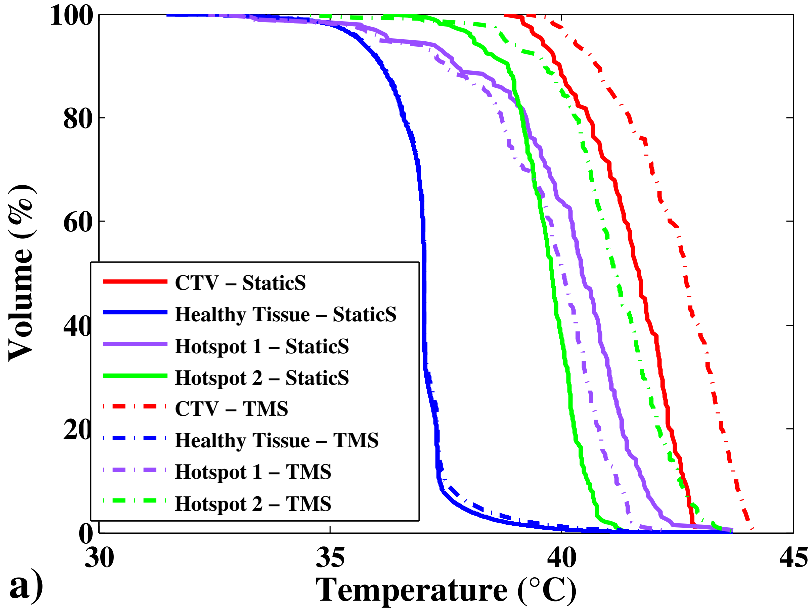

(a)

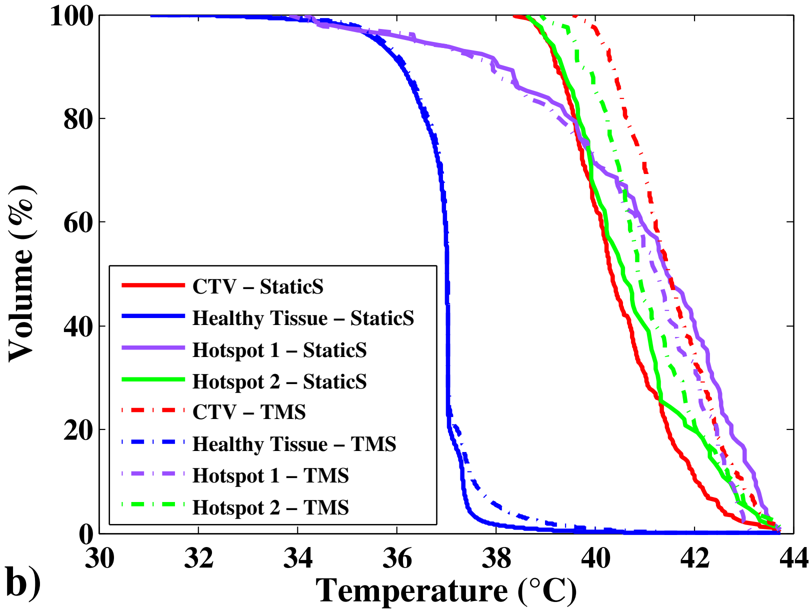

(b)

Figure 4.10: Cumulative Temperature-Volume (T-V) histograms representing the 3D temperature distribution within CTV (red), healthy tissue (blue), Hotspot 1 (violet), Hotspot 2 (green) for Patient 2 (a) and Patient 4 (b). The static (solid line) and the time-multiplexed (dash-dot line) thermal performances are compared. Hotspots 2 (green) arising in Patient 2 during time-multiplexed steering is also illustrated in (a).

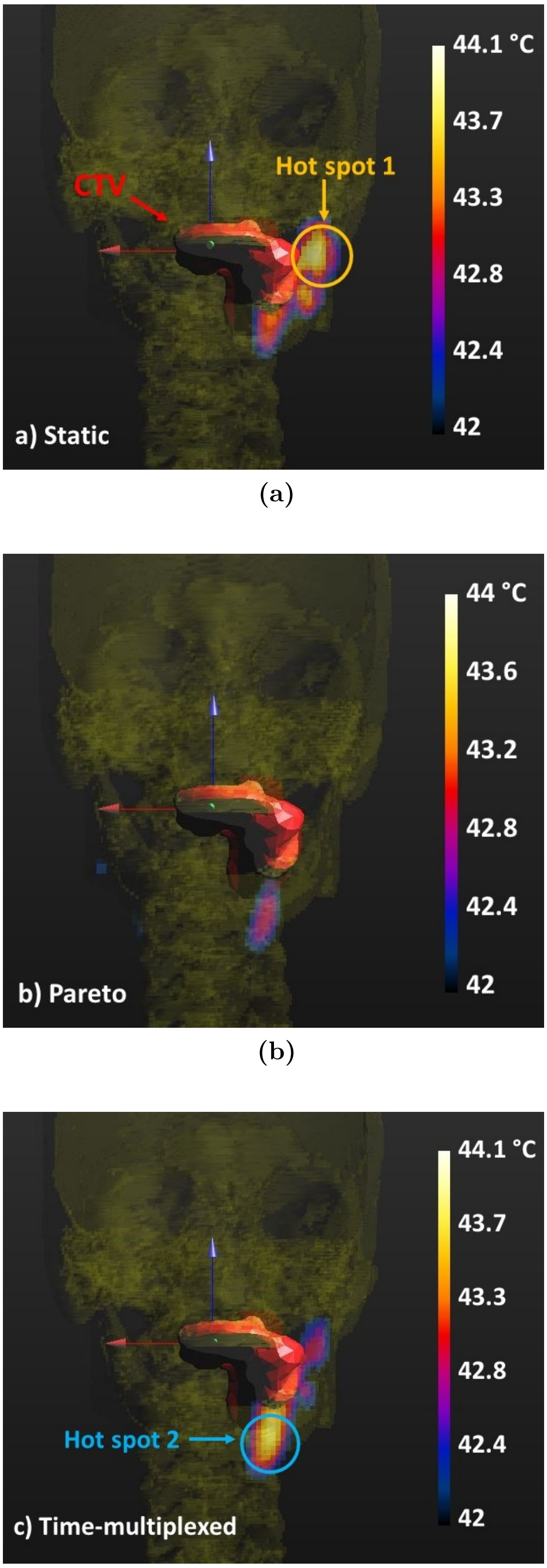

(a)

(b)

(c)

Figure 4.11: Patient 1. Simulated 3D temperature distribution (range of 42-44.1 °C) on a coronal view obtained through the static (a), selected Pareto (b) and time-multiplexed (c) settings. Figures were produced by SEMCAD X software. CTV and Hotspot 1 are indicated in (a). Hotspot 1 suppression is evident in (b). Hotspot 1 reduction and the Hotspot 2 appearance are shown in (c) while a T_{50} gain of 0.3 °C is achieved in the target region.

4.3.3.3 Temperature Distributions

Figure 4.11 shows the temperature patterns (range of 42-44.1 °C) after 20 minutes of irradiation predicted by SEMCAD X for Patient 1 when using static, the selected Pareto solution by itself, and time-multiplexed settings. The CTV and Hotspot 1 are highlighted in the static distribution(Figure 4.11a). In Figure 4.11b, it can clearly be seen that Hotspot 1 is totally suppressed, while a second region is being heated. Then, the temperatures of the new hotspot increases when time-multiplexed steering is applied until the occurrence of Hotspot 2; however, Hotspot 1 remains at a lower temperature than in the static temperature pattern (Figure 4.11c).

4.4 Discussion

For time-multiplexed hyperthermia treatment, the characteristics of the applicator system are important. One of the great difficulties in hyperthermia systems in maintaining amplitude and phase stability during the whole hyperthermia treatment are well known problems. However, the work of [48] showed excellent phase (±5°) and amplitude (5%) stability of the Erasmus MC custom-made amplifier system. Furthermore, the progress in RF amplifier technology has made possible devices with improved efficiency that absorb less power and hence have even greater stability. These developments point to the feasibility of the techniques described in this chapter.

An important aspect addressed in this work concerned the correlation between SAR and temperature. Previous research has also examined the correlation between SAR and temperature, with varying conclusions.

Several studies [126]–[129] show a good correlation between SAR and temperature. For example, Hirata and Fujiwara [126] studied the correlation in head models using a generic dipole antenna, and found SAR averaged over 10 g correlated well with local temperature increase for frequencies from 3 to 6 GHz. Razmadze *et al.* [128] studied the mass-averaged SAR and the correlation with temperature elevation using a full-body numerical model exposed to plane waves in the frequency range between 30 MHz and 800 MHz. Results showed that better correlation with temperature was obtained with an averaging mass of 10 g.

On the other hand, other studies have also found a weak correlation between SAR and temperature, in common with the investigations in this thesis. For example, Hirata *et al.* [130] investigated the correlation between peak spatial-average SARs and maximum temperature increase for different SAR averaging schemes and masses. The correlation was obtained by using two head models and a dipole antenna was used as a wave source at different frequencies. Results showed a weak correlation in the brain tissue when using 1 g and 10 g averaged SAR. Samaras *et al.* [131] investigated the uncertainty in the temperature calculations due to tissue composition and thermal properties in the head of mobile phone users. Frequencies of 900 MHz and 1800 MHz were examined. They found that the maximum temperature rise in the brain was not correlated to maximum 10 g averaged SAR in the head.

Most of the aforementioned studies reported that the average SAR over 10 g correlates well with the temperature rise when models are exposed to high frequencies from a dipole antenna. However, our scenario is different in that a lower frequency was used (434 MHz vs $\geq$ 800 MHz), a phased array was applied and heating was done to maximum tolerance (max 44°C vs max 38°C). In our simulations, steady state was reached within 20 minutes while other studies report longer periods to reach steady state. Further, the cooling effect by the water bolus in H&N hyperthermia can also affect the SAR temperature correlation particularly in the hotspots near to the skin. Therefore, a direct comparison between previous studies and our specific scenario is difficult. Our analysis indicates that the correlation between SAR and temperature is low and SAR cannot be readily used to assess hotspot location and intensity during H&N hyperthermia.

Further research is needed to establish the true correlation for this specific scenario. However, overall, the results obtained in this chapter indicate the clinical potential of this approach.

4.5 Conclusions

In this chapter, time-multiplexed hyperthermia was proposed for the treatment of H&N cancers and compared with the static method clinically deployed at Erasmus MC, using 3D models derived from five patients treated by HYPERcollar3D.

Sequentially applied SAR patterns were used as the source for thermal simulations. MOGA was used for the optimisation of HTQ and HTQ_{HS} to find the time-multiplexed setting of amplitudes and phases, the so called Pareto optimal solutions, whereas PSO of HTQ was used to optimise the static settings. SAR results obtained by MOGA indicate the feasibility of applying time-multiplexed hyperthermia.

Time-multiplexed hyperthermia for H&N cancers showed improved performance over the static method clinically deployed at Erasmus MC. A substantial gain of the CTV temperatures is observed, which indicates that more effective heat focusing to the target volume is possible for these five patients. The temperature simulations predict a reduction in the average maximum temperature (-1.2 °C) and hence a clinically relevant average improvement in target temperatures, i.e. 0.8 °C in T_{50}. SAR results obtained by MOGA, i.e. TC_{25} values grater than 75% and hotspot energy suppression indicate the potential of time-multiplexed steering via MOGA optimisation. From this analysis, a steering period of ten seconds is found to be sufficient to ensure a stable temperature increment in the target (< 0.1 °C).

In the following chapter, the robustness of time-multiplexed hyperthermia will be tested against thermal tissue properties variation by using a thermal dependent perfusion model.

5

Robustness of Time-multiplexed Hyperthermia to Temperature Dependent Thermal Tissue Properties

5.1 Introduction

As discussed previously, the principal need in hyperthermia treatments is to optimally focus the heating into the target while protecting the surrounding healthy tissue. Patient-specific treatment planning is done to optimise the specific absorption rate and the resulting temperature distribution. Uncertainties related to the thermal model used for temperature simulations present another important challenge. For example, uncertainty exists as to the exact thermal properties of tissues and as to whether SAR or temperature simulations are a better basis for optimisation. Additionally, neither the mechanism for heat dissipation in tissues, nor changes in perfusion with respect to temperature, are fully understood.

The previous chapter proposed a time-multiplexed steering procedure and evaluated its performance using several sets of real patient data. The procedure was found to result in better performance than a static procedure based on a single solution. The previous chapter assumed constant thermal properties. In this chapter, the benefits of time-multiplexed hyperthermia are further evaluated using temperature dependent thermal properties. The work evaluates the robustness of the time-multiplexed hyperthermia algorithm from Chapter 4 using the thermal dependent perfusion model developed in [132].

The remainder of this chapter is organised as follows: Section 5.2 describes the methods, including the different sets of thermal properties used for evaluation. Section 5.3 presents the results and compares the temperature distributions achieved using constant and temperature-dependent perfusion properties. Finally, Section 5.5 concludes the chapter.

5.2 Methodology

In this section, the time-multiplexed steering, previously introduced in Chapter 4, is reviewed, together with the thermal models employed to perform the thermal evaluation. The criteria adopted to test the robustness of the method are also described.

5.2.1 Temperature Properties

To assess the robustness of time-multiplexed hyperthermia, temperature simulations were performed in SEMCAD X using the Pennes' bio-heat equation [83] where a Scaling Factor (SF) is used to implement a temperature dependent blood perfusion model [132], [133]:

$$\rho c\frac{\partial T}{\partial t} = \bigtriangledown \cdot (k \bigtriangledown T) + \rho Q + \rho S - SF\rho_b c_b \rho\omega\,(T - T_b) \tag{5.1}$$

where T $({}^oC)$ is the temperature, t (s) is the time, ρ $(kg \cdot m^{-3})$ is the volume density of mass, c $(J \cdot kg^{-1} \cdot^{\circ} C^{-1})$ is the specific heat capacity, k $(W \cdot m^{-1} \cdot^{o} C^{-1})$ is the thermal conductivity, ω $(m^3 \cdot s^{-1} \cdot kg^{-1})$ is the volumetric blood perfusion rate, Q $(W \cdot kg^{-1})$ is the metabolic heat generation rate, S $(W \cdot kg^{-1})$ is the SAR and the subscript b indicates a blood property. Transient thermal simulations were done using the tissue dielectric and thermal properties reported as detailed in Chapter 3 (3.6). Previous research has shown that the response of vasculature in tissues to heat stress depends on the temperature [133]. In this chapter, two different cases are considered:

- Constant values of blood perfusion and thermal conductivity for muscle, fat and tumor tissue were optimised in [105]. This is referred to as the Constant Thermal Model (CTM).

- Temperature dependent perfusion [104]: blood perfusion for muscle was piecewise linearly scaled by a factor of 8.9, for fat by a factor of 2 and for tumor by a factor of 0.5 between temperatures of 37 °C and 45 °C as indicated in Figure 5.1. Temperature-dependent perfusion was modelled only for muscle, fat and tumour; for other tissues, the scaling factor is equal to 1 [104]. This is referred to as the Thermal Dependent Perfusion Model (TDPM).

The manner in which the thermal properties vary with temperature is taken into account in the thermal behaviour of the tissue by the inclusion of the scaling factor SF in equation 5.1. Figure 5.1 shows the linear temperature dependent perfusion scaling factors for fat, muscle and tumor. The blood perfusion increases between 37 °C and 45 °C for fat and muscle. This is described by sigmoidal curves consisting of a Gaussian profile followed by a plateau for temperatures above 45 °C. In contrast, the blood perfusion in the tumor decreases with temperature.

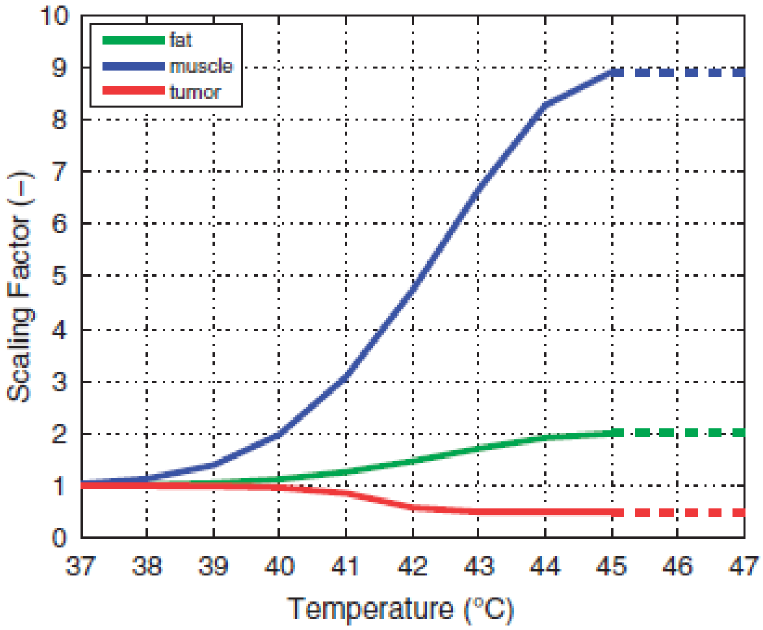

Figure 5.1: Linear temperature dependent perfusion scaling factors for fat, muscle and tumour [104].

To evaluate the robustness of time-multiplexed hyperthermia, results obtained using the CTM and the TDPM have been compared. The same procedure that was used in Chapter 4 was applied with both thermal models (CTM and TDPM), and is summarised here for completeness:

- Individual StaticS thermal simulations were run for 1200 s to obtain the total input power required to reach the maximum temperature of 44 °C in the healthy tissue and/or 40 °C in critical organs (eyes, brains and spinal cord).
- The hotspot was selected on the StaticS temperature distribution delineating the area with the highest temperature (44 °C). The hotspot volume varies over a range between 0.5 and 0.2 % of the healthy tissue among all patients. After finding the PoptS settings by MOGA, individual PoptS thermal simulations were run to reach the maximum temperature of 44 °C in the healthy tissue and/or 40 °C in critical organs.
- Thermal simulations for time-multiplexed steering were run applying StaticS and PoptS antenna settings in a sequence over a simulation period of 1200 s and using a steering interval of 10 s. The steering interval is the time length for which each antenna setting is applied.

5.2.2 Hotspot Delineation and Localisation

As described in Section 5.2.1, the selection of the primary hotspot (Hotspot 1) was done on the static temperature distribution and the region with the highest temperature was delineated. In Chapter 4 it was found that additional hotspots occurred in the healthy tissue during time-multiplexed steering, hence a second hotspot (Hotspot 2) was selected based on the time-multiplexed temperature distribution obtained by using the constant thermal model.

To evaluate the robustness of static and time-multiplexed hyperthermia, the highest temperature was identified from the static TDPM distribution. Hence, Hotspot 1 related to CTM, (Hotspot 1-CTM) and Hotspot 1 related to TDPM (Hotspot 1-$TDPM$) were found.

To verify whether Hotspot 1-$TDPM$ occurred in the same or a nearby location as Hotspot 1-CTM, the Euclidean distance was calculated between the two hotspots, using the highest temperatures in the CTM and TDPM distributions as comparison points. Lastly, the time-multiplexed steering was run using TDPM.

5.2.3 Experimental Dataset and Evaluation Parameters

The five patient models selected in Section 4.2.5 were also used in this study. The patient group included one neck node metastasis, one oral cavity, one parotid gland and two oropharynx tumors. All patients were treated with the HYPERcollar3D at Erasmus MC Cancer Institute.

The StaticS and the PoptS solutions were evaluated based on SAR performance metrics as described in 4.2.5. In particular, Target Coverage by 25% iso-SAR (TC_{25}) and Target Coverage 50% (TC_{50}) were used to select the best Pareto solution which supplied a balance between providing sufficient SAR in the target and SAR reduction in the healthy tissue and these results were discussed in Section 4.3.

The thermal performance of the StaticS and the PoptS configurations and the robustness of the time-multiplexed steering to temperature dependent thermal tissue properties was evaluated using cumulative Temperature-Volume (T-V) histograms and thermal indices such as the median temperature, T_{50} in the CTV, and the maximum temperature T_{max} in the hotspot, to quantify the hotspot suppression.

5.3 Results

Experimental results obtained by running the time-multiplexed steering using constant and thermal dependent perfusion model are presented in this section. Firstly, the hotspots based on the TDPM distributions are identified. Then, static and time-multiplexed thermal performances are compared and discussed.

5.3.1 Hotspot location: CTM and TDPM Distributions

The StaticS and PoptS settings used to run the CTM thermal simulation were the ones selected in Chapter 4 for five patient models. PoptS was selected by ensuring adequate focusing in the target area, i.e. $TC_{25} \geq 75\%$ [51] and suppression of the hotspot energy, i.e. 30-60% SAR reduction compared to the HTQ-optimised distribution for each patient. Static temperature distributions for Patient 5 for CTM and TDPM are given in Figure 5.2a and 5.2b respectively.

The location of the highest temperature in the static TDPM temperature distribution was identified as shown in Figure 5.2b and it was found that the maximum Euclidean distance between the highest temperatures in CTM and TDPM was 5.4 mm, and was generally much less than that. Euclidean distance values (D) for the five patient models are reported in Table 5.1.

Since the hotspot location does not vary significantly between CTM and TDPM over the patient population, in the following analyses the same hotspot delineation was used for both CTM and TDPM. We also used the PoptS-CTM antenna settings to assess the effectiveness of time-multiplexing steering using TDPM.

Table 5.1: Euclidean distance between Hotspot 1-CTM (in constant thermal model distribution) and Hotspot 2-$TDMP$ (in thermal dependent perfusion model) for five cases treated with the HYPERcollar3D.

Patient no.	P1	P2	P3	P4	P5
D (mm)	3.7	5.4	2.2	2.8	1.7

5.3.2 Cumulative Temperature-Volume Histograms and Thermal Indicators

5.3.2.1 Impact of thermal model: Static Performance

Static performance using CTM and TDPM was considered for all five patients using cumulative T-V histograms. The temperature in the CTV and in Hotspot 1 was calculated based on the static temperature distributions and the thermal quantifiers are reported in Table 5.2. The variation ($\Delta T_{StaticS-TDPMvsCTM}$) arising from the static CTM and the static TDPM performances is also shown in Table 5.2. For all clinical records, the static performance obtained with TDPM provides a temperature increase of T_{50} in CTV of between 1.5 °C and 2.1 °C compared to the static CTM performance. Figure 5.3 is an example of the cumulative T-V

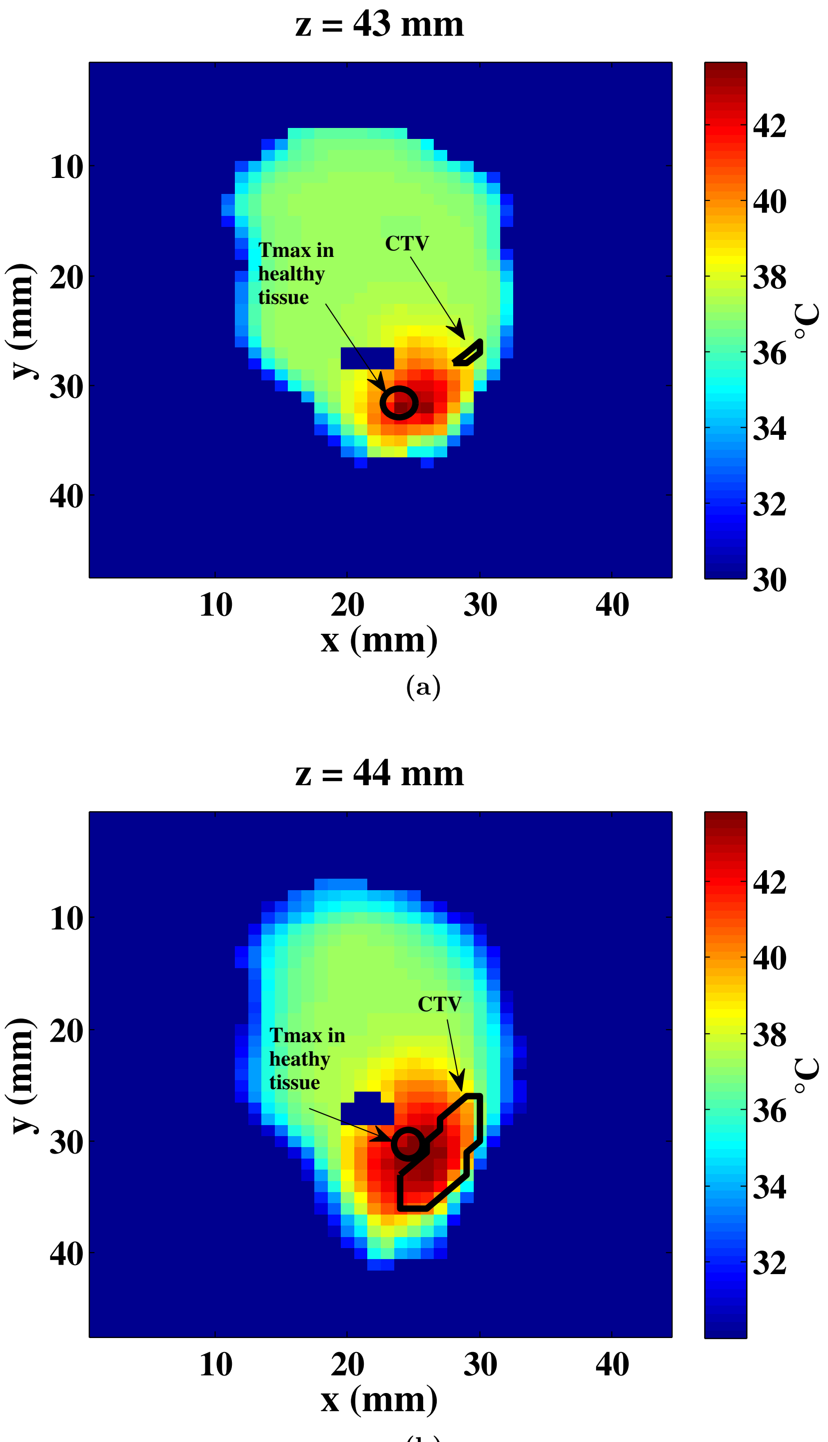

(a)

(b)

Figure 5.2: Patient 5. 3D temperature distribution on a transversal view obtained using *StaticS* settings with Constant Thermal Model (CTM) (z=43 mm) (a) and Thermal Dependent Perfusion Model (TDPM) (z=44 mm)(b). CTV and the location of maximum temperature achieved in the healthy tissue are are in the oral cavity in both cases but with a difference of 1 mm in the *z*-location.

histogram for the static thermal performance using CTM and TDPM. Similar trend are observed in all other patients.

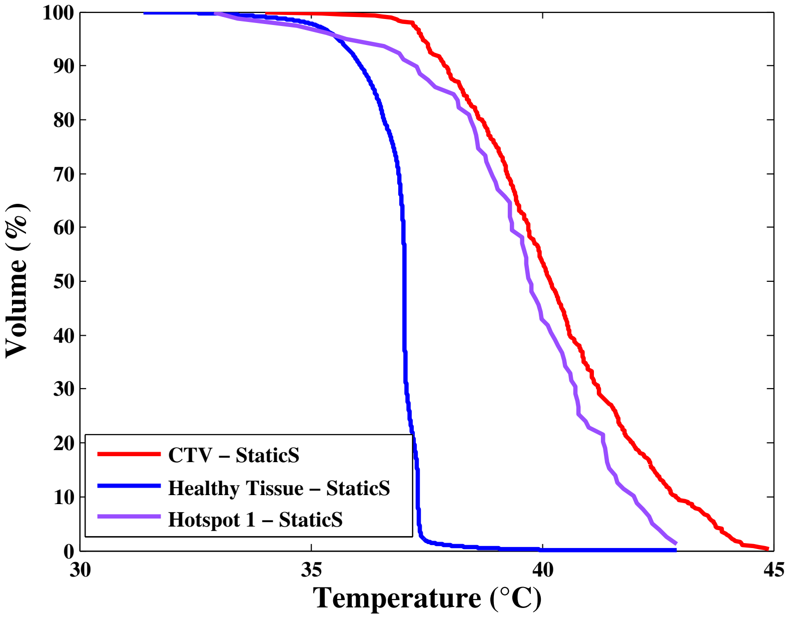

(a)

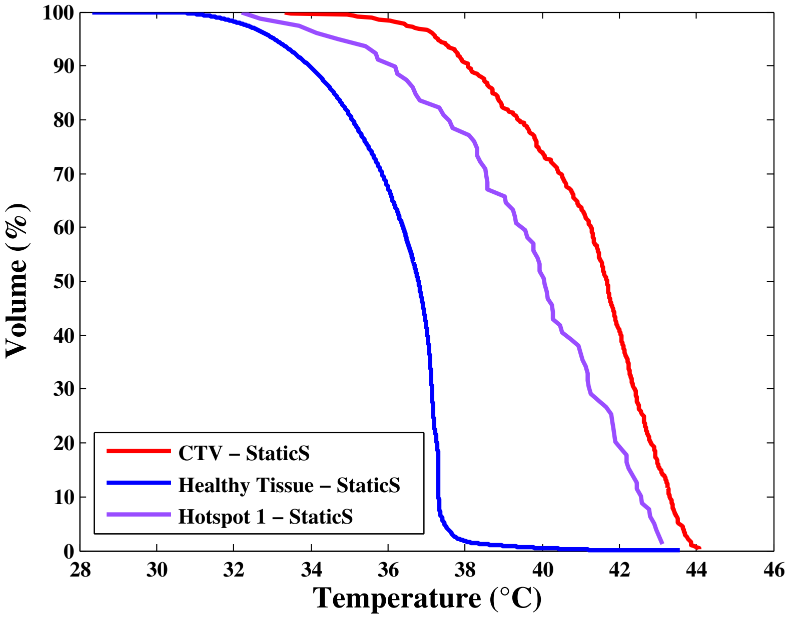

(b)

Figure 5.3: CTV (red) and Hotspot 1 (violet) cumulative T-V histograms for Patient 3. The static thermal performance using CTM and TDPM are shown in (a) and (b) respectively.

Table 5.2: Thermal quantifier T_{50} that is exceeded by 50 percent of all temperature readings in the CTV and T_{max} in the hotspot for five cases treated with the HYPERcollar3D. Temperature changes from StaticS (single SAR steering) to TMS (time-multiplexed steering) obtained by CTM (constant thermal model) and TDPM (thermal dependent perfusion model) are given in bold

Patient no.	Thermal model	Antenna settings	CTV	Hotspot 1	Hotspot 2	Hotspot 3
			T50 (°C)	Tmax (°C)	Tmax (°C)	Tmax (°C)
P1	CTM	StaticS	40.4	44	43.1	42
		TMS	40.7	42.9	43.9	43.5
		$\Delta T_{TMS-StaticS}$ (°C)	**+0.3**	**-1.4**	**+0.8**	**+1.5**
	TDPM	StaticS	42.1	42.6	42.6	41.8
		TMS	42.1	41.6	42.7	42.3
		$\Delta T_{TMS-StaticS}$ (°C)	**0**	**-1**	**+0.1**	**+0.5**
	$\Delta T_{StaticS-TDPMvsCTM}$ (°C)		**+1.7**			
P2	CTM	StaticS	41.7	43.7	41.3	
		TMS	42.7	42.2	43.7	
		$\Delta T_{TMS-StaticS}$ (°C)	**+1**	**-1.5**	**+2.4**	
	TDPM	StaticS	43.2	43.5	43.1	
		TMS	43.4	42.9	44.3	
		$\Delta T_{TMS-StaticS}$ (°C)	**+0.2**	**-0.6**	**+0.2**	
	$\Delta T_{StaticS-TDPMvsCTM}$ (°C)		**+1.5**			
P3	CTM	StaticS	40.2	42.9	42.7	
		TMS	40.7	41.4	43.6	
		$\Delta T_{TMS-StaticS}$ (°C)	**+0.5**	**-1.5**	**+0.9**	
	TDPM	StaticS	41.7	43.1	42.3	
		TMS	42.5	42.5	43.5	
		$\Delta T_{TMS-StaticS}$ (°C)	**+0.8**	**-0.6**	**+1.2**	
	$\Delta T_{StaticS-TDPMvsCTM}$ (°C)		**+1.5**			
P4	CTM	StaticS	40.3	43.7	43.6	
		TMS	41.5	43.1	43.7	
		$\Delta T_{TMS-StaticS}$ (°C)	**+1.2**	**-0.6**	**+0.1**	
	TDPM	StaticS	42.4	43.7	43.7	
		TMS	42.5	42.9	43.1	
		$\Delta T_{TMS-StaticS}$ (°C)	**+0.1**	**-0.8**	**-0.6**	
	$\Delta T_{StaticS-TDPMvsCTM}$ (°C)		**+2.1**			
P5	CTM	StaticS	39.9	43.7	42	
		TMS	40.7	42.7	43.9	
		$\Delta T_{TMS-StaticS}$ (°C)	**+0.8**	**-1**	**+1.9**	
	TDPM	StaticS	41.9	43.7	42.9	
		TMS	42.5	43.1	43.8	
		$\Delta T_{TMS-StaticS}$ (°C)	**+0.6**	**-0.6**	**+0.9**	
	$\Delta T_{StaticS-TDPMvsCTM}$ (°C)		**+2**			

5.3.2.2 Impact of thermal model: Time-multiplexed performance

In addition to the static settings, the performance of the time-multiplexed steering procedure using CTM and TDPM was considered for the five patient models. The median temperature in CTV, the maximum temperature in Hotspot 1 and the additional hotspot temperatures raising from time-multiplexed steering, Hotspot 2 and Hotspot 3 (following the definition of Hotspot 1 and Hotspot 2) are reported in Table 5.2, together with the variation resulting from static and time-multiplexed steering ($\Delta T_{TMS-StaticS}$) both for constant thermal and thermal dependent perfusion performances.

Figure 5.4 shows an example of cumulative T-V histograms for static and time-multiplexed steering using CTM and TDPM. Results obtained with time-multiplexed steering using the constant thermal model have been discussed in Section 4.3. The temperature simulations predicted an average improvement in target temperatures, i.e. 0.8 °C in T_{50} and a reduction in the average maximum temperature of 1.2 °C in the healthy tissue. The time-multiplexed steering using TDPM provides an increase in T_{50} of the CTV in the range of 0.1 °C and 0.8 °C for four out of five patients, and identical T_{50} is achieved for Patient 1 compared to the static TDPM performance. Also, a hotspot reduction varying between 0.6 °C and 1 °C is observed for all patients studied.

Results show that the static performance arising from TDPM predicts higher T_{50} values in CTV compared to the static performance obtained with CTM. Hence, the improvements achieved by TMS when using TDPM is not high as for the TMS using CTM. Nevertheless, there is still improvement and these findings demonstrate the robustness of time-multiplexed hyperthermia to temperature dependent thermal tissue properties and the benefit both in terms of CTV coverage and hotspot suppression.

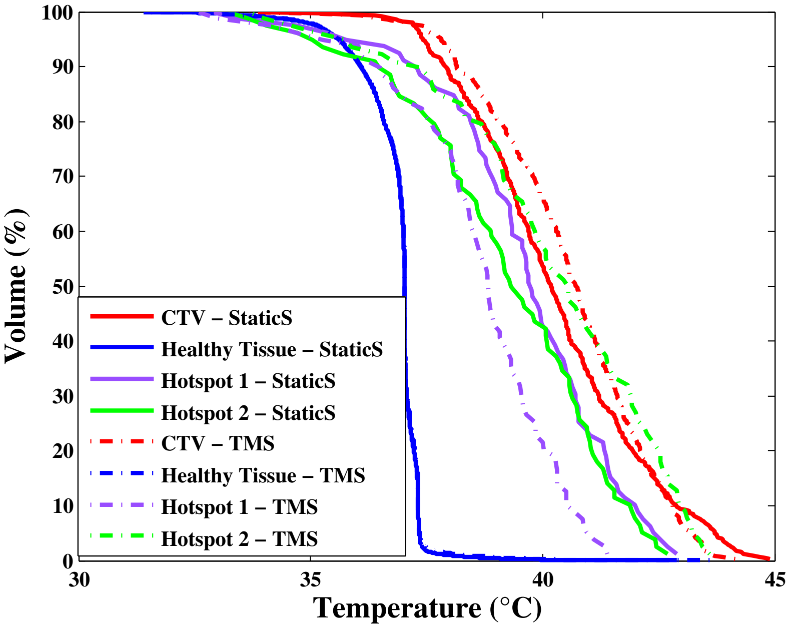

(a)

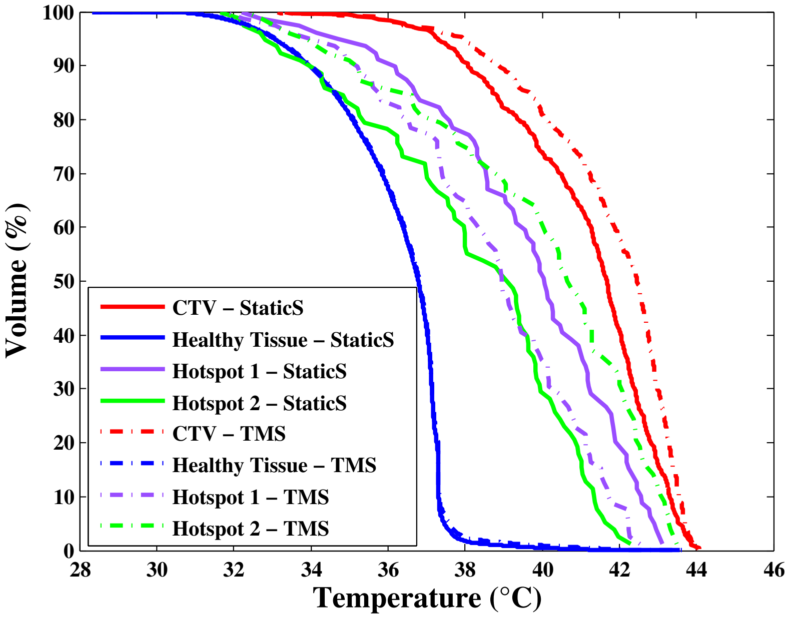

(b)

Figure 5.4: CTV (red), Hotspot 1 (violet) and Hotspot 2 (green) cumulative T-V histograms for Patient 3. The static (solid line) and the time-multiplexed (dash-dot line) thermal performances are compared using CTM (a) and TDPM (b).

5.4 Discussion

The novelty of the work described in this chapter is the additional development of TMS by means of non-linear thermal simulations where the blood perfusion coefficient of selected tissues depends on the temperature itself. Results indicated that the temperature in the target could be increased by 0.8 °C while hotspots could be reduced by 1.2 °C on average between all patients. These results show that TMS using thermal dependent perfusion model still yields thermal distribution comparable with those obtained with constant tissue properties, with a lower improvement in the target temperature.

As described in Chapter 4, the predicted temperatures in the healthy tissue cannot exceed a specified temperature limit, i.e. 44 °C. Additional hotspots arise in the healthy tissue during time-multiplexed steering leading to higher maximum temperatures in some cases as compared to the maximum temperature of the hotspots obtained in the static simulation. For example, T_{max} of Hotspot 2 and Hotspot 3 resulting from TDPM show increases in the range of 0.1-1.2 °C; however, their median temperatures are still below the CTV temperatures. While it is also possible in some cases that hotspot temperatures may exceed the specified limit of 44 °C with TMS (e.g. with Patient 2), these cases are relatively rare and the TMS method allows flexibility in controlling the steering rate to compensate for these effects if necessary. In an extreme case, if an increase in hotspot temperature was deemed to be clinically unacceptable relative to the beneficial increase in CTV, the steering rate may be set to zero so that treatment reverts to the static settings only for that patient. Further investigation of these factors will be the subject of future research.

In TDPM, while the perfusion of the tumour with increasing temperature is reduced relative to CTM, the relative increase in the perfusion of muscle with increasing temperature is substantially larger, and likely dominates the thermal behaviour.

Clinical experience in Erasmus MC Cancer Institute suggests that increases in CTV temperature on the order of only 0.3 °C are beneficial [113], [114]. While the relative increase in CTV temperature using TMS is smaller with TDPM, these increases are still clinically useful in many patients.

These findings demonstrate the general robustness and utility of time-multiplexed hyperthermia to temperature dependent thermal tissue properties and the benefit both in terms of CTV coverage and hotspot suppression.

5.5 Conclusions

In this chapter, the robustness of the time-multiplexed steering method for hyperthermia treatment planning presented in Chapter 4 with different thermal models of tissue behaviour was evaluated. In particular, the effects on performance as determined through thermal simulations of assuming that the thermal properties vary with temperature, as opposed to being constant, were examined. Multiple heating patterns, i.e. antenna phases and amplitudes, were generated by a multi-objective genetic algorithm and applied sequentially in thermal simulations.

The proposed strategy was compared with the particle swarm optimisation used in the clinic and the thermal performance was assessed. Using the temperature dependent perfusion model, an increase in T_{50}, i.e. 0.2-0.8 °C, and a decrease in the hotspot temperature, i.e. 0.6-1 °C was observed for four out of five patients.

The work presented in Chapter 4 has suggested that time-multiplexed hyperthermia can achieve higher temperatures in the tumour and decrease temperatures in the healthy tissue when constant thermal properties are used in thermal simulations. Similarly, the work presented in this chapter, has found that time-multiplexed hyperthermia increases the temperature in the tumour and lowers the temperature in the hotspot when using temperature dependent perfusion models. Overall, the results in this chapter indicate that time-multiplexed hyperthermia via MOGA optimisation is robust to variations in thermal properties due to temperature increases.

6

Conclusions and Future Work

The principal conclusions and findings of the thesis are described in this final chapter. The primary contributions are revisited and suggestions for future work are presented.

6.1 Summary of Thesis

This thesis dealt with the development of optimisation techniques for use in planning of non-invasive microwave hyperthermia treatment of cancer. The investigation was focused on the application of H&N cancers. Studies on SAR and temperature-based optimisation algorithms were carried out with the goal of focusing EM energy to heat tumours, while preserving the healthy tissue. The delivery of the desired heating in cancerous and healthy tissue was validated using thermal simulations.

Firstly, evolutionary optimisation algorithms were investigated to optimise the SAR distributions and find optimal antenna settings for antenna amplitude and phase. Then, a novel time-multiplexed steering approach was developed to further focus the heating into the target and reduce hotspot prominence. The robustness of the time-multiplexed hyperthermia to temperature dependent thermal tissue properties was also assessed. The performance of the various algorithms was evaluated using clinical patient data and through metrics informed by clinical practice.

Chapter 2 of the thesis presented an overview of the anatomy of H&N cancer and introduced the biological aspects of the hyperthermia treatment. Different hyperthermia systems and modalities were discussed and the clinical benefits as found in clinical trials were described. The stages of pre-treatment planning were described, together with the performance metrics used in the clinic. Furthermore, several objective functions and optimisation algorithms were reviewed.

Chapter 3 proposed the differential evolution algorithm for treatment planning, and compared it with the particle swarm optimisation clinically used at the Erasmus MC. Different optimisation settings were investigated to find the best antenna configuration which provided optimal SAR distribution. The algorithms were applied to a set of patients clinically treated with the HYPERcollar system in clinical use at Erasmus MC. Thermal simulations were carried out to assess effective target heating and hotspot reduction. The performance of both algorithms was compared in terms of target coverage, SAR distributions, thermal indicators and cumulative T-V histograms.

Chapter 4 presented the development of a novel time-multiplexed hyperthermia strategy via MOGA optimisation to dynamically generate a heating distribution. Similar to the DE optimisation, the proposed method was compared with the static solution obtained by PSO and the results were presented in terms of SAR and thermal indicators. For this analysis, data from patients treated with the next generation HYPERcollar3D system at Erasmus MC were used. Given that some uncertainty exists in relation to specific thermal behaviour of tissue, Chapter 5 evaluated the efficacy of the time-multiplexed steering system proposed in Chapter 4 in the presence of variation in thermal properties of tissues due to temperature increase. The robustness was assessed based on thermal quantifiers and using data from patients treated with the HYPERcollar3D system at Erasmus MC.

6.2 Main Contributions

The primary contributions of this thesis are as follows. A list of the publications derived from the research described in this thesis was given in Section 1.2.1.

1. A Differential Evolution (DE) algorithm for SAR optimisation was proposed to improve the SAR coverage of the target region, and compared with an existing algorithm (PSO) in clinical use. Evaluation indicated that while both algorithms are capable of finding the optimal power deposition, the proposed DE algorithm is more consistently superior to PSO in locating the optimum solution. DE performs better in terms of HTQ average and standard deviation, reporting a range of improvement of HTQ standard deviation of between 40.1-96.8% across six patients.

2. A Multi-Objective Genetic Algorithm (MOGA) for target focusing and hotspot suppression was proposed, involving optimisation of two objective functions. Furthermore, a novel objective function was formulated in such a way to find a tradeoff between the EM energy in the target and suppression of a pre-defined hotspot. The efficacy of the novel objective function was demonstrated in terms of SAR metrics and when applying TMS using thermal simulations. SAR results obtained by MOGA, in particular TC_{25} values greater than 75%, showed improved target coverage and hotspot energy reduction of 59-71% compared to PSO, indicated the feasibility of implementing time-multiplexed hyperthermia.

3. A new approach for phased array hyperthermia focusing was proposed, whereby multiple solutions produced by MOGA were applied in a time-multiplexed fashion in order to improve treatment planning. Studies were conducted to determine the best multiplexing parameters, in particular the steering rate. The results demonstrated that the predicted time-averaged temperature is increased when using time-multiplexing. Realistic steering periods of 10 seconds were found to stabilise temperatures within 0.04 °C. Target heating was

enhanced and hotspots reduced by the time-multiplexed approach, resulting in 0.3-1.2 °C improvement in T_{50} and 0.6-1.5 °C reduction in hotspot temperatures compared to the static method currently used in clinic.

4. A SAR-temperature correlation analysis was carried out before applying time-multiplexed hyperthermia. A low correlation was found between EM energy and temperature values leading to the selection of the hotspots based on temperature distribution. This analysis showed the importance of thermal simulations as a means of treatment validation and that the selection of hotspots based on SAR distribution alone may not always be appropriate.
5. The time-multiplexed hyperthermia system proposed in Chapter 4 was evaluated using temperature dependent thermal tissue properties in order to determine its robustness to uncertainty in thermal model parameters. The novel technique was shown to be robust to variations in thermal properties.

6.3 Future Work

The primary conclusions of this thesis show that the proposed techniques have the potential to be used for the treatment of H&N cancer. However, several potential areas of research remain that may improve the effectiveness of the optimisation methods and more generally, the accuracy and reliability of the hyperthermia treatment planning.

Firstly, a larger population of patients should be tested to confirm the capability of the proposed focusing algorithms in heating H&N tumors. Moreover, the application of the optimisation methods can be extended to other types of cancers such as pelvic cancer and to different hyperthermia applicators such as BSD 2000 system.

The differential evolution algorithm proposed in this thesis was tested on a set of patients treated by the HYPERcollar system designed with a total of twelve antennas. Researchers at the Erasmus MC demonstrated that increasing the number of antenna elements, as in HYPERcollar3D, enhances heat focusing into the tumor; however, one of the limitations when applying H&N hyperthermia treatment with

HYPERcollar3D was that only twelve antennas out of twenty could be used due to a limited number of power amplifiers. The selection of the antennas was based on the highest mean SAR individually achieved in the target region. Further analysis could focus on evaluating the SAR distribution using different combinations or subgroups of antennas. This may result in a total field pattern characterised by a smaller number of hotspots in the healthy tissue and better target focusing.

An additional area of research concerns the application of time-multiplexed hyperthermia in larger CTV to exclusively enhance the target heating. The CTV volume could be divided in multiple sub-volumes and the multi objective genetic algorithm could be exploited for each sub-volume. Pareto optimal solutions could be obtained for each area of interest and selected in such a way to achieve substantial SAR coverage. Then, the Pareto antenna settings could be sequentially applied in thermal simulation to run time-multiplexed hyperthermia and evaluate the temperature distribution. For this approach, the number and the location of the selected antennas of the HYPERcollar3D system is critical to achieve good SAR coverage.

The accuracy of tissue thermal and dielectric properties represent another important challenge in hyperthermia treatment planning. While the robustness of the time-multiplexed steering has been tested in this thesis, further research can be devoted to evaluate the robustness of the proposed technique against dielectric properties uncertainties.

Finally, analysis conducted as part of this research shows a low correlation between SAR and temperature values. Hence, accurate modeling to predict as closely as possible the SAR and temperature distribution within the patient should be examined in future work. However, despite the uncertainties in thermal tissue properties, the lack of knowledge on the physiological response of the body to temperature increase, thermal modeling remains an important tool to evaluate the temperature distribution in the treated area.

References

[1] W. H. Organization, “The Global Burden of Disease: 2004 update”, *Update*, vol. 2010, p. 146, 2008.

[2] J. Ferlay, H. R. Shin, F. Bray, D. Forman, C. Mathers, and D. M. Parkin, “Estimates of worldwide burden of cancer in 2008: GLOBOCAN 2008”, *International Journal of Cancer*, vol. 127, no. 12, pp. 2893–2917, 2010.

[3] A. K. Chaturvedi, W. F. Anderson, J. Lortet-Tieulent, M. Paula Curado, J. Ferlay, S. Franceschi, P. S. Rosenberg, F. Bray, and M. L. Gillison, “Worldwide trends in incidence rates for oral cavity and oropharyngeal cancers”, *Journal of Clinical Oncology*, vol. 31, no. 36, pp. 4550–4559, 2013.

[4] B. A. Conley, “Treatment of advanced head and neck cancer: what lessons have we learned?”, *Journal of clinical oncology : official journal of the American Society of Clinical Oncology*, vol. 24, no. 7, pp. 1023–1025, 2006.

[5] A. Trotti, “Toxicity in head and neck cancer: a review of trends and issues.”, *International journal of radiation oncology, biology, physics*, vol. 47, no. 1, pp. 1–12, 2000.

[6] R. Issels, E. Kampmann, R. Kanaar, and L. H. Lindner, “Hallmarks of hyperthermia in driving the future of clinical hyperthermia as targeted therapy: translation into clinical application”, *International Journal of Hyperthermia*, vol. 32, no. 1, pp. 89–95, 2016.

[7] N. van den Tempel, M. R. Horsman, and R. Kanaar, “Improving efficacy of hyperthermia in oncology by exploiting biological mechanisms”, *International Journal of Hyperthermia*, vol. 32, no. 4, pp. 446–454, 2016.

[8] N. Cihoric, A. Tsikkinis, G. van Rhoon, H. Crezee, D. M. Aebersold, S. Bodis, M. Beck, J. Nadobny, V. Budach, P. Wust, and P. Ghadjar, “Hyperthermia-related clinical trials on cancer treatment within the ClinicalTrials.gov registry”, *International Journal of Hyperthermia*, vol. 31, no. 6, pp. 609–614, 2015.

[9] M. Franckena, L. J. A. Stalpers, P. C. M. Koper, R. G. J. Wiggenraad, W. J. Hoogenraad, J. D. P. van Dijk, C. C. Wárlám-Rodenhuis, J. J. Jobsen, G. C. van Rhoon, and J. van der Zee, “Long-Term Improvement in Treatment Outcome After Radiotherapy and Hyperthermia in Locoregionally Advanced Cervix Cancer: An Update of the Dutch Deep Hyperthermia Trial”, *International Journal of Radiation Oncology Biology Physics*, vol. 70, no. 4, pp. 1176–1182, 2008.

[10] N. R. Datta, S. Rogers, S. G. Ordóñez, E. Puric, N. R. Datta, S. Rogers, S. G. Ordóñez, E. Puric, E. Puric, and S. Bodis, "Hyperthermia and radiotherapy in the management of head and neck cancers : A systematic review and meta-analysis", *International Journal of Hyperthermia*, vol. 32, no. 1, pp. 31–40, 2016.

[11] N. Datta, S. G. Ordóñez, U. Gaipl, M. Paulides, H. Crezee, J. Gellermann, D. Marder, E. Puric, and S. Bodis, "Local hyperthermia combined with radiotherapy and-/or chemotherapy: Recent advances and promises for the future", *Cancer Treatment Reviews*, vol. 41, no. 9, pp. 742–753, 2015.

[12] R. Valdagni and M. Amichetti, "Report of long-term follow-up in a randomized trial comparing radiation therapy and radiation therapy plus hyperthermia to metastatic lymphnodes in stage IV head and neck patients", *International Journal of Radiation Oncology Biology Physics*, vol. 28, pp. 163–169, 1994.

[13] J. van der Zee, D. González, G. C. van Rhoon, J. D. P. van Dijk, W. L. J. van Putten, and A. A. M. Hart, "Comparison of radiotherapy alone with radiotherapy plus hyperthermia in locally advanced pelvic tumours: a prospective, randomised, multicentre trial", *Lancet*, vol. 355, no. 9210, pp. 1119–1125, 2000.

[14] C. C. Vernon, J. W. Hand, S. B. Field, D. Machin, J. B. Whaley, J. van der Zee, W. L. van Putten, G. C. van Rhoon, J. D. van Dijk, D. Gonzalez Gonzalez, F. F. Liu, P. Goodman, and M. Sherar, "Radiotherapy with or without hyperthermia in the treatment of superficial localized breast cancer: results from five randomized controlled trials.", *International Journal of Radiation Oncology Biology Physics*, vol. 35, no. 4, pp. 731–744, 1996.

[15] P. R. Stauffer, "Evolving technology for thermal therapy of cancer", *International Journal of Hyperthermia*, vol. 21, no. 8, pp. 731–744, 2005.

[16] G. Bruggmoser, S. Bauchowitz, R. Canters, H. Crezee, M. Ehmann, J. Gellermann, U. Lamprecht, N. Lomax, M. B. Messmer, O. Ott, S. Abdel-Rahman, R. Sauer, M. Schmidt, A. Thomsen, R. Wessalowski, and G. van Rhoon, "Quality assurance for clinical studies in regional deep hyperthermia", *Strahlentherapie und Onkologie*, vol. 187, no. 10, pp. 605–610, 2011.

[17] J. Crezee, P. M. Van Haaren, H. Westendorp, M. De Greef, H. P. Kok, J. Wiersma, G. Van Stam, J. Sijbrands, P. Zum Vörde Sive Vörding, J. D. Van Dijk, M. C. Hulshof, and A. Bel, "Improving locoregional hyperthermia delivery using the 3-D controlled AMC-8 phased array hyperthermia system: A preclinical study", *International Journal of Hyperthermia*, vol. 25, no. 7, pp. 581–592, 2009.

[18] M. M. Paulides, J. F. Bakker, E. Neufeld, J. van der Zee, P. P. Jansen, P. C. Levendag, and G. C. van Rhoon, "The HYPERcollar: a novel applicator for hyperthermia in the head and neck.", *International Journal of Hyperthermia*, vol. 23, no. 7, pp. 567–576, 2007.

[19] P. Turner, “Regional hyperthermia with an annular phased array”, *IEEE Transactions on Biomedical Engineering*, vol. 31, pp. 106–14, 1984.

[20] F. Bardati and P. Tognolatti, “Hyperthermia phased arrays pre-treatment evaluation”, *International Journal of Hyperthermia*, vol. 32, no. 8, pp. 911–922, 2016.

[21] M. Converse, E. J. Bond, B. D. Van Veen, and S. C. Hagness, “A computational study of ultra-wideband versus narrowband microwave hyperthermia for breast cancer treatment”, *IEEE Transactions on Microwave Theory and Techniques*, vol. 54, no. 5, pp. 2169–2180, 2006.

[22] D. Iero, T. Isernia, and A. F. Morabito, “Optimal Constrained Field Focusing for Hyperthermia Cancer Therapy: A Feasibility Assessment on Realistic Phantoms”, *Progress In Electromagnetics Research*, vol. 102, pp. 125–141, 2010.

[23] T. Köhler, P. Maass, P. Wust, and M. Seebass, “A fast algorithm to find optimal controls of multiantenna applicators in regional hyperthermia.”, *Physics in Medicine and Biology*, vol. 46, no. 9, pp. 2503–2514, 2001.

[24] P. T. Nguyen, A. Abbosh, and S. Crozier, “Three-Dimensional Microwave Hyperthermia for Breast Cancer Treatment in a Realistic Environment Using Particle Swarm Optimization”, *IEEE Transactions on Biomedical Engineering*, vol. 64, no. 6, pp. 1335–1344, 2017.

[25] H. D. Trefna, J. Vrba, and M. Persson, “Time-reversal focusing in microwave hyperthermia for deep-seated tumors”, *Physics in Medicine and Biology*, vol. 55, no. 1361-6560 (Electronic), pp. 2167–2185, 2010.

[26] R. A. M. Canters, P. Wust, J. F. Bakker, and G. C. van Rhoon, “A literature survey on indicators for characterisation and optimisation of SAR distributions in deep hyperthermia, a plea for standardisation.”, *International Journal of Hyperthermia*, vol. 25, no. 7, pp. 593–608, 2009.

[27] S. K. Das, S. T. Clegg, and T. V. Samulski, “Electromagnetic thermal therapy power optimization for multiple source applicators.”, *International Journal of Hyperthermia*, vol. 15, no. 4, pp. 291–308, 1999.

[28] H. P. Kok, P. M. a. van Haaren, J. B. van de Kamer, P. J. Zum Vörde Sive Vörding, J. Wiersma, M. C. C. M. Hulshof, E. D. Geijsen, J. J. B. van Lanschot, and J. Crezee, “Prospective treatment planning to improve locoregional hyperthermia for oesophageal cancer.”, *International Journal of Hyperthermia*, vol. 22, no. 5, pp. 375–389, 2006.

[29] J. P. Pignon, J. Bourhis, C. Domenge, and L. Designé, “Chemotherapy added to locoregional treatment for head and neck squamous-cell carcinoma: three meta-analyses of updated individual data. MACH-NC Collaborative Group. Meta-Analysis of Chemotherapy on Head and Neck Cancer.”, *Lancet*, vol. 355, no. 9208, pp. 949–955, 2000.

[30] H. H. Kampinga, "Cell biological effects of hyperthermia alone or combined with radiation or drugs: a short introduction to newcomers in the field", *International Journal of Hyperthermia*, vol. 22, no. 3, pp. 191–196, 2006.

[31] M. W. Dewhirst, Z. Vujaskovic, E. Jones, and D. Thrall, "Re-setting the biologic rationale for thermal therapy", *International Journal of Hyperthermia*, vol. 21, no. 8, pp. 779–790, 2005.

[32] J. van der Zee, "Heating the patient: A promising approach?", *Annals of Oncology*, vol. 13, no. 8, pp. 1173–1184, 2002.

[33] L. Roizin-Towle and J. P. Pirro, "The response of human and rodent cells to hyperthermia", *International Journal of Radiation Oncology, Biology, Physics*, vol. 20, no. 4, pp. 751–756, 1991.

[34] S. A. Sapareto and W. C. Dewey, "Thermal dose determination in cancer therapy", *International Journal of Radiation Oncology, Biology, Physics*, vol. 10, no. 6, pp. 787–800, 1984.

[35] B. Hildebrandt and P. Wust, "The biologic rationale of hyperthermia", *Peritoneal Carcinomatosis: A Multidisciplinary Approach*, no. Table 1, pp. 171–184, 2007.

[36] P. Wust, B. Hildebrandt, G. Sreenivasa, B. Rau, J. Gellermann, H. Riess, R. Felix, and P. M. Schlag, "Hyperthermia in combined treatment of cancer.", *The lancet oncology*, vol. 3, no. 8, pp. 487–497, 2002.

[37] H. D. Trefna, "Advances in microwave hyperthermia treatment using time reversal", PhD thesis, Chalmers University of Technology, 2010.

[38] G. C. van Rhoon, P. J. Rietveld, and J. van der Zee, "A 433 MHz Lucite cone waveguide applicator for superficial hyperthermia.", *International Journal of Hyperthermia*, vol. 14, no. 1, pp. 13–27, 1998.

[39] P. J. Rietveld, M. L. Lumori, J. Van der Zee, and G. C. Van Rhoon, "Quantitative evaluation of 2 x 2 arrays of Lucite cone applicators in flat layered phantoms using Gaussian-beam-predicted and thermographically measured SAR distributions", *Physics in Medicine and Biology*, vol. 43, no. 8, pp. 2207–2220, 1998.

[40] M. de Bruijne, J. Van der Zee, A. Ameziane, and G. C. Van Rhoon, "Quality control of superficial hyperthermia by treatment evaluation.", *International Journal of Hyperthermia*, vol. 27, no. 3, pp. 199–213, 2011.

[41] A. Chicheł, J. Skowronek, M. Kubaszewska, and M. Kanikowski, "Hyperthermia - Description of a method and a review of clinical applications", *Reports of Practical Oncology and Radiotherapy*, vol. 12, no. 5, pp. 267–275, 2007.

[42] A. A. C. De Leeuw and J. J. W. Lagendijk, "Design of a clinical deep-body hyperthermia system based on the 'coaxial TEM' applicator", *International Journal of Hyperthermia*, vol. 3, no. 5, pp. 413–421, 1987.

[43] P. Raskmark, S. N. Hornsleth, L. N. Salling, J. C. Lindegaard, and J. Overgaard, “Deep heating using a movable applicator phased array hyperthermia system: A preclinical feasibility study”, *Acta Oncologica*, vol. 33, no. 4, pp. 451–455, 1994.

[44] H. Kroeze, J. B. Van de Kamer, A. A. C. De Leeaw, and J. J. W. Lagendijk, “Regional hyperthermia applicator design using FDTD modelling”, *Physics in Medicine and Biology*, vol. 46, no. 7, pp. 1919–1935, 2001.

[45] P. Togni, Z. Rijnen, W. C. M. Numan, R. F. Verhaart, J. F. Bakker, G. C. van Rhoon, and M. M. Paulides, “Electromagnetic redesign of the HYPERcollar applicator: toward improved deep local head-and-neck hyperthermia.”, *Physics in medicine and biology*, vol. 58, no. 17, pp. 5997–6009, 2013.

[46] W. R. Hendee, *Physics of Thermal Therapy: Fundamental and Clinical Applications*, E. G. Moros, Ed. CRC Press, Taylor and Francis, 2012, pp. 139–158.

[47] M. M. Paulides, J. F. Bakker, M. Linthorst, J. van der Zee, Z. Rijnen, E. Neufeld, P. M. T. Pattynama, P. P. Jansen, P. C. Levendag, and G. C. van Rhoon, “The clinical feasibility of deep hyperthermia treatment in the head and neck: new challenges for positioning and temperature measurement.”, *Physics in medicine and biology*, vol. 55, no. 9, pp. 2465–2480, 2010.

[48] J. F. Bakker, M. M. Paulides, A. H. Westra, H. Schippers, and G. C. van Rhoon, “Design and test of a 434 MHz multi-channel amplifier system for targeted hyperthermia applicators.”, *International journal of hyperthermia*, vol. 26, no. 2, pp. 158–170, 2010.

[49] Z. Rijnen, P. Togni, R. Roskam, S. G. van de Geer, R. H. Goossens, and M. M. Paulides, “Quality and comfort in head and neck hyperthermia: A redesign according to clinical experience and simulation studies”, *International Journal of Hyperthermia*, vol. 31, no. 8, pp. 823–830, 2015.

[50] M. M. Paulides, Z. Rijnen, P. Togni, R. F. Verhaart, T. Drizdal, D. D. Jong, M. Franckena, G. M. Verduijn, and G. C. V. Rhoon, “Clinical Introduction of Novel Microwave Hyperthermia Technology : the HYPERcollar3D Applicator for Head and Neck Hyperthermia”, in *European Conference on Antennas and Propagation (EuCAP)*, 2015, pp. 1–4.

[51] Z. Rijnen, J. F. Bakker, R. a. M. Canters, P. Togni, G. M. Verduijn, P. C. Levendag, G. C. van Rhoon, and M. M. Paulides, “Clinical integration of software tool VEDO for adaptive and quantitative application of phased array hyperthermia in the head and neck.”, *International Journal of Hyperthermia*, vol. 29, no. 3, pp. 181–93, 2013.

[52] R. Valdagni, M. Amichetti, and G. Pani, “Radical radiation alone versus radical radiation plus microwave hyperthermia for N3 (TNM-UICC) neck nodes: a prospective randomized clinical trial”, *International Journal of Radiation Oncology Biology Physics*, vol. 15, pp. 13–24, 1988.

[53] P. K. Sneed, P. R. Stauffer, M. W. McDermott, C. J. Diederich, K. R. Lamborn, M. D. Prados, S. Chang, K. A. Weaver, L. Spry, M. K. Malec, S. A. Lamb, B. Voss, R. L. Davis, W. M. Wara, D. A. Larson, T. L. Phillips, and P. H. Gutin, "Survival benefit of hyperthermia in a prospective randomized trial of brachytherapy boost ± hyperthermia for glioblastoma multiforme", *International Journal of Radiation Oncology Biology Physics*, vol. 40, no. 2, pp. 287–295, 1998.

[54] J. Overgaard, D. G. Gonzalez, M. C. C. M. Hulshof, G. Arcangeli, O. Dahl, O. Mella, and S. M. Bentzen, "Randomized Trial of Hyperthermia as Adjuvant to Radiotherapy for Recurrent or Metastatic Malignant-Melanoma", *Lancet*, vol. 345, no. 8949, pp. 540–543, 1995.

[55] E. L. Jones, J. R. Oleson, L. R. Prosnitz, T. V. Samulski, Z. Vujaskovic, D. Yu, L. L. Sanders, and M. W. Dewhirst, "Randomized trial of hyperthermia and radiation for superficial tumors", *Journal of Clinical Oncology*, vol. 23, no. 13, pp. 3079–3085, 2005.

[56] J. P. Pignon, A. le Maıtre, E. Maillard, and J. Bourhis, "Meta-analysis of chemotherapy in head and neck cancer (MACH-NC): An update on 93 randomised trials and 17,346 patients", *Radiotherapy and Oncology*, vol. 92, no. 1, pp. 4–14, 2009.

[57] N. R. Datta, A. K. Bose, H. K. Kapoor, and S. Gupta, "Head and neck cancers: Results of thermoradiotherapy versus radiotherapy", *International Journal of Hyperthermia*, vol. 6, no. 3, pp. 479–486, 1990.

[58] N. Huilgol, S. Gupta, and C. R. Sridhar, "Hyperthermia with radiation in the treatment of locally advanced head and neck cancer: A report of randomized trial", *Journal of Cancer Research and Therapeutics*, vol. 6, no. 4, pp. 492–496, 2010.

[59] Y. Hua, S. Ma, Z. Fu, Q. Hu, L. Wang, and Y. Piao, "Intracavity hyperthermia in nasopharyngeal cancer: A phase III clinical study", *International Journal of Hyperthermia*, vol. 27, no. 2, pp. 180–186, 2011.

[60] C. Zhao, J. Chen, B. Yu, and X. Chen, "Improvement in quality of life in patients with nasopharyngeal carcinoma treated with non-invasive extracorporeal radiofrequency in combination with chemoradiotherapy", *International Journal of Radiation Biology*, vol. 90, no. 10, pp. 853–858, 2014.

[61] M. M. Paulides, G. M. Verduijn, and N. Van Holthe, "Status quo and directions in deep head and neck hyperthermia", *Radiatiation Oncology*, vol. 11, p. 21, 2016.

[62] M. M. Paulides, P. R. Stauffer, E. Neufeld, P. F. Maccarini, A. Kyriakou, R. a. M. Canters, C. J. Diederich, J. F. Bakker, and G. C. van Rhoon, "Simulation techniques in hyperthermia treatment planning.", *International Journal of Hyperthermia*, vol. 29, no. 4, pp. 346–57, 2013.

[63] V. Fortunati, R. F. Verhaart, F. van der Lijn, W. J. Niessen, J. F. Veenland, M. M. Paulides, and T. van Walsum, “Tissue segmentation of head and neck CT images for treatment planning: a multiatlas approach combined with intensity modeling.”, *Medical physics*, vol. 40, no. 7, p. 071 905, 2013.

[64] R. A. M. Canters, M. Franckena, M. M. Paulides, and G. C. Van Rhoon, “Patient positioning in deep hyperthermia: influences of inaccuracies, signal correction possibilities and optimization potential.”, *Physics in Medicine and Biology*, vol. 54, no. 12, pp. 3923–3936, 2009.

[65] R. A. M. Canters, M. M. Paulides, M. Franckena, J. W. Mens, and G. C. van Rhoon, “Benefit of replacing the Sigma-60 by the Sigma-Eye applicator: A Monte Carlo-based uncertainty analysis”, *Strahlentherapie und Onkologie*, vol. 189, no. 1, pp. 74–80, 2012.

[66] P. Wust, M. Seebass, J. Nadobny, P. Deuflhard, G. Mönich, and R. Felix, “Simulation studies promote technological development of radiofrequency phased array hyperthermia.”, *International Journal of Hyperthermia*, vol. 12, no. 4, pp. 477–494, 1996.

[67] K. D. Paulsen, S. Geimer, J. Tang, and W. E. Boyse, “Optimization of pelvic heating rate distributions with electromagnetic phased arrays.”, *International Journal of Hyperthermia*, vol. 15, no. 3, pp. 157–186, 1999.

[68] M. Seebass, R. Beck, J. Gellermann, J. Nadobny, and P. Wust, “Electromagnetic phased arrays for regional hyperthermia: optimal frequency and antenna arrangement.”, *International Journal of Hyperthermia*, vol. 17, no. 4, pp. 321–336, 2001.

[69] J. Gellermann, J. Göke, R. Figiel, M. Weihrauch, C. H. Cho, V. Budach, R. Felix, and P. Wust, “Simulation of different applicator positions for treatment of a presacral tumour”, *International Journal of Hyperthermia*, vol. 23, no. 1, pp. 37–47, 2007.

[70] L. Sandrini, A. Vaccari, C. Malacarne, L. Cristoforetti, and R. Pontalti, “RF dosimetry: A comparison between power absorption of female and male numerical models from 0.1 to 4 GHz”, *Physics in Medicine and Biology*, vol. 49, no. 22, pp. 5185–5201, 2004.

[71] N. Kuster, V. B. Torres, N. Nikoloski, M. Frauscher, and W. Kainz, “Methodology of detailed dosimetry and treatment of uncertainty and variations for in vivo studies”, *Bioelectromagnetics*, vol. 27, no. 5, pp. 378–391, 2006.

[72] *Recommended practice for determining the peak spatial-average specific absoption rate (SAR) associated with the use of wireless handsets - Computational techniques. Draft standard, IEEE-1529.*

[73] P. Bernardi, M. Cavagnaro, S. Pisa, and E. Piuzzi, “Specific absorption rate and temperature elevation in a subject exposed in the far-field of radiofrequency sources operating in the 10-900-MHz range”, *IEEE Transactions on Biomedical Engineering*, vol. 50, no. 3, pp. 295–304, 2003.

[74] D. G. Neuman, P. R. Stauffer, S. Jacobsen, and F. Rossetto, “SAR pattern perturbations from resonance effects in water bolus layers used with superficial microwave hyperthermia applicators”, *International Journal of Hyperthermia*, vol. 18, no. 3, pp. 180–193, 2002.

[75] M. de Bruijne, D. H. M. Wielheesen, J. van der Zee, N. Chavannes, and G. C. van Rhoon, “Benefits of superficial hyperthermia treatment planning: Five case studies”, *International Journal of Hyperthermia*, vol. 23, no. 5, pp. 417–429, 2007.

[76] E. A. Gelvich, V. N. Mazokhin, and I. I. Troshin, “An attempt at quantitative specification of SAR distribution homogeneity”, *International Journal of Hyperthermia*, vol. 12, no. 3, pp. 431–436, 1996.

[77] F. Bardati, A. Borrani, A. Gerardino, and G. a. Lovisolo, “SAR optimization in a phased array radiofrequency hyperthermia system”, *IEEE Transactions on Biomedical Engineering*, vol. 42, no. 12, pp. 1201–1207, 1995.

[78] A. J. Fenn and G. a. King, “Experimental investigation of an adaptive feedback algorithm for hot spot reduction in radio-frequency phased-array hyperthermia”, *IEEE Transactions on Biomedical Engineering*, vol. 43, no. 3, pp. 273–280, 1996.

[79] M. Bohm, J. Kremer, and A. K. Louis, “Efficient algorithm for computing optimal control of antennas in hyperthermia”, *Surv. Math. Indust.*, vol. 3, pp. 233–51, 1993.

[80] E. Zastrow, S. C. Hagness, and B. D. Van Veen, “3D computational study of non-invasive patient-specific microwave hyperthermia treatment of breast cancer.”, *Physics in Medicine and Biology*, vol. 55, no. 13, pp. 3611–3629, 2010.

[81] O. Schenk, M. Manguoglu, A. Sameh, M. Christen, and M. Sathe, “Parallel scalable PDE-constrained optimization: Antenna identification in hyperthermia cancer treatment planning”, *Computer Science - Research and Development*, vol. 23, no. 3-4, pp. 177–183, 2009.

[82] E. Neufeld, “High Resolution Hyperthermia Treatment Planning”, PhD thesis, Swiss Federal Institute of Technology, Zurich, 2008.

[83] H. Pennes, “Analysis of tissue and arterial blood temperatures in the resting human forearm”, *Journal of Applied Physiology*, vol. 1, no. 2, pp. 93–122, 1948.

[84] F. E. Curtis, O. Schenk, and A. Wachter, “An Interior-Point Algorithm for Large Scale Nonlinear Optimization with Inexact Step Computations”, *Society for Indistrial and Applied Mathematics*, vol. 32, no. 6, pp. 3447–3475, 2010.

[85] T. Isernia, P. D. Iorio, and F. Soldovieri, “An effective approach for the optimal focusing of array fields subject to arbitrary upper bounds”, *IEEE Transactions on Antennas and Propagation*, vol. 48, no. 12, pp. 1837–1847, 2000.

[86] T. Isernia and G. Panariello, “Optimal focusing of scalar fields subject to arbitrary upper bounds”, *Electronics Letters*, vol. 34, no. 2, pp. 162–164, 1998.

[87] R. Fletcher, *Practical Methods of Optimization.* Wiley, New York, 1990.

[88] M. Converse, E. J. Bond, S. C. Hagness, and B. D. Van Veen, “Ultrawideband microwave space-time beamforming for hyperthermia treatment of breast cancer: A computational feasibility study”, *IEEE Transactions on Microwave Theory and Techniques*, vol. 52, no. 8 II, pp. 1876–1889, 2004.

[89] K. S. Cheng, V. Stakhursky, O. I. Craciunescu, P. Stauffer, M. Dewhirst, and S. K. Das, “Fast temperature optimization of multi-source hyperthermia applicators with reduced-order modeling of ’virtual sources’.”, *Physics in medicine and biology*, vol. 53, no. 6, pp. 1619–1635, 2008.

[90] B. Guo, L. Xu, and J. Li, “Time Reversal Based Microwave Hyperthermia Treatment of Breast Cancer”, *Microwave and Optical Technology Letters*, vol. 47, no. 4, pp. 335–338, 2005.

[91] D. A. M. Iero, L. Crocco, and T. Isernia, “Thermal and microwave constrained focusing for patient-specific breast cancer hyperthermia: A robustness assessment”, *IEEE Transactions on Antennas and Propagation*, vol. 62, no. 2, pp. 814–821, 2014.

[92] D. A. Iero, L. Crocco, and T. Isernia, “Advances in 3-D electromagnetic focusing: Optimized time reversal and optimal constrained power focusing”, *Radio Science*, vol. 52, no. 1, pp. 166–175, 2017.

[93] D. A. M. Iero, L. Crocco, S. Member, and T. Isernia, “On the Role and Choice of Source Polarization in Time-Reversal Focusing of Vector Fields”, *IEEE Antennas and Wirless Propagation Letters*, vol. 15, no. 1, pp. 214–217, 2016.

[94] D. A. M. Iero, L. Crocco, and T. Isernia, “Constrained power focusing of vector fields: An innovative globally optimal strategy”, *Journal of Electromagnetic Waves and Applications*, vol. 29, no. 13, pp. 1708–1719, 2015.

[95] G. G. Bellizzi, L. Crocco, G. M. Battaglia, and T. Isernia, “Multi-Frequency Constrained SAR Focusing For Patient Specific Hyperthermia Treatment”, *IEEE Journal of Electromagnetics, RF and Microwaves in Medicine and Biology*, vol. 1, no. 2, pp. 74–80, 2017.

[96] G. G. Bellizzi, L. Crocco, and T. Isernia, “SAR Constrained Focusing Through Multi-Frequency Array Applicators”, in *2017 First IEEE MTT-S International Microwave Bio Conference (IMBIOC)*, 2017, pp. 2–5.

[97] E. Zastrow, S. C. Hagness, B. D. Van Veen, and J. E. Medow, “Time-multiplexed beamforming for noninvasive microwave hyperthermia treatment”, *IEEE Transactions on Biomedical Engineering*, vol. 58, no. 6, pp. 1574–1584, 2011.

[98] J. Wiersma, R. A. M. Van Maarseveen, and J. D. P. Van Dijk, “A flexible optimization tool for hyperthermia treatments with RF phased array systems”, *International Journal of Hyperthermia*, vol. 18, no. 2, pp. 73–85, 2002.

[99] D. Cassereau and M. Fink, “Time-Reversal of Ultrasonic Fields—Part III: Theory of the Closed Time-Reversal Cavity”, *IEEE Transactions on Ultrasonics, Ferroelectrics, and Frequency Control*, vol. 39, no. 5, pp. 579–592, 1992.

[100] M. M. Paulides, S. H. J. a. Vossen, A. P. M. Zwamborn, and G. C. Van Rhoon, “Theoretical investigation into the feasibility to deposit RF energy centrally in the head-and-neck region”, *International Journal of Radiation Oncology Biology Physics*, vol. 63, no. 2, pp. 634–642, 2005.

[101] S. K. Das, S. T. Clegg, and T. V. Samulski, “Computational techniques for fast hyperthermia temperature optimization”, *Medical Physics*, vol. 26, pp. 319–328, 1999.

[102] M. De Greef, H. P. Kok, D. Correia, A. Bel, and J. Crezee, “Optimization in hyperthermia treatment planning: The impact of tissue perfusion uncertainty”, *Medical Physics*, vol. 37, no. 9, pp. 4540–4550, 2010.

[103] H. K. Lee, A. G. Antell, C. A. Perez, W. L. Straube, G. Ramachandran, R. J. Myerson, B. Emami, E. P. Molmenti, A. Buckner, and M. A. Lockett, “Superficial hyperthermia and irradiation for recurrent breast carcinoma of the chest wall: Prognostic factors in 196 tumors”, *International Journal of Radiation Oncology Biology Physics*, vol. 40, no. 2, pp. 365–375, 1998.

[104] T. Drizdal, M. M. Paulides, N. van Holthe, and G. C. van Rhoon, “Hyperthermia treatment planning guided applicator selection for sub-superficial head and neck tumors heating”, *International Journal of Hyperthermia*, vol. 34, no. 6, pp. 704–713, 2017.

[105] R. F. Verhaart, G. M. Verduijn, V. Fortunati, Z. Rijnen, T. van Walsum, J. F. Veenland, and M. M. Paulides, “Accurate 3D temperature dosimetry during hyperthermia therapy by combining invasive measurements and patient-specific simulations”, *International Journal of Hyperthermia*, vol. 31, no. 6, pp. 686–692, 2015.

[106] D. Fatehi, J. van der Zee, A. Notenboom, and G. C. van Rhoon, “Comparison of intratumor and intraluminal temperatures during locoregional deep hyperthermia of pelvic tumors”, *Strahlentherapie und Onkologie*, vol. 183, no. 9, pp. 479–486, 2007.

[107] G. Cappiello, B. Mc Ginley, M. A. Elahi, T. Drizdal, M. M. Paulides, M. Glavin, M. O’Halloran, and E. Jones, “Differential Evolution Optimization of the SAR Distribution for Head and Neck Hyperthermia”, *IEEE Transactions on Biomedical Engineering*, vol. 64, no. 8, pp. 1875–1885, 2016.

[108] R. Eberhart and J. Kennedy, “A new optimizer using particle swarm theory”, *MHS’95. Proceedings of the Sixth International Symposium on Micro Machine and Human Science*, pp. 39–43, 1995.

[109] S. Chen, *Constrained Particle Swarm Optimization.* [Online]. Available: `https://www.mathworks.com/matlabcentral/fileexchange/25986-constrained-particle-swarm-optimization` (visited on 12/12/2018).

[110] R. Storn and K. Price, "Differential evolution–a simple and efficient heuristic for global optimization over continuous spaces", *Journal of Global Optimization*, pp. 341–359, 1997.

[111] J. L. K. Price, R. Storn, *Differential Evolution - A Practical Approach to Global Optimization.* Springer, 2005.

[112] P. Hasgall, E. Neufeld, M. C. Gosselin, A. Klingenbock, and N. Kuster, *ITIS Database for thermal and electromagnetic parameters of biological tissues.* [Online]. Available: `http://www.itis.ethz.ch/database` (visited on 12/12/2018).

[113] M. Franckena, R. Canters, F. Termorshuizen, J. Van Der Zee, and G. Van Rhoon, "Clinical implementation of hyperthermia treatment planning guided steering: A cross over trial to assess its current contribution to treatment quality", *International Journal of Hyperthermia*, vol. 26, no. 2, pp. 145–157, 2010.

[114] M. Kroesen, H. T. Mulder, J. M. van Holthe, A. A. Aangeenbrug, J. W. M. Mens, H. C. van Doorn, M. M. Paulides, E. Oomen-de Hoop, R. M. Vernhout, L. C. Lutgens, G. C. van Rhoon, and M. Franckena, "Confirmation of thermal dose as a predictor of local control in cervical carcinoma patients treated with state-of-the-art radiation therapy and hyperthermia", *Radiotherapy and Oncology*, vol. 140, no. July 2005, pp. 150–158, 2019.

[115] G. Cappiello, T. Drizdal, B. Mc Ginley, M. O'Halloran, M. Glavin, G. C. Van Rhoon, E. Jones, and M. M. Paulides, "The potential of time-multiplexed steering in phased array microwave hyperthermia for head and neck cancer treatment", *Physics in Medicine and Biology*, vol. 63, no. 13, 2018.

[116] K. Deb, A. Pratap, S. Agarwal, and T. Meyarivan, "A fast and elitist multi-objective genetic algorithm: NSGA-II", *IEEE Transactions on Evolutionary Computation*, vol. 6, no. 2, pp. 182–197, 2002.

[117] E. Zitzler and L. Thiele, "Multiobjective optimization using evolutionary algorithms - A comparative case study", *Parallel Problem Solving from Nature - PPSN V*, pp. 292–301, 1998.

[118] K. Deb, *Multi-objective optimization using evolutionary algorithms.* Chichester, England: John Wiley & Sons, 2001.

[119] A. Konak, D. W. Coit, and A. E. Smith, "Multi-objective optimization using genetic algorithms: A tutorial", *Reliability Engineering and System Safety*, vol. 91, no. 9, pp. 992–1007, 2006.

[120] J. F. Bakker, M. M. Paulides, A. Christ, N. Kuster, and G. C. van Rhoon, "Assessment of induced SAR in children exposed to electromagnetic plane waves between 10 MHz and 5.6 GHz.", *Physics in Medicine and Biology*, vol. 55, no. 11, pp. 3115–3130, 2010.

[121] L. Sachs, *Applied Statistics: A Handbook of Techniques*, 2nd. New York: Springer Verlag, 1982.

[122] M. M. Paulides, R. M. C. Mestrom, G. Salim, B. B. Adela, W. C. M. Numan, T. Drizdal, D. T. B. Yeo, and A. B. Smolders, "A printed Yagi–Uda antenna for application in magnetic resonance thermometry guided microwave hyperthermia applicators", *Physics in Medicine and Biology*, vol. 62, no. 5, pp. 1831–1847, 2017.

[123] M. Franckena, D. Fatehi, M. D. Bruijne, R. a. M. Canters, Y. V. Norden, J. W. Mens, G. C. V. Rhoon, and J. V. D. Zee, "Hyperthermia dose-effect relationship in 420 patients with cervical cancer treated with combined radiotherapy and hyperthermia", *European Journal of Cancer*, vol. 45, no. 11, pp. 1969–1978, 2009.

[124] J. Gellermann, B. Hildebrandt, R. Issels, H. Ganter, W. Wlodarczyk, V. Budach, R. Felix, P. U. Tunn, P. Reichardt, and P. Wust, "Noninvasive magnetic resonance thermography of soft tissue sarcomas during regional hyperthermia: Correlation with response and direct thermometry", *Cancer*, vol. 107, no. 6, pp. 1373–1382, 2006.

[125] G. C. van Rhoon, "Is CEM43 still a relevant thermal dose parameter for hyperthermia treatment monitoring?", *International Journal of Hyperthermia*, vol. 32, no. 1, pp. 50–62, 2016.

[126] A. Hirata and O. Fujiwara, "The correlation between mass-averaged SAR and temperature elevation in the human head model exposed to RF near-fields from 1 to 6 GHz", *Physics in Medicine and Biology*, vol. 54, no. 23, pp. 7227–7238, 2009.

[127] A. Hirata, K. Shirai, and O. Fujiwara, "Temperature Elevation Due To a Dipole Antenna", *Progress In Electromagnetics Research*, vol. 84, pp. 221–237, 2008.

[128] A. Razmadze, L. Shoshiashvili, D. Kakulia, R. Zaridze, G. Bit-Babik, and A. Faraone, "Influence of specific absorption rate averaging schemes on correlation between mass-averaged specific absorption rate and temperature rise", *Electromagnetics*, vol. 29, no. 1, pp. 77–90, 2009.

[129] A. Razmadze, L. Shoshiashvili, D. Kakulia, and R. Zaridze, "Correlation between SAR and temperature rise distributions with different masses and schemes of averaging, child head, dipole antenna radiation at 1800 MHz", *Proceedings of DIPED-2007*, pp. 48–53, 2007.

[130] A. Hirata, M. Fujimoto, T. Asano, J. Wang, O. Fujiwara, and T. Shiozawa, "Correlation between maximum temperature increase and peak SAR with different average schemes and masses", *IEEE Transactions on Electromagnetic Compatibility*, vol. 48, no. 3, pp. 569–577, 2006.

[131] T. Samaras, E. Kalampaliki, and J. N. Sahalos, "Influence of thermophysiological parameters on the calculations of temperature rise in the head of mobile phone users", *IEEE Transactions on Electromagnetic Compatibility*, vol. 49, no. 4, pp. 936–939, 2007.

[132] J. Lang, B. Erdmann, and M. Seebass, “Impact of Nonlinear Heat Transfer onTemperature Control in Regional Hyperthermia”, *IEEE Transactions on Biomedical Engineering*, vol. 46, no. 9, pp. 1129–38, 1999.

[133] C. W. Song, A. Lokshina, J. G. Rhee, M. Patten, and S. H. Levitt, “Implication of Blood Flow in Hyperthermic Treatment of Tumors”, *IEEE Transactions on Biomedical Engineering*, vol. 31, pp. 9–16, 1984.